6-2004

Crystallization kinetics study of the glasses in Se–Te system

Fareed Abdul Raheem Al-Gheyath

CRYSTALLIZATION KINETICS STUDY OF GLASSES IN THE SE -TE SYSTEM

Thesis submitted to

Deanship of Graduate Studies

United Arab Emirates University

By

Fareed Abdul Raheem Al-Gheyath

In Partial Fulfillment of the Requirements for the Degree of M. Sc.

In Materials Science and Engineering

Supervisors

Prof. Ossama El-Shazly
Department of Physics
Faculty of Science
UAE University

Prof. Rashed Alsaeed
Department of Chemistry
Faculty of Science
UAE University

June 2004

To my beloved Mother,
For every wonderful
thing she taught me

ACKNOWLEDGMENTS

The achievement of any millstone requires a wide group of advisors and genuine support. Hence my first and foremost thanks go to my supervisor Prof. Ossama El-Shazly for his valuable advice, encouragements & alteration, for his sincere caring and effectual guidance, and for truly having the interest of my success in his heart. I would also like to thank Prof. Rashed Alsaeed for his assistance and supervision.

My thanks are extended to Dr. Hadif Elowais and Dr. Yousef Hayek for their moral supports. I would like to thank Dr. Salah Makhlouf, Physics Department, for his assistance in handling the x-ray data. Then I would like to thank Mr. Ahmad Ayesh, Mr. Mohammad, Mr. Ayman and Mr. Ali Dewidar for their technical support in regards of materials preparation, glass work, x-ray measurements and DSC measurements, respectively.

I am in dept to my parents, for their care which kept pouring in during the good and bad times of throughout my life course. Further I would like to acknowledge my brothers and sister, my friends and my colleagues and coworkers from the past and present for their wonderful company. My thanks are also due to all my professors in the master program, and the management of UAE University and the University assisting staff for facilitating my success all through my master. Special thanks to Prof. Adel Hamamy, for his enthusiastic guidance and backing

Above all I would like to express my deepest gratitude to my Mother Fatima for her sincere caring and loving support.

Abstract

ABSTRACT

The aim of the present work is to study the crystallization kinetics of some chalcogenide glassy alloys in the Selenium-Tellurium system. Four glassy systems have been prepared: $Se_{80}Te_{20-x}Sb_x$ (x = 0, 4, 6, 8, 10); $Se_{70}Te_{30-x}Sb_x$ (x = 2, 6, 8, 10); $Se_{80}Te_{20-x}Cd_x$ (x = 2, 4, 10); and $Se_{80}Te_{20-x}Sn_x$ (x = 2, 4, 10). The starting materials of (99.999%) purity were weighted according to their atomic percentages and sealed in evacuated silica tubes, under a pressure of about 10^{-5} torr. The tubes were heated in a furnace at the required temperature and then quenched in ice-water mixture.

X-ray diffraction measurements indicated that all samples in the first two systems are amorphous, while all samples in the other two systems indicated the existence of some degree of crystallinity, except only the sample ($Se_{20}Te_{16}Cd_4$). Therefore it was decided to confine the study on the first two systems and ($Se_{20}Te_{16}Cd_4$) alloy.

From the DSC measurements, the glass transition temperature (T_g) and the onset temperature of crystallization (T_c) were determined at different heating rates. It was found that (T_g) and (T_c) shift to higher values as the heating rate (α) is increased. This dependence of (T_g) and (T_g) on (α) was used to calculate the activation energy of glass transition (E_t) and the activation energy of crystallization (E_c), respectively. The activation energy values of glass transition using several equations were found to be in good agreement with each other, for each glassy alloy. Similarly the

activation energy for crystallization was calculated using several equations and they were in good agreement with each other.

From the value of (T_c-T_g), which gives an indication of the kinetic resistance to crystallization, it was found that the alloy with 6 at.% Sb is the most stable alloy for both systems (1 and 2).

Crystallizations using partial area analysis were studied where the crystallization mechanism was concluded for each glassy alloy.

Table of Contents

List of figures

List of Tables

Chapter 1

Introduction

Today we live in a world that is both dependent upon and highly determined by materials. Specific materials are designed within the potentiality of its properties. Properties are derived from certain characteristics that result from carefully selecting the materials, and from controlling the manufacturing processes used to convert the basic materials into the final engineered product. Exciting new product developments are frequently possible only through new materials and/or processing. Most likely, material technologies would continue to develop more in the coming decades. During the last 3 decades of the 20^{th} century, glasses with new characteristics have attracted the attention of scientists to the extent of calling this age the Glass age [1]. This is due to its wide range of applications, and exhibiting interesting phenomenon.

1.1 Amorphous and Crystalline State of Matter:

Solids lacking long range order (position order) are called noncrystalline solids (NCS) Non-Crystalline solids can be divided into two classes: and amorphous solids. Glasses are amorphous in nature [2, 3], i.e. they form a disordered and metastable structure.

Disorder can occur in several forms, of which topological (or geometric), spin (or magnetic), substitutional, and vibrational disorder are the most important. These types of disorder are illustrated schematically in Fig. 1.1. Topological disorder is that form of randomness in which there is no translational periodicity whatsoever as shown in (Fig. 1.1-a). In spin disorder, the underlying perfect crystalline is preserved, but each atomic site possessed a spin or magnetic moment,

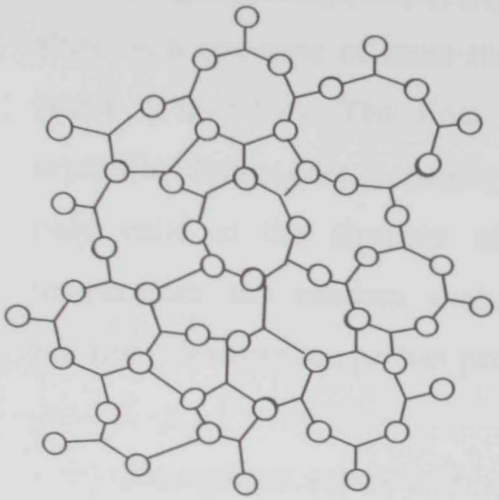

(a)

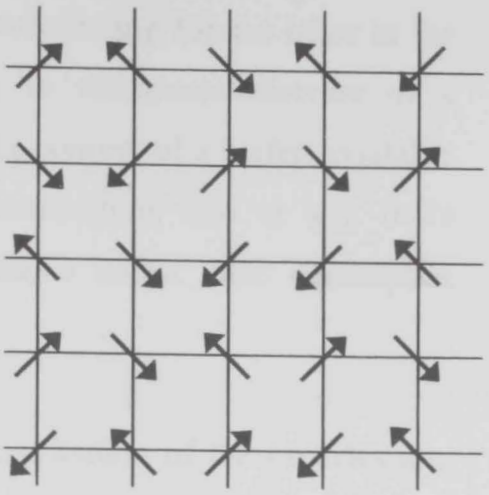

(b)

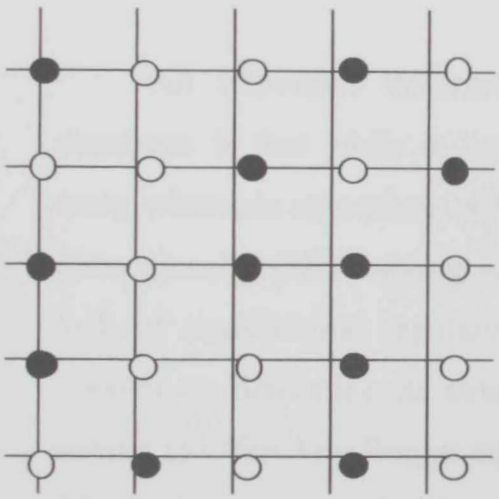

(c)

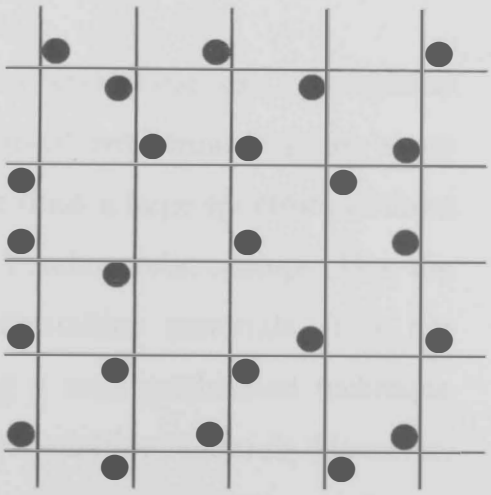

(d)

Fig 1.1 Types of disorder: (a) Topological disorder. (b) Spin disorder. (c) Substitutional disorder. (d) Vibrational disorder.

that is oriented randomly (Fig. 1.1-b). In substitutional disorder, the underlying crystalline lattice is preserved but in fact the material is in an alloy with one type of atom randomly substituting for the other in the lattice (Fig. 1.1-c). The final category is vibrational disorder of a crystalline lattice (Fig. 1.1-d) in which the concept of a perfect crystal is only valid at the absolute zero of temperature, and at any finite temperature the random motion of atoms about their equilibrium positions destroys the perfect periodicity.

Amorphous solids with random distribution of the particles are, like liquids, isotropic and do not form regular shapes. With respect to the set of their physical and chemical properties, amorphous solids occupy an intermediate position between the solid crystalline state and the liquid state.

An important difference between crystalline and amorphous structures is that while in crystals the local environment is the same every where, in amorphous materials one finds a large spectrum of three dimensionally (3D) varying spatial and bonding relationships. Due the lack of translational regularity in noncrystalline materials, it is not possible to determine its structure using a well established technique similar to offered by Braggs equation for crystalline materials. However, this lack of translational regularity makes it possible to change continuously the elemental ratios in noncrystalline compounds allowing systematic compositional studies to be made.

The rate of molecular regrouping, (i.e. relaxation process) plays an important role in the glass formation. When the liquid is cooled, its

structure becomes rearranged and the relative positions of the atoms and molecules are changed. The completion of the rearrangement is slower the temperature. When the temperature is such that the relaxation time and the viscosity become very large, the probability of rearrangement of the structure becomes negligibly small.

Amorphous solids can be prepared by different ways [4], and the characteristics of the material obtained, are, in general, strongly dependent on the mode of preparation. There are two standard ways of preparing amorphous solids:

(i) by condensation from vapor as in the thermal evaporation, sputtering, glow discharge decomposition of a gas, or other methods of deposition, and

(ii) by cooling from a melt.

The first methods produce thin films, while the second method produces bulk materials. Materials that are obtained from the molten state are called glasses and generally have smaller tendency to crystallize compared to those prepared by deposition.

1.2 Chalcogenide Glasses:

Continuous progress in science and technology imposes new and increased requirements on semiconducting materials. Silicon and germanium on longer satisfy all these varied and specific requirements. The search is for new more effective semiconducting materials with properties that can be varied in a wide range. Chalcogenide glasses are promising in many respects.

The word Chalcogenide is derived from 'chalcogen', which is the Latin name for sulfur [5]. Now a days, The term Chalcogenide Glass is used for inorganic material alloys composed of two or more chemical elements, when at least the major composite of the system is Sulfur (S), Selenium (Se) or Tellurium (Te), which are elements from group (VI-A) of the periodic table [6]. The other composites that form a chalcogenide system are more electropositive elements of group V, Tathogen elements of group IV-A such as Si, Ge, Sn, Pb, or Pnictides elements of group V-A such as P, As, Sb, & Bi[7] as shown in Fig. 1.2.

Therefore chalcogens can combine with other elements to form glasses in wide ranges of proportion, while oxide glasses are essentially composed of stoichiometric oxides [5]. Unlike oxygen, which in the liquid state consists of O2 molecules that crystallize on cooling, S, Se, and Te form elemental glasses containing disordered rings or chains. The structures of these large classes of glasses are based on rings, chains, or three-dimensional networks as well as combinations of such structural groupings. Most chalcogenides form glasses very easily. Several glass forming systems have been identified containing these elements and combination of several other elements [5-7].

Chalcogenide glasses have been studied for over one hundred years [8] but intensive investigation began only after the discovery that many of these materials transmit light well in the infrared out to 12 μm [9-11]. A systematic study of chalcogenide glasses was initiated by B. T. Kolomiets and N. A. Goryunova with their coworkers [12] discovered their semiconducting properties. This is how chalcogenide glasses have acquired their second name "glassy semiconductors".

IB	IIB	III	IV	V	VI
		Al	Si	P	S
Cu	Zn	Ga	Ge	As	Se
Ag	Cd	In	Sn	Sb	Te
Au	Hg	Ti	Pb	Bi	Po

Chalcogen element

Additive elements to chalcogenide glasses

Fig. 1.2 The main components of the Chalcogenide Glasses in the periodic table.

1.3 Synthesis of Chalcogenide Alloys:

There are many methods by which chalcogenide materials can be obtained, some of which allow the production of the materials in bulk form. Others produce a thin layer of film deposited upon a substrate. Some methods also produce the chalcogens in fiber forms. The compositional range depends on the preparation method used e.g. the rapid vapor quenching technique allows a wider composition range to be produced in amorphous form than by melt quenching which enables bulk materials to be produced.

1.3.1 Melt Quenching

The technique of preparing bulk glasses by rapid quenching of a melt is the most established and widely used method in the preparation of amorphous chalcogenide materials. Many chalcogenide materials are good glass formers, and the melts of these materials will vitrify (change into glass) when cooled by quenching in air or water. Thermodynamic, kinetic and structural factors also can influence the process in generic and specific ways. The viscosity of the melt is also important in glass formation. The thicker the melt at a given temperature above the melting point is, the greater the chances for glass formation exist. On cooling, the viscosity increases even further as it is usually activated due to heat flow [16].

The formation of crystals is avoided by making the movement of the atoms in the liquid increasingly difficult, by using suitable amounts of kinetic energy. Hence, the kinetics (speed) of the quenching process is also a factor influencing the glass forming abilities of the chalcogenide materials. The faster the quenching process the greater the likelihood of

forming glassy and not a crystalline product. Another influencing factor is the process of 'frustration', i.e. crystallization in a multi-component melt is avoided by encouraging competition between formation of several different types (crystal of different composition) or simply by inducing difficulty of rearranging many different types of atoms to form a multi-component crystal. Chemical factors also can determine the ease of glass formation for chalcogenide materials [17].

Glassy semiconductor alloys are synthesized as rule from elemental substance of equal degree of purity. To obtain most glassy alloys, materials of very pure grade are used. The total weight of the obtained glassy alloys is determined mainly by its crystallization ability. Glasses of low crystallization ability can be synthesized in any amount. Easily crystallization glasses can be synthesized in amounts of 5-10 g. The smaller the total weight of the melt, the higher the rate at which this melt can be cooled uniformly.

The synthesis is carried out in evacuated (10^{-5} Torr) quartz ampoules. The synthesis regimes are highly varied. They depend on the melting temperature of the glass components, on their vapor pressure, and others. The presence of even traces of oxygen in chalcogenide glasses is highly undesirable, and is especially harmful to their optical properties.

To obtain homogeneous glassy alloys it is necessary to use forced homogenization of the melt. This can be done by vibration mixing of the melt or by synthesizing the glasses in rotating furnaces.

The melt cooling regimes vary, depending on its composition and on its crystallization ability. One procedure is to cool the melt slowly together with turned – off furnace for 10-12 h. slow cooling in the furnace, while offering certain advantages, has also serious shortcomings. In a slowly cooling melt, all the sheared bonds that can exist in the liquid state have time to be restored. The stress that can arise in fast cooling is eliminated However, the greatest shortcoming is that when the cooling is slow the structure of the melt itself is gradually altered and a complicated equilibrium, not always reproducible, is established between the structural formations; this equilibrium is reflected in the physical and chemical properties of the alloys produced. It is therefore more advantageous to cool the obtained melts rapidly by removing the ampoules from the furnace to the air (quenching in air) , to allow the glass to retain, as much possible, a definite structure corresponding approximately to the structure of the melt at the synthesis temperatures[8, 18].

1.3.2 Vapor Deposition

Vapor deposition methods can be used to obtain amorphous thin films deposited onto substrates. These techniques have extremely fast quenching rates and are therefore ideal for obtaining amorphous chalcogenide products from those materials that are difficult to vitrify. It is also possible to extend the compositional range for which a given system can be made amorphous in these techniques, compared to the ranges available using conventional melt-quenching techniques. Vapor deposition methods are mainly divided into two categories: physical deposition involving the conversion of atoms and molecules into vapor

phase from solid or liquid sources with no chemical modification; and reactive deposition in which the vapor is chemically modified with respect to the source material. Main types of these techniques are thermal evaporation, sputtering, and chemical vapor deposition [19- 21].

1.4 Regularities of Glass Formation in Chalcogenide Systems:

The tendency of chalcogenide systems to form glasses, as well as the physical and chemical properties of the glasses, determined by the character of the chemical bond between the atoms that make up the glass. An increased tendency to glass formation is possessed by chalcogenide compounds and alloys with predominantly covalent chemical bonds. This is attested by the position of the main components of the chalcogenide glasses

In the periodic Table of the elements (Fig. 1.2), they belong to groups IV – VII of neighboring periods and are compactly placed. This group includes also the elemental semiconductors germanium and silicon. When these elements interact, the ion–bond component that hinders glass formation should be minimal. The excellent glass forming ability of the chalcogenides originates from the large size of the anions which can be combined with other elements to form glasses in a wide range of proportion.

It was found that the binary chalcogenide systems: As- Se, Ge-Se and As-S, have large glass forming regions. The As-Se glasses were obtained with composition ranging from 44 to 100 at.% Se. In the Ge –

Se system, glasses were obtained with 60-100 at. % Se. In As-S system, glasses containing from 55to 95 at. % S were obtained [12].

A relatively large region of glass formation was obtained in the sulfur-selenium system , where glassy alloys containing Se from 60 to 100 at. % can be found [12].Glasses with a large S content, are exceedingly unstable.

With increasing the number of components, the ability of the alloys to form glass increases. The more complicated the alloy composition, the greater the variety of spatially different structural units produced in it [12]. It is difficult to separate the individual crystal phases in the complicated composition of the alloy.

1.5 The Structure of Glassy Chalcogenides:

In order to understand the structure of chalcogenide glasses, it is important to understand the framework within which the structural features can be explained. It is convenient to divide the structure in materials in general into three different ascending length scales.

Short Range Order (SRO): In covalently bonded amorphous materials with strongly directed bonding such as chalcogenides, SRO can be defined in terms of a rather well defined coordination polyhedra as shown in Fig 1.3.

Medium Range Order (MRO): This group is defined by as simply the next highest level of structural organization beyond SRO.

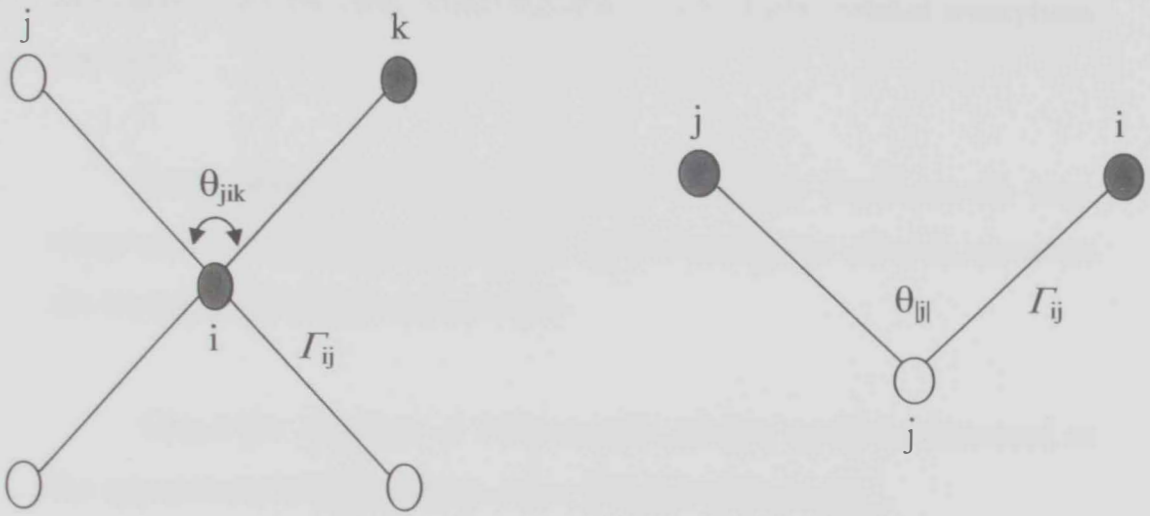

Fig. 2.3 Short range order of covalent materials in terms of coordination polyhedral molecular structure.

In practice for covalently bonded materials, it is convenient to divide MRO into three categories corresponding to progressively increasing scales: short range MRO (SRMRO) which are marked if the degrees of freedom associated with the relative orientation of pairs of neighboring polyhedra are restricted in some way. (Fig. 1.4); intermediate range MRO (IRMRO) which are associated with correlations between pairs of dihedral angles for neighboring bonds; and long range MRO (LRMRO) which is associated with the local dimensionality of covalently bonded amorphous network.

Long Range Order (structure): Although there are no long range order in amorphous materials, by definition, not all such materials are isotropic on a macroscopic scale.

Hence the structure of chalcogenide glasses could be discussed as the appearance of these groups in a chalcogenide system.

SRO in Chalcogenides: In the case of pure amorphous chalcogens the fundamental structural unit is based on a single atom and as such the SRO is straightforward. In the case of binary (or more complex) compositions, the situation is more sophisticated. In the case of Group III-VI glass, the structural unit is a planar triangular unit. In the case of Group V-VI glasses the structural unit is also triangular, but pyramidal, with the pnictogen atom raised above the plane defined by the three chalcogens. The polyhedral unit, for materials in Group IV-VI, is a tetrahedron on a tetragen. This geometry is consistent with the vibrational characteristics found from inelastic neutron scattering measurements. It has been assumed that these materials are completely chemically ordered, and hence each apex of the polyhedral units is

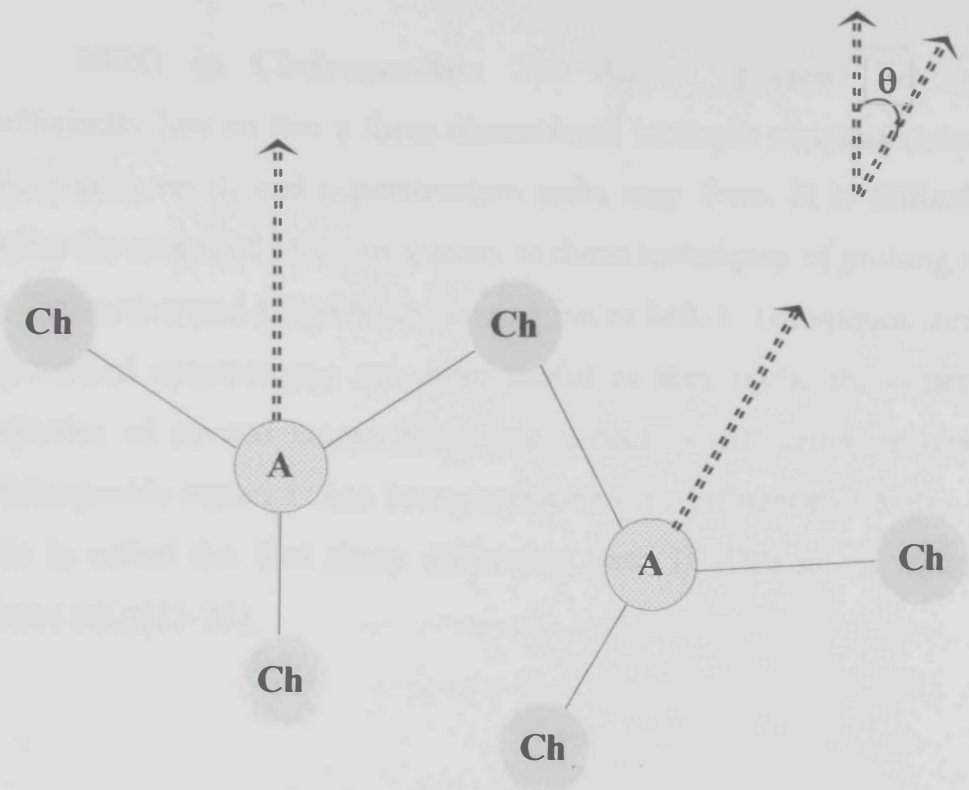

Ch Chalcogen element (S, Se or Te)

A Additive elements to chalcogenide glasses

Fig 1.4 Two neighboring polyhedral structure.

occupied by a chalcogens atom, which acts as a bridging link between two units. In the case of more complicated system or those containing wrong bonds, the structure remains the same but the chalcogens atoms are substituted by other elements.

MRO in Chalcogenides: The degree of cross linking is sufficiently low so that a three dimensional isotropic structure does not necessarily result and superstructure units may form. It is difficult to probe the extent of MRO in glasses as those techniques of probing such as Diffraction and EXAFS; are insensitive to MRO. Techniques such as vibrational spectroscopy are more useful as they probe the collective behavior of several atoms. Only one aspect of diffraction results on chalcogenide materials has been ascribed to the influence of MRO, and this is called the first sharp diffraction peak (FSDP) in the structure factor S(Q)[23-25].

Structure of Pure Chalcogens

The structural configurations which can be formed are limited essentially to rings or chains. The structure configurations are held by Van-Der-Waal interactions. For the case of Sulfur, there are several crystalline allotropic forms, each of them based on the packing of (cyclootasulfur) rings.

As for Selenium (Se) There are 3 crystalline forms including: The triagonal or hexagonal (most stable) form consists of helical(spiral) chains that are packed in a parallel fashion; The α and β monoclinic forms are composed of cyclootaselenium rings but packed differently;

and The dihedral angle polymorphs form. Unlike Sulfur or Selenium, Tellurium has only one crystalline form. It is a triagonal modification that comprises of infinite spiral chains packed in a parallel arrangement of molecules [26].

Structure of Chalcogenic Composites

As for (V-VI Materials), the most commonly studied materials in this system are the Arsenic (As) chalcogenides, which is based upon the stoichiometric compositions. The structure of As_2S_3 in both bulk glassy and amorphous thin films are superficially similar. Yet the bulk glass is more ordered than that of film. The structure of As_2Te_3 contains As sites which are octahedrally coordinated by Te, whereas the glass contains mainly $AsTe_{3/2}$ pyramidal units. The structure of Antimony (Sb) chalcogenides have trigonal pyramidal coordination of Sb atoms. The structure of amorphous phosphorus chalcogenides materials form cage like molecules [6, 7].

As for (IV-VI Materials), Germanium(Ge) and Silicon(Si) chalcogenides also exhibit a rich variety of structural features, particularly related to the MRO, as a result of the propensity for the formation of edge sharing tetrahedra compared with their oxide counterparts. As for III-VI Materials, there has been little structural work undertaken on boron chalcogenide glasses mainly because of their great sensitivity to hydrolysis and neutron scattering measurements are not possible with the naturally occurring isotopic mixture of boron due to the very high absorption cross section of the boron isotope nucleus. Other famous chalcogenic systems are metallic and halogennic chalcogenide glasses [6, 7].

1.6 Technological Applications for Chalcogenide Glasses:

A variety of stable chalcogenide glasses can be prepared in bulk, thin film, and multilayer forms. This led to a wide range of practical and potential technological applications. Generally four kinds of applications are commercially available for practical utilization. These rely upon the unique features of chalcogenide glasses, which are quasistability, photoconductive properties, infrared transparency, and ionic conduction. The 1st category is the phase-change phenomenon used in erasable high-density optical memories. The 2nd category is photoconductive applications such as photoreceptors in copying machines and X-ray imaging plates. The 3rd category of applications is purely optical. That is, since the chalcogenide glass is transparent in IR regions, it can be utilized for IR optical components such as lenses and windows. It can also be utilized for IR-transmitting optical fibers. Lastly, chalcogenide glasses containing group I elements such as silver are used as high-sensitivity ionic sensors [25].

On the other hand, Kaplan, et.al. [26] studied the potentiality of utilizing Se based chalcogenide glassy systems in the realization of ultra-fast all-optical switches suitable for telecommunication applications. Sanghera et.al. [27] showed applications that include laser power delivery, chemical sensing, and imaging, scanning near field microscopy/spectroscopy, IR sources/lasers, amplifiers. K. Hirao and K. Miura. [28] conducted a structural analysis of chalcogenide waveguides and demonstrated their stability under variation of ambient conditions.

Chapter 2

Theoretical background

2.1 Thermal Analysis:

The theoretical basis for interpreting differential thermal analysis (DTA) or differential scanning calorimetry (DSC) data is provided by the formal theory of transformation kinetics as the volume fraction (χ) crystallized in time (t), using the Tohns-Mehl-Avrami equation [29]:

$$\chi = 1 - \exp[-(Kt)^n] \qquad (2.1)$$

where (n) is an integer or haft integer, which depends on the mechanism of growth and the dimensionality of the crystal. (K) is defined as the effective overall reaction rate, which is usually assumed to have an Arrhenian temperature dependence:

$$K = K_o \exp[-E/RT] \qquad (2.2)$$

where (E) is the effective activation energy describing the overall crystallization process, which can be approximated as follows:

$$E \cong (E_N + mE_G)/n \qquad (2.3)$$

where (E_N) and (E_G) are the effective activation energies for nucleation and growth, respectively, and (n = m) for the nucleation frequency ($I_v = 0$)[30] and ($n = m + 1$) for ($I_v \neq 0$) [29].

If E_N is negligible over the temperature range of concern in the thermoanalytical study [29], then:

$$E \cong (m/n)\, E_g \qquad (2.4)$$

2.2 Method of Piloyan Borchardt:

In non-isothermal crystallization, it is assumed that there is a constant heating rate (α) in the DTA and DSC experiments. The relation between the sample temperature (T) and the heating rate (α) can be written in the form of :

$$T = T_0 + \alpha t \tag{2.5}$$

where (T_0) is the initial temperature. Differentiating equation (2.1) results in the following expression:

$$\chi' = (1-\chi)\, n K^n\, t^{(n-1)}\, [1 + \frac{t}{K} K'] \tag{2.6}$$

where ($\chi' = d\chi/dt$) and ($K' = dk/dt$). The derivation of K with respect to time is obtained from equations (2.2) and (2.5)

$$K' = \frac{dK}{dT}\frac{dT}{dt} = \frac{\alpha E}{RT^2} K \tag{2.7}$$

Thus equation (2.6) becomes:

$$\chi' = (1-\chi)\, n\, K^n\, t^{(n-1)}\, [1 + at] \tag{2.8}$$

where

$$a = (\alpha E / R T^2)$$

In the Piloyan [31] – Borchardt [32] method, the term (at) was neglected in comparison to unity assuming that ($E/RT << 1$). A better approach seems reasonable, if T_0 in Equation (2.5) is much smaller than T, the term ($at \cong E/RT$), and equation (2.8) becomes

$$\chi' = (1-\chi)\, n\, K^n\, t^{(n-1)}\, E/RT \qquad (2.9)$$

If ($T_0 << T$) and ($E/RT << 0$), equation (2.9) becomes:

$$\chi' = (1-\chi)\, n\, K^n\, t^{(n-1)} \qquad (2.10)$$

Combining equation (2.9) with the concept stated by Borchardt [30], that, at least for ($\chi < 0.5$), the reaction rate (χ') at a particular temperature (T) is proportional to the heat flow difference between the sample and inert reference (Δq), leads for DSC to

$$\chi' = C\, \Delta q \qquad (2.11)$$

In preceding further, the following operations are performed

(a) expressing (t) in terms of (χ) in equation (2.11),

$$t = (1/K)\, [-\ln(1-\chi)]^{1/n} \qquad (2.12)$$

(b) substituting for t in equation (2.9) gives

$$\chi' = (n\, K\, E/R\, T)\, F(\chi) \qquad (2.13)$$

The function $F(\chi)$ is defined as:

$$F(\chi) = (1-\chi)[-\ln(1-\chi)]^{\{(n-1)/n\}} \qquad (2.14)$$

(c) combining equations (2.2), (2.11) and (2.13) gives

$$C\, \Delta q = nK_0\, (E/R\, T)\, F(\chi)\, exp(-E/R\, T) \qquad (2.15)$$

(d) taking the logarithm and rearranging equation (2.15) gives

$$\ln[\frac{T\Delta q}{F(\chi)}] = \ln(\frac{n K_0}{C}) + \ln(\frac{E}{R}) - \frac{E}{RT} \qquad (2.16)$$

$\ln[T\Delta q/F(\chi)]$ is a linear function of (1/T). The slope of this relation yields the effective activation energy of crystal growth (E_c).

2.3 Method of Coats-Redfern-Sestak:

Coast-Redfern-Sestak (CRS) [33] suggested a method of determining the crystallization energy (E) by using the following equation:

$$\chi' = g(\chi)\, K_0 \exp(-E/RT) \qquad (2.17)$$

where ($\chi' = d\chi/dT$), the activation energy of reaction $\{g(\chi) = (1-\chi)^n\}$.
By rearranging equation (2.17) and integrating one obtains

$$\int_0^{\chi'} \frac{d\chi}{g(\chi)} = K_0 \int_0^1 \exp(-E/RT)dt \equiv G(\chi') \qquad (2.18)$$

The integration is carried out from the beginning from the reaction of crystallization until some fraction is crystallized. The function $G(\chi')$ is independent from the heating rate used to obtain the crystallized fraction (χ'). The time integral in equation (2.18) is transformed to a temperature integral yielding:

$$G(\chi') = \frac{K_0}{\alpha} \int_{T_0}^{T'} \exp(-E/RT)dT \qquad (2.19)$$

where (T_0) is the initial temperature.

If ($T_0 << T'$) and ($E/RT >> 1$), the solution of equation (2.19) is [34, 45, 36]

$$G(\chi') = [-\ln(1-\chi')]^{1/n} = (K_0\, R\, T^2/E\alpha) \exp(-E/R\, T') \qquad (2.20)$$

Or in logarithmic form

$$\ln[\{-\ln(1-\chi')\}/\{T'^{2n}\}] = -n\ln(\alpha) - \frac{nE}{RT'} + n\ln(\frac{K_0 R}{nE}) \qquad (2.21)$$

At constant α the relation between $\ln[\{-\ln(1-\chi')\}/\{T'^{2n}\}]$ and $(1/T')$ gives the value of (E).

The order of crystallization reaction (n) was proposed by Ozawa[37] method by differentiating equation (2.21) at constant temperature gives

$$d\{ln[-ln(1-\chi)]\}/d\{ln(\alpha)\} = -n \qquad (2.22)$$

On this basis plotting $\{\ln[-\ln(1-\chi)]\}$ versus $(\ln \alpha)$, which is obtained at the same temperature from a number of crystallization exotherms taken at different heating rates should yield the value of (n).

2.4 The Kissinger Method:

The method which is commonly used in analyzing the data in DSC and DTA experiments was developed by Kissinger [38, 39]. By using equation (2.10) and substituting from equation (2.12), the rate of reaction can be expressed as

$$\chi' = n\,K\,(1-\chi)\,[-ln(1-\chi)]^{(n-1)/n} \qquad (2.23)$$

In taking the derivative of equation (2.23) with respect to time it is convenient to assume that, near the crystallization peak, $\{[-\ln(1-\chi)]^{(n-1)/n}\}$ is a constant denoted A. taking the derivative of equation (2.23) with respect of time one obtains

$$\chi'' = AK_0[\frac{E}{RT^2} - \{\frac{AK_0}{\alpha}\exp(-E/RT_p)\}]\alpha(1-\chi_p)\exp(\frac{-E}{RT_p}) = 0 \quad (2.24)$$

i.e.

$$\alpha/T_p^2 = \frac{ARK_0}{E}\exp(-E/RT_p) \quad (2.25)$$

or

$$ln(\alpha/T_p^2) = -E/R\,T_p + Constant \quad (2.26)$$

The value of E can be evaluated from the relation between $\ln(\alpha/T_p^2)$and $(1/T_p)$ in equation (2.26).

2.5 Theories for Glass-Transition:

The heating rate dependence of the glass transition temperature is interpreted in terms of thermal relaxation phenomena. In this kinetic interpretation, the enthalpy of the glassy system at a particular temperature and time, towards a new equilibrium value $\{H_e(T)\}$. The relaxation equation can be written if the following form

$$(\frac{\partial H}{\partial t})_\tau = -(H - H_e)/\tau \quad (2.27)$$

where (τ) is a temperature dependent structural relaxation time and is given by the following relation

$$\tau = \tau_0\exp(\frac{\Delta E_t}{RT})\exp[\quad (2.28)$$

where (τ_0) and (c) are constant and (ΔE_t) is the activation energy of the relaxation time. Using the above equation, it can be shown that

$$\frac{d \ln \alpha}{d(1/T_g)} = -\frac{\Delta E_t}{R} \qquad (2.29)$$

(α) being the heating rate.

The dependence of the glass transition (T_g) on the heating rate (α) can be analyzed in two approaches, one is the empirical relationship of the form

$$T_g = A + B\, ln(\alpha) \qquad (2.30)$$

where A and B are constants for a given glass composition. This equation was suggested by lasocka [40]. The other approach is the use of so called Kissinger formula [39] for the evaluation of the activation energy for glass transition (E_t). For homogenous crystallization with spherical nuclei, it has been suggested that the dependence of (T_c) on a is given by the following equation [41, 42]

$$ln\left(\frac{\alpha}{T_g^2}\right) = -\frac{E_t}{RT_g} + Constant \qquad (2.31)$$

where (E_t) is the effective activation energy of crystallization. Although originally derived for the crystallization process, it is suggested that this expression is valid for glass transition [43] and has often been used [41, 44] to calculate the value of (E_t). The Kissinger can be approximated by the form

$$ln(\alpha) = -\frac{E_t}{RT_g} + Constant \qquad (2.32)$$

Chapter 3

Experimental Techniques

3.1 Sample Preparation:

Glassy alloys in the Se-Te system were prepared by using high purity (99.999 %) elements. Selenium (Se), Tellurium (Te), Antimony (Sb), Cadmium (Cd) and Tin (Sn) (from Aldrich) were weighted in appropriate at.% proportions by using electrical sensitive balance with accuracy of 10^{-4} g.

The appropriate sample weight of each element (S_i) is calculated form the equation:

$$S_i = \frac{\omega_i}{\sum_i \omega_i} W_t \qquad (3.1)$$

where ω_i is the weight of each element in the sample,

ω_i = concentration of the element × atomic mass,

$\sum_i \omega_i$ = $\sum$ weight of all elements in the sample, and

W_t is the total weight needed for preparing the sample.

Five grams of the starting sample composition were weighted and placed in a silica tube and sealed in a vacuum of about 10^{-5} torr. The tubes were heated in a furnace at the corresponding temperature for the specified time as indicated in Table 3.1.

The tubes were shaken several times during the heating process to ensure the homogeneous mixing of the constituent elements. The tubes

Alloy	Heating Temperature (°C)	Time (Hours)
Se_{80} Te_{20} Se_{80} Te_{16} Sb_4 Se_{80} Te_{14} Sb_6 Se_{80} Te_{12} Sb_8 Se_{80} Te_{10} Sb_{10}	700	24
Se_{70} Te_{28} Sb_2 Se_{70} Te_{24} Sb_6 Se_{70} Te_{22} Sb_8 Se_{70} Te_{20} Sb_{10}	700	24
Se_{80} Te_{16} Cd_4	800	20
Se_{80} Te_{18} Cd_2 Se_{80} Te_{10} Cd_{10}	800	20
Se_{80} Te_{18} Sn_2 Se_{80} Te_{16} Sn_4 Se_{80} Te_{10} Sn_{10}	700	8

Table 3.1 Prepared alloys.

were quenched in ice-water mixture and the glassy samples were obtained.

3.2 X-ray Diffraction Measurements

X-ray diffraction measurements were used to confirm the glassy nature of the prepared samples. A Philips x-ray diffractometer model PW/1840, with Ni filter, Cu-Kα radiation (λ = 1.542 A°) at 40 kV, 30 mA and scanning speed of (0.02°/s) was used.

Measurements were carried out at room temperature on the powder samples. The diffracted intensity as a function of the reflection angle was measured automatically by the x-ray diffractometer. The x-ray diffractograms of the prepared samples are shown in Figs. 3.1 - 3.15. The absence of any peak in the x-ray diffractograms (Fig. 3.1 – Fig. 3.10) indicates that $Se_{80}Te_{20-x}Sb_x$ (x = 0, 4, 6, 8, 10), $Se_{70}Te_{30-x}Sb_x$ (x = 2, 6, 8, 10) and $Se_{80}Te_{16}Cd_4$ alloys are in the glassy state. On the other hand, $Se_{80}Te_{20-x}Cd_x$ (x = 2, 10); and $Se_{80}Te_{20-x}Sn_x$ (x = 2, 4, 10) alloys have some degree of crystallinity as shown in Fig. 3.11 - Fig. 3.15.

3.3 Thermal Analysis Measurements

When heated to high enough temperatures, all materials undergo physical or chemical changes. These changes alter the enthalpy and heat capacity of the material which in turn results in the release or absorption of heat. By determining the instantaneous heat flow, differential

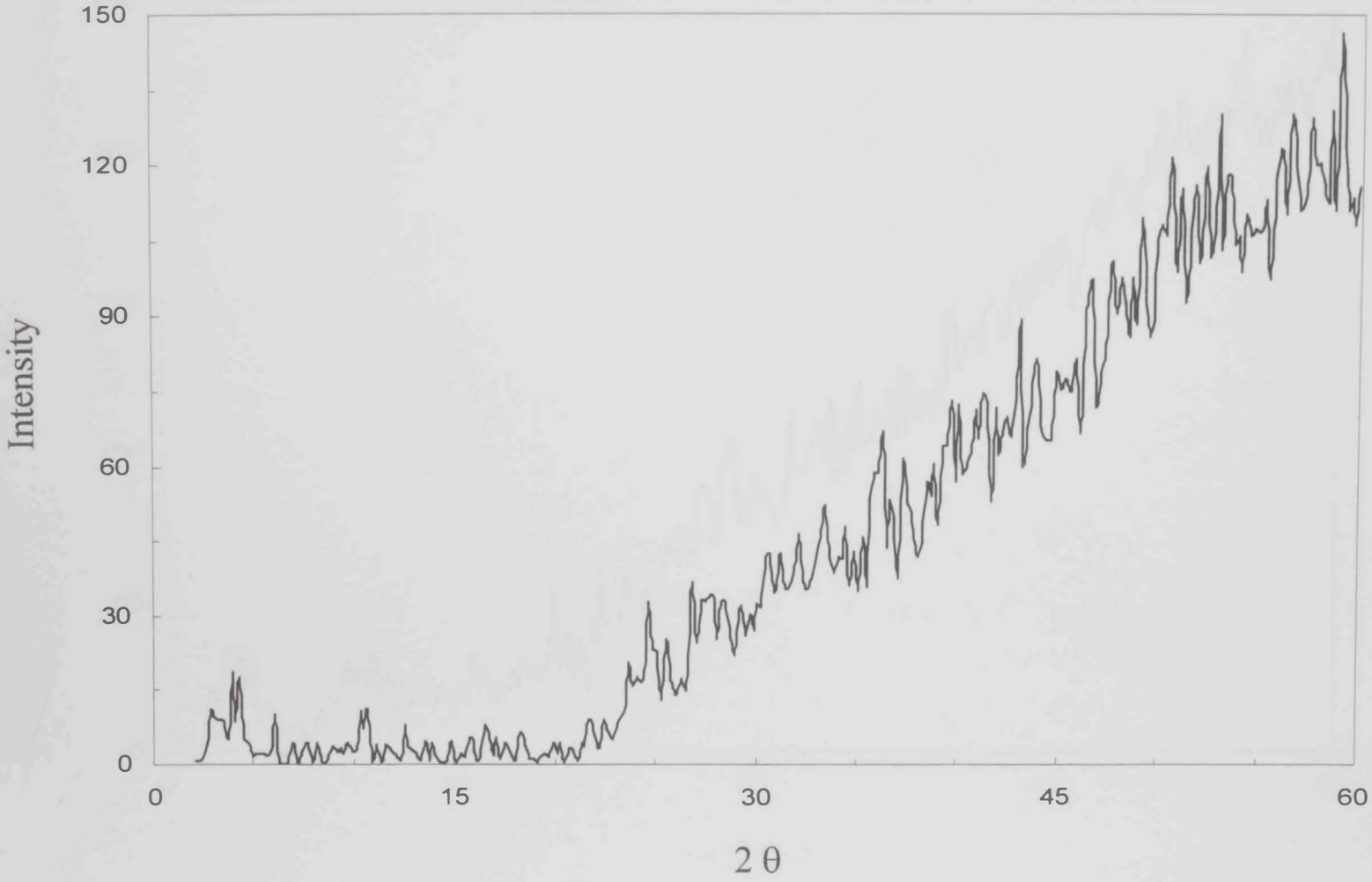

Fig. 3.1 X-ray diffraction pattern of $Se_{80}Te_{20}$ glassy alloy.

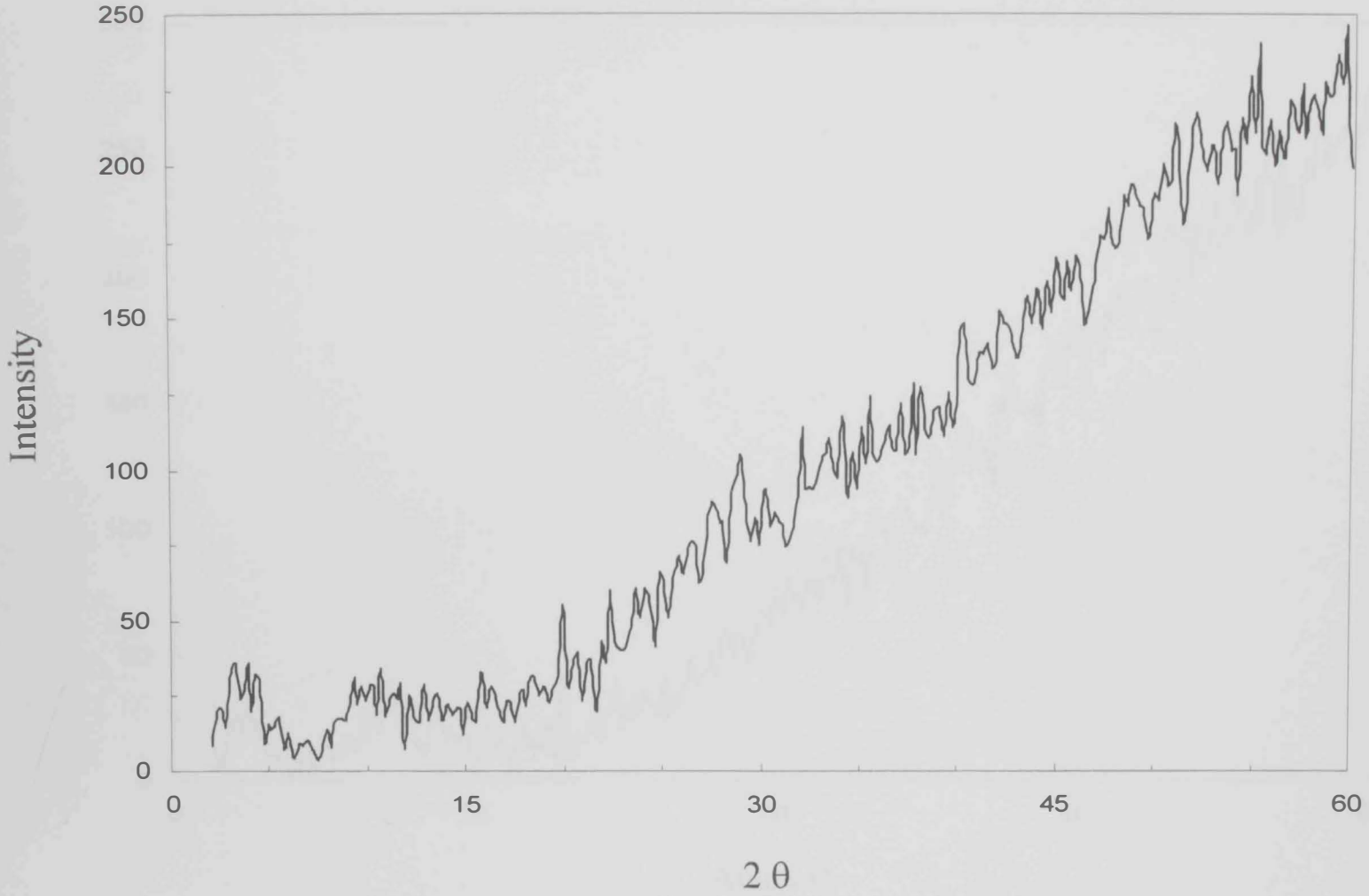

Fig. 3.2 X-ray diffraction pattern of $Se_{80}Te_{16}Sb_4$ glassesy alloy.

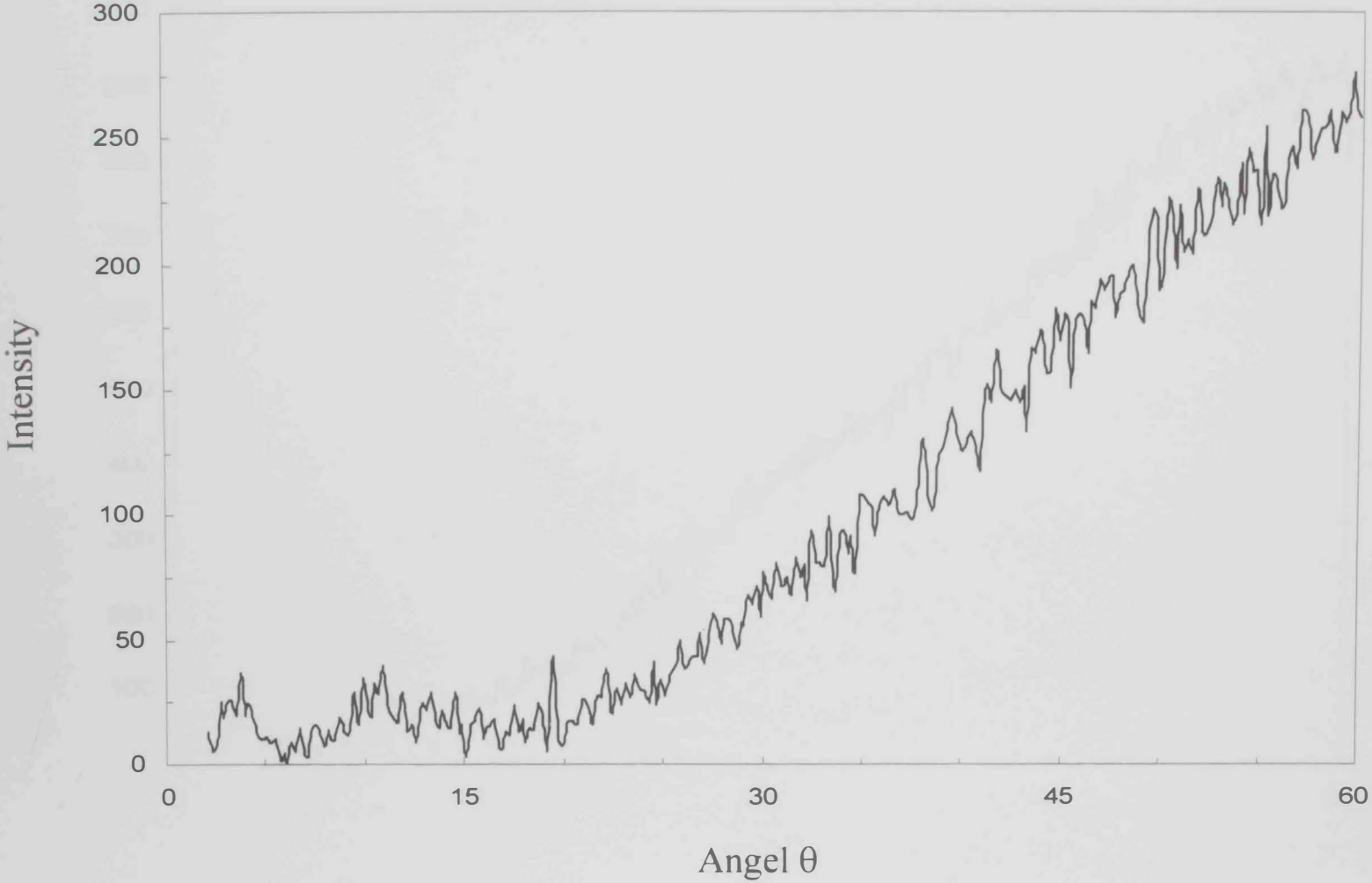

Fig. 3.3 X-ray diffraction pattern of $Se_{80}Te_{14}Sb_6$ glassesy alloy.

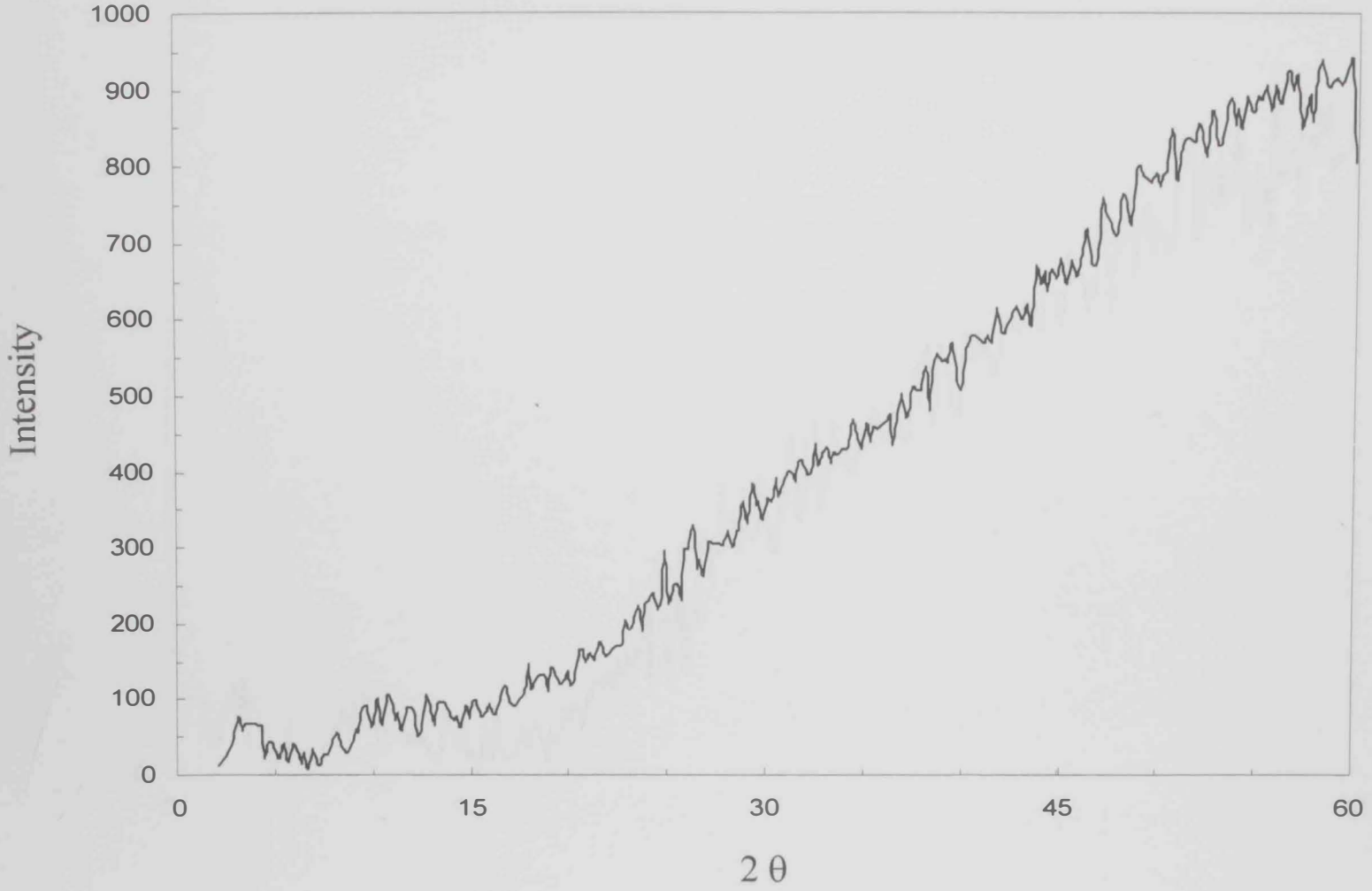

Fig. 3.4 X-ray diffraction pattern of $Se_{80}Te_{12}Sb_8$ glassesy alloy.

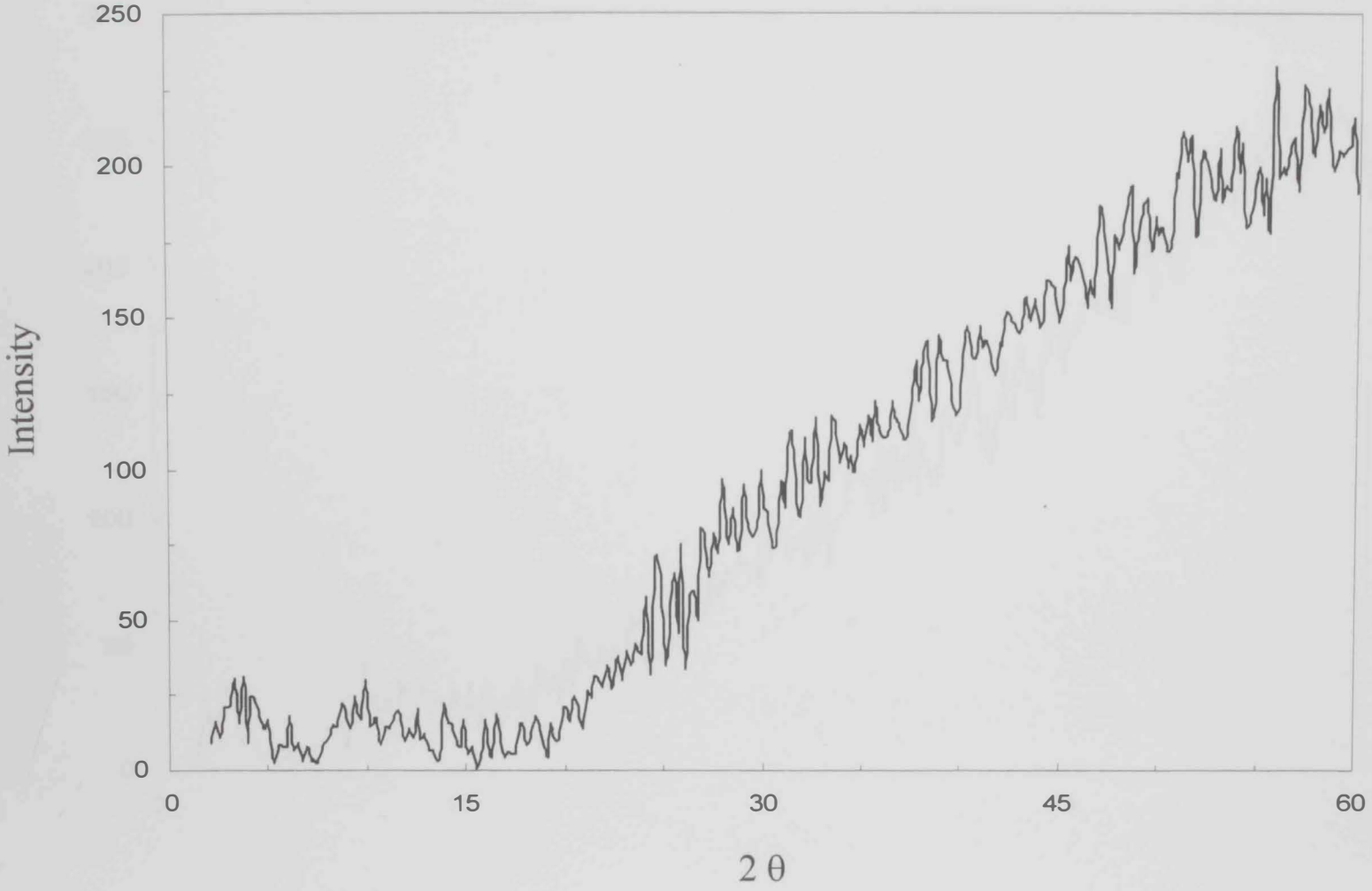

Fig. 3.5 X-ray diffraction pattern of $Se_{80}Te_{10}Sb_{10}$ glassesy alloy.

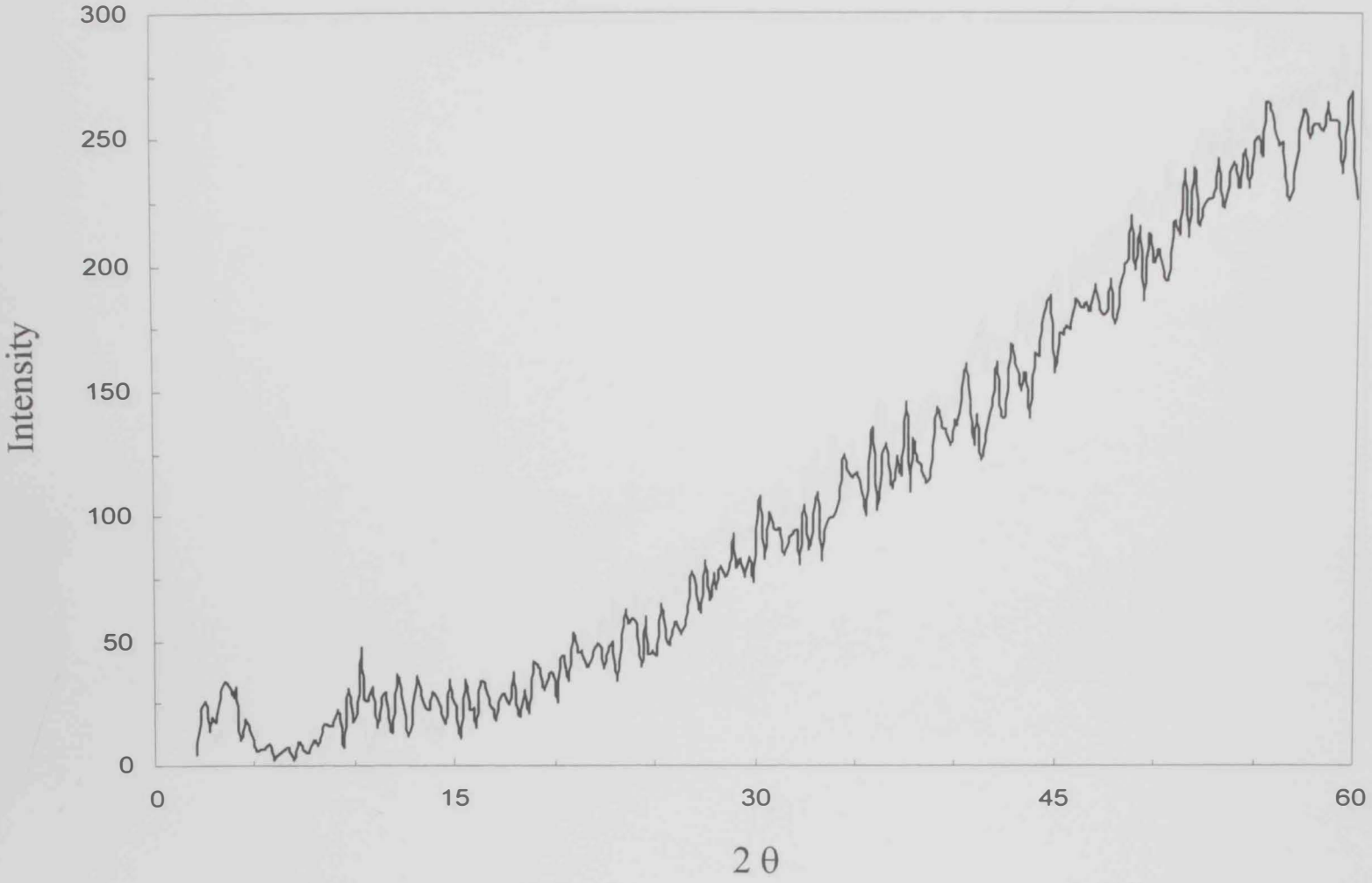

Fig. 3.6 X-ray diffraction pattern of Se_{70} Te_{28} Sb_2 glassy alloy.

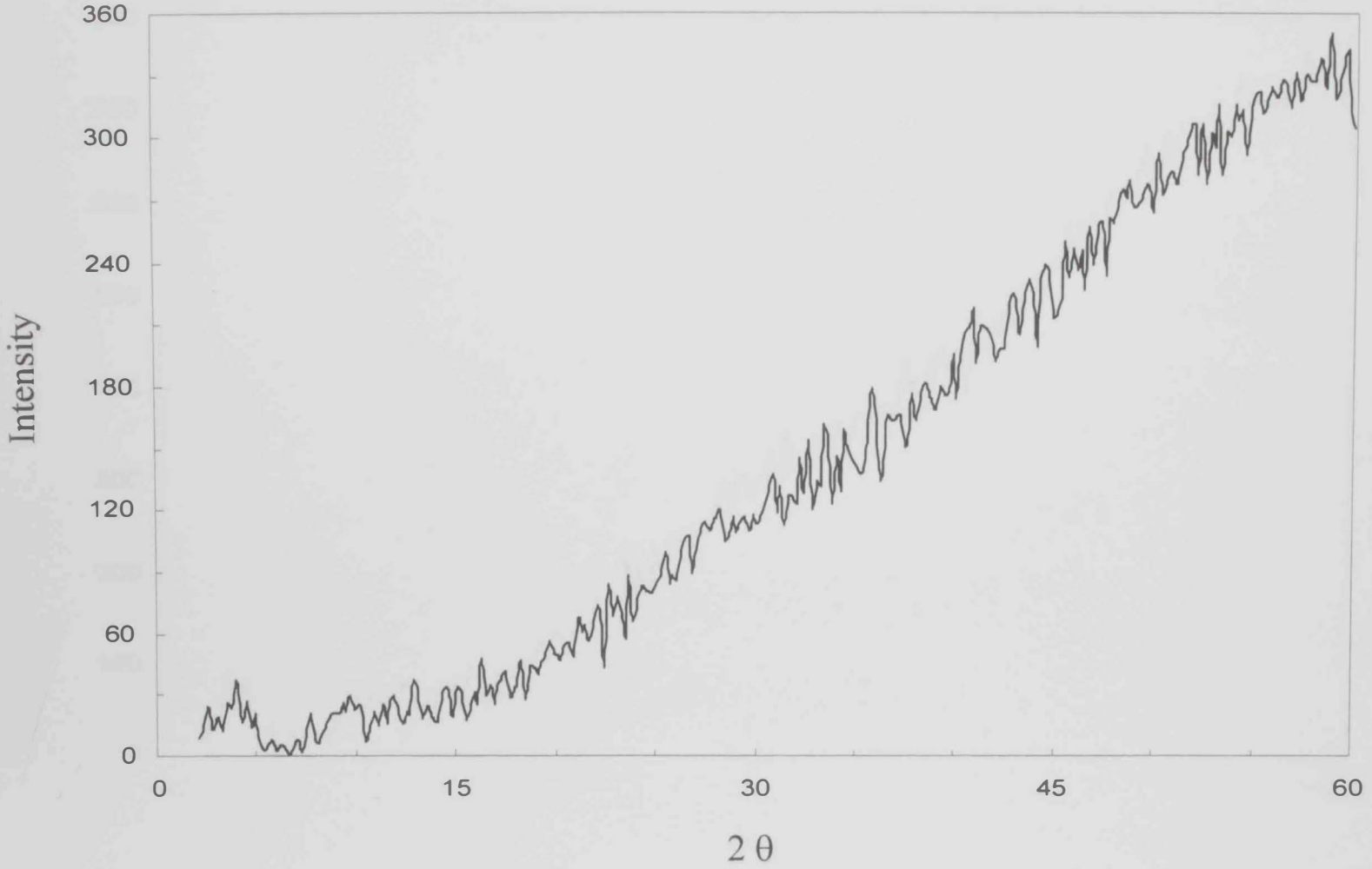

Fig. 3.7 X-ray diffraction pattern of Se_{70} Te_{24} Sb_6 glassy alloy.

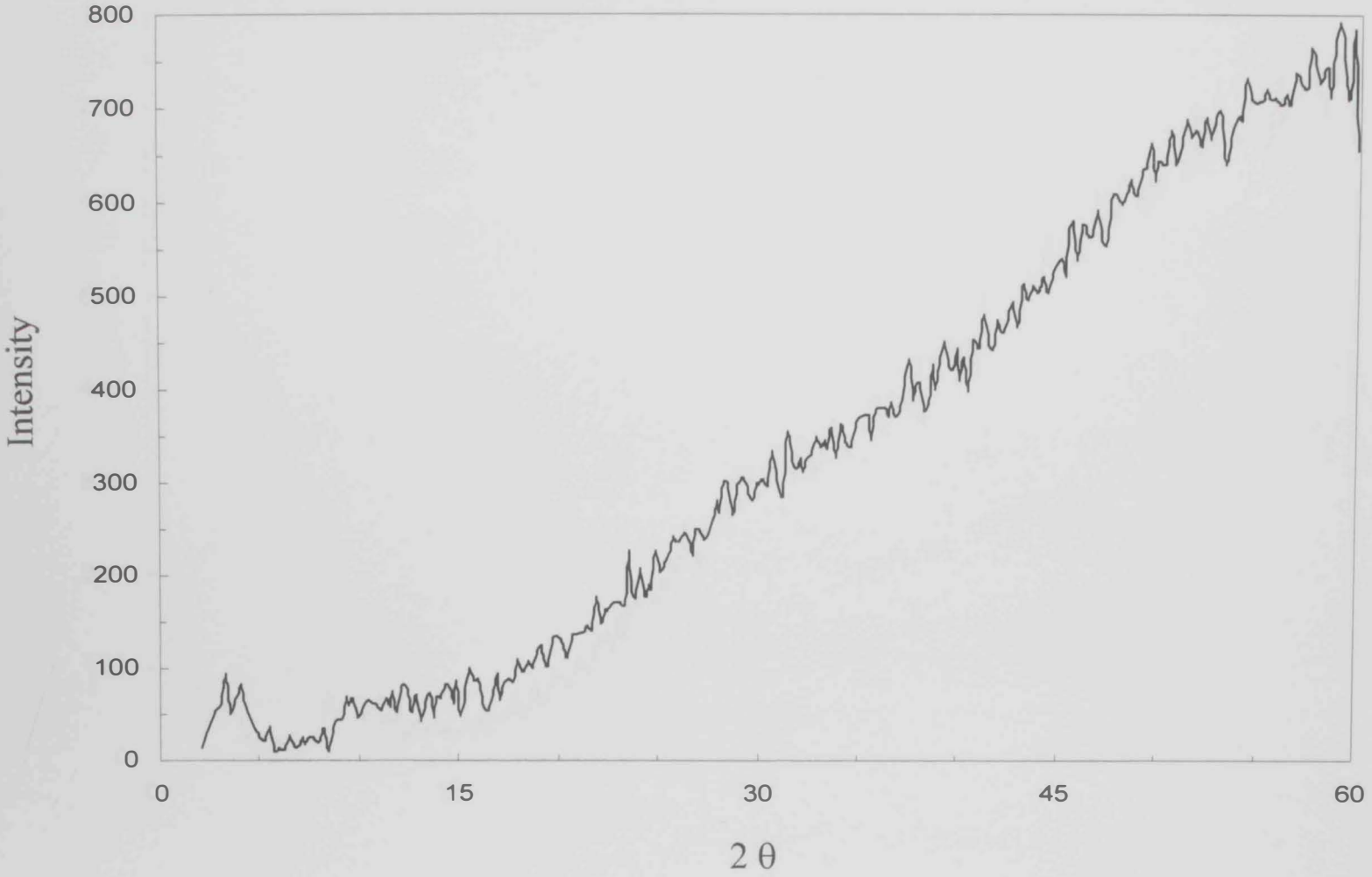

Fig. 3.8 X-ray diffraction pattern of Se_{70} Te_{22} Sb_8 glassy alloy.

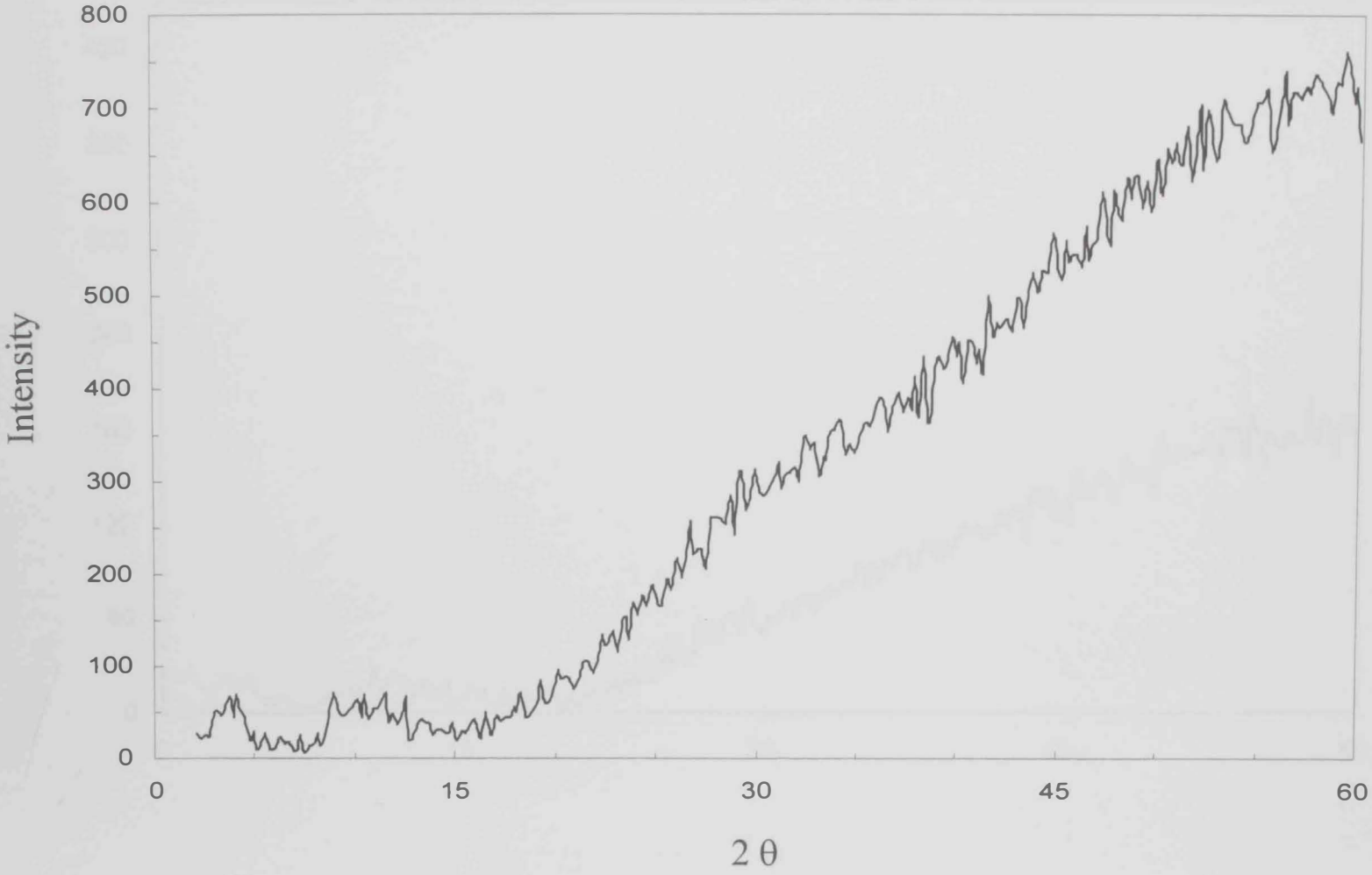

Fig. 3.9 X-ray diffraction pattern of Se_{70} Te_{20} Sb_{10} glassy alloy.

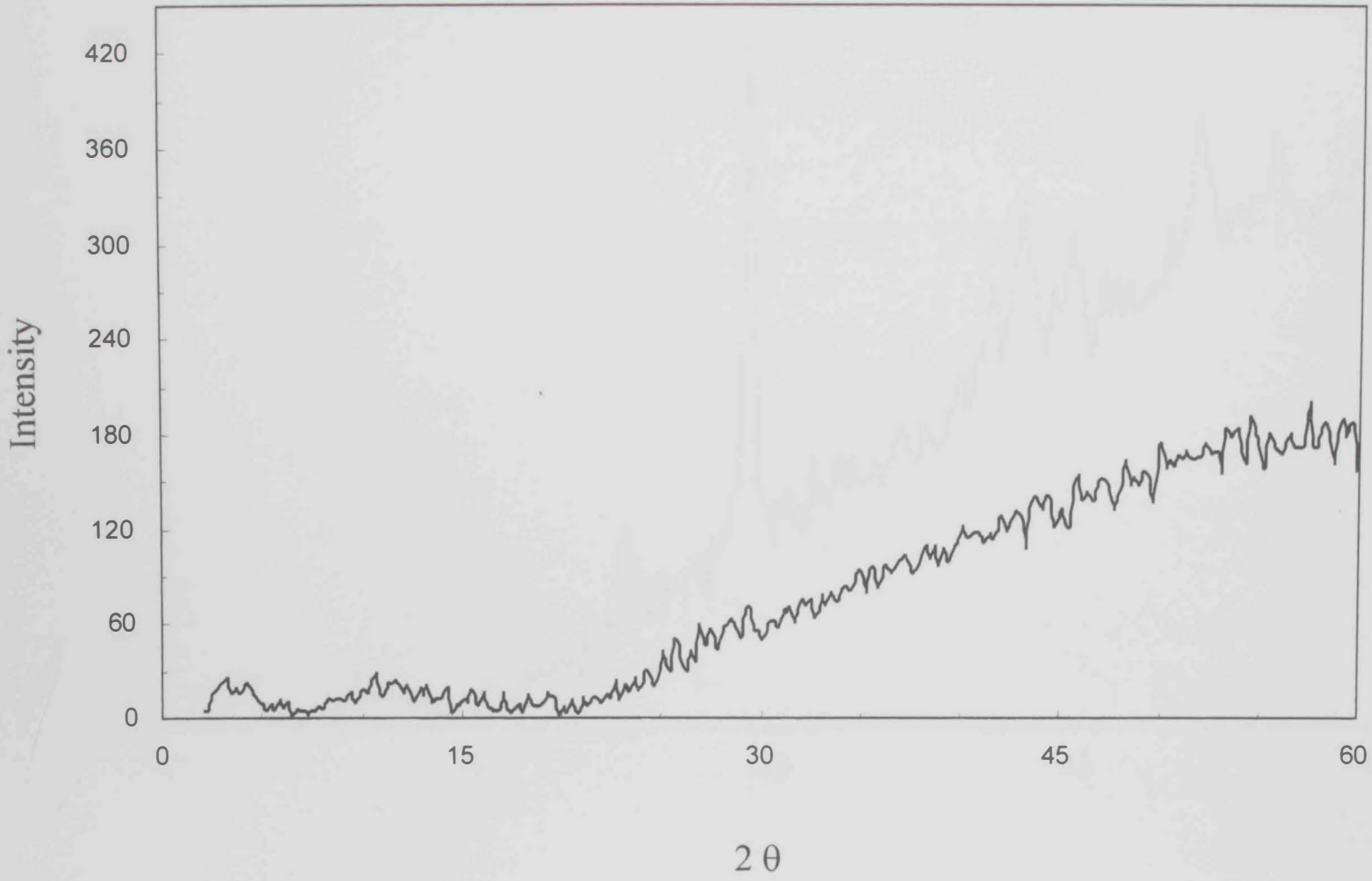

Fig. 3.10 X-ray diffraction pattern of $Se_{70}Te_{16}Cd_4$ glassy alloy.

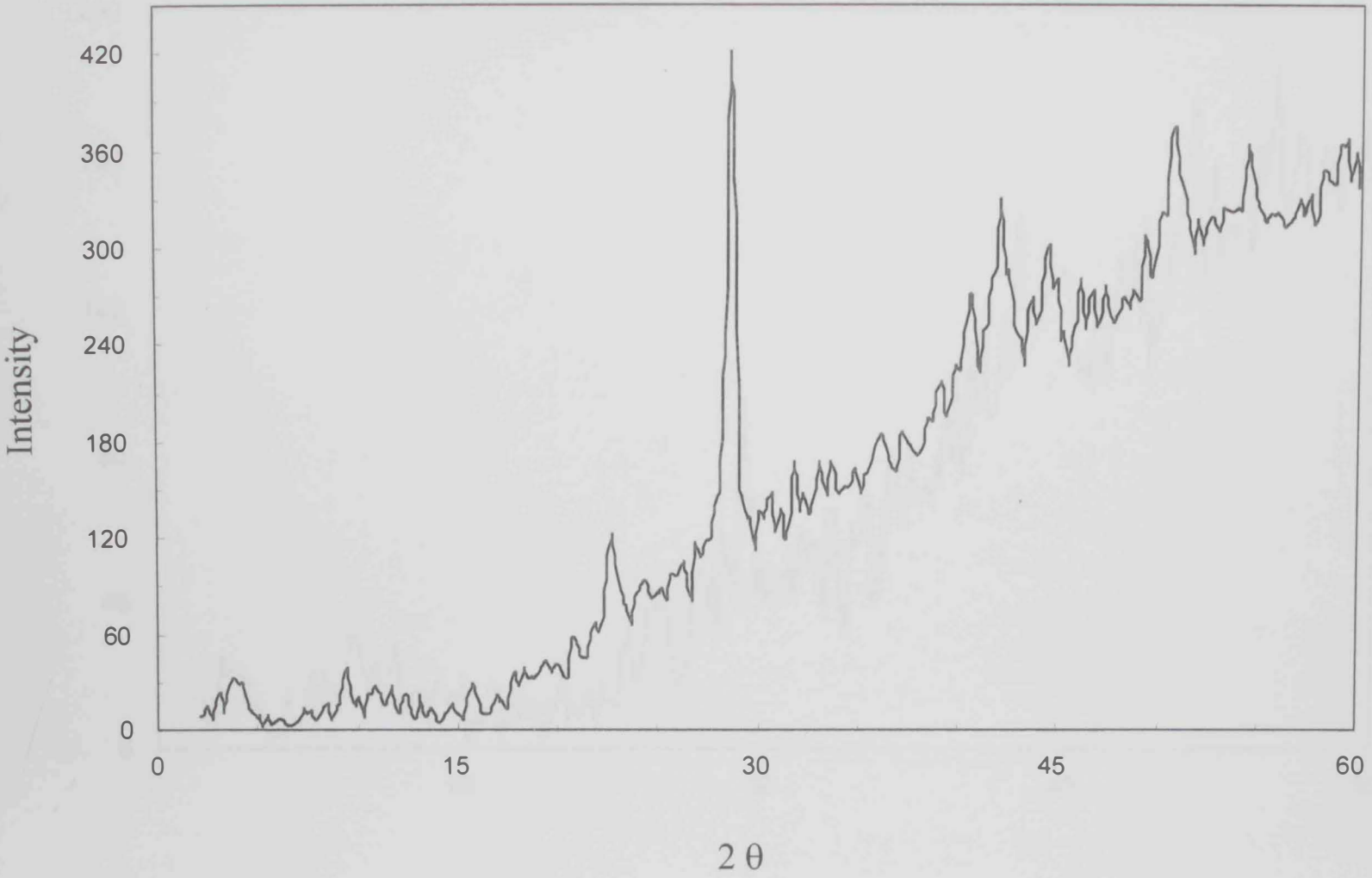

Fig. 3.11 X-ray diffraction pattern of $Se_{70}Te_{18}Cd_2$ glassy alloy.

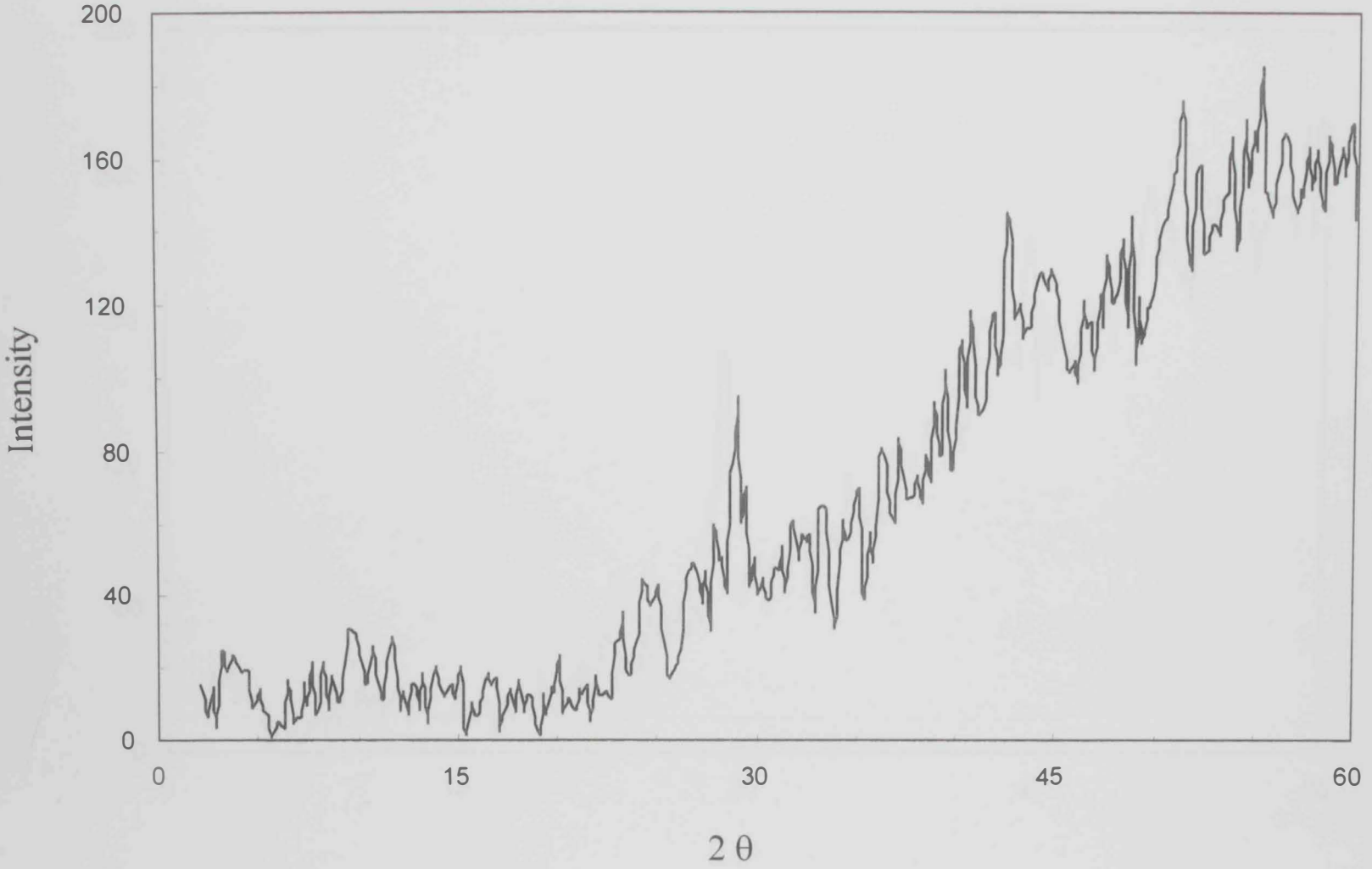

Fig. 3.12 X-ray diffraction pattern of $Se_{70}Te_{10}Cd_{10}$ glassy alloy.

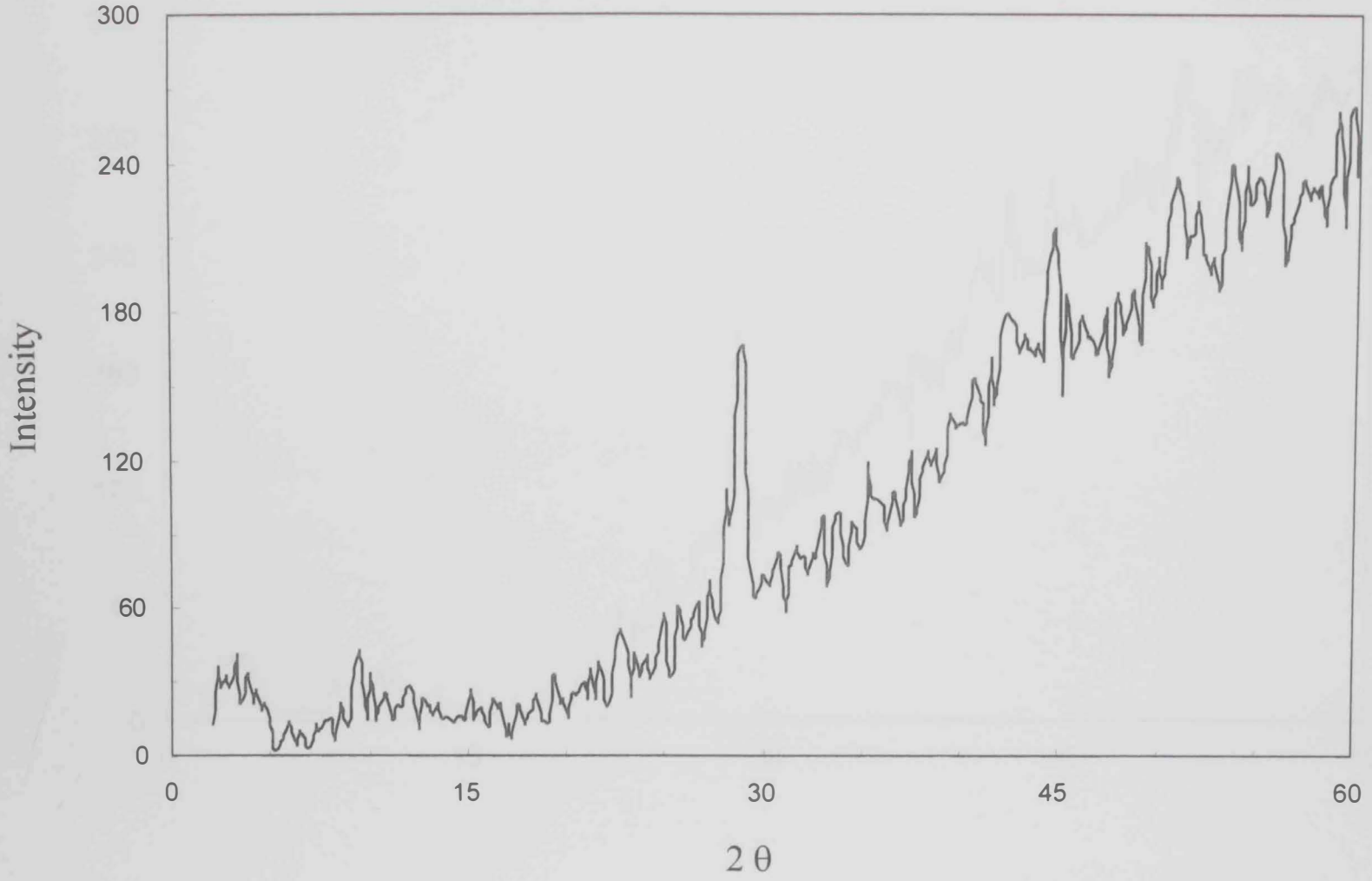

Fig. 3.13 X-ray diffraction pattern of $Se_{70}Te_{18}Sn_2$ glassy alloy.

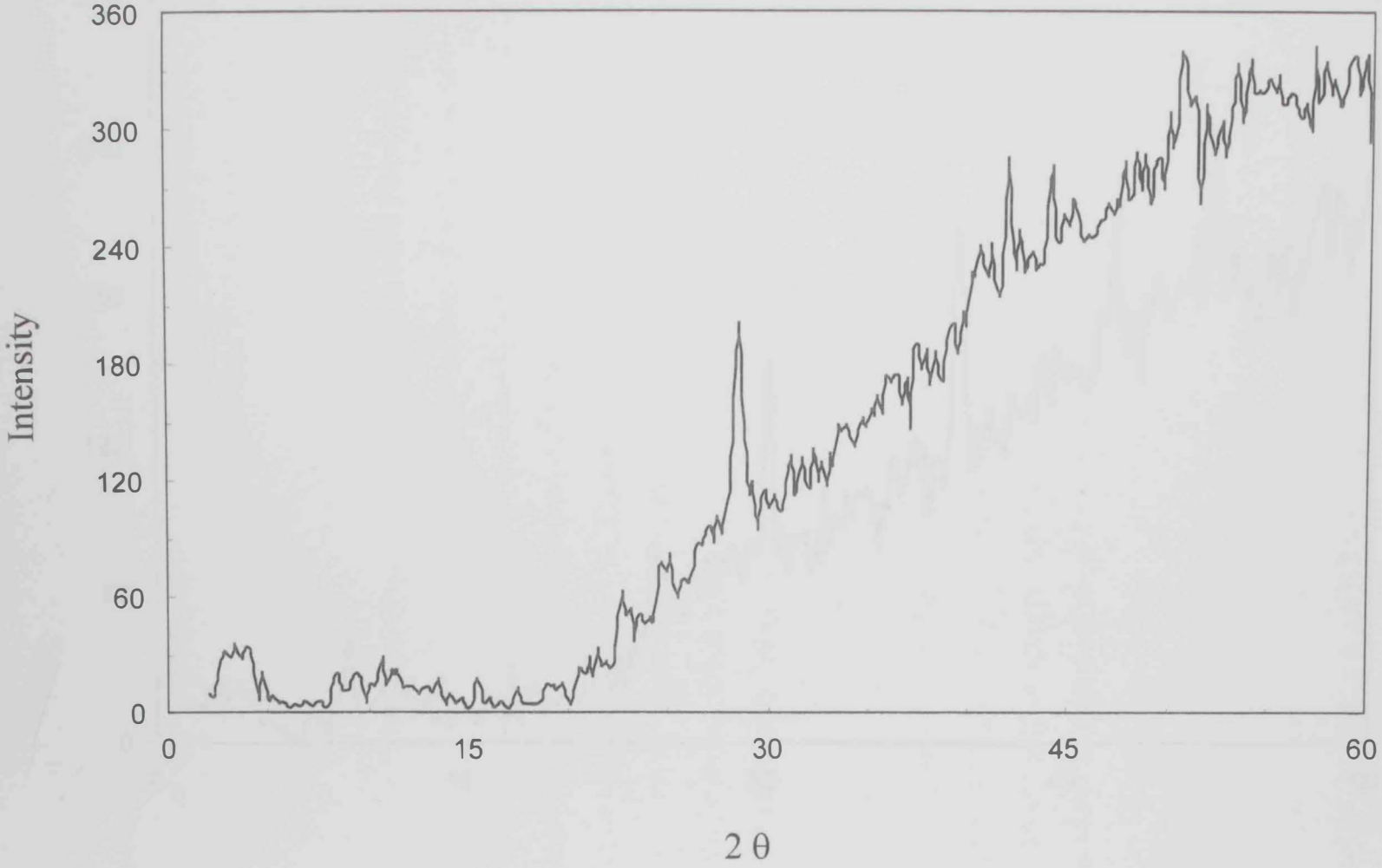

Fig. 3.14 X-ray diffraction pattern of $Se_{70}Te_{16}Sn_4$ glassy alloy.

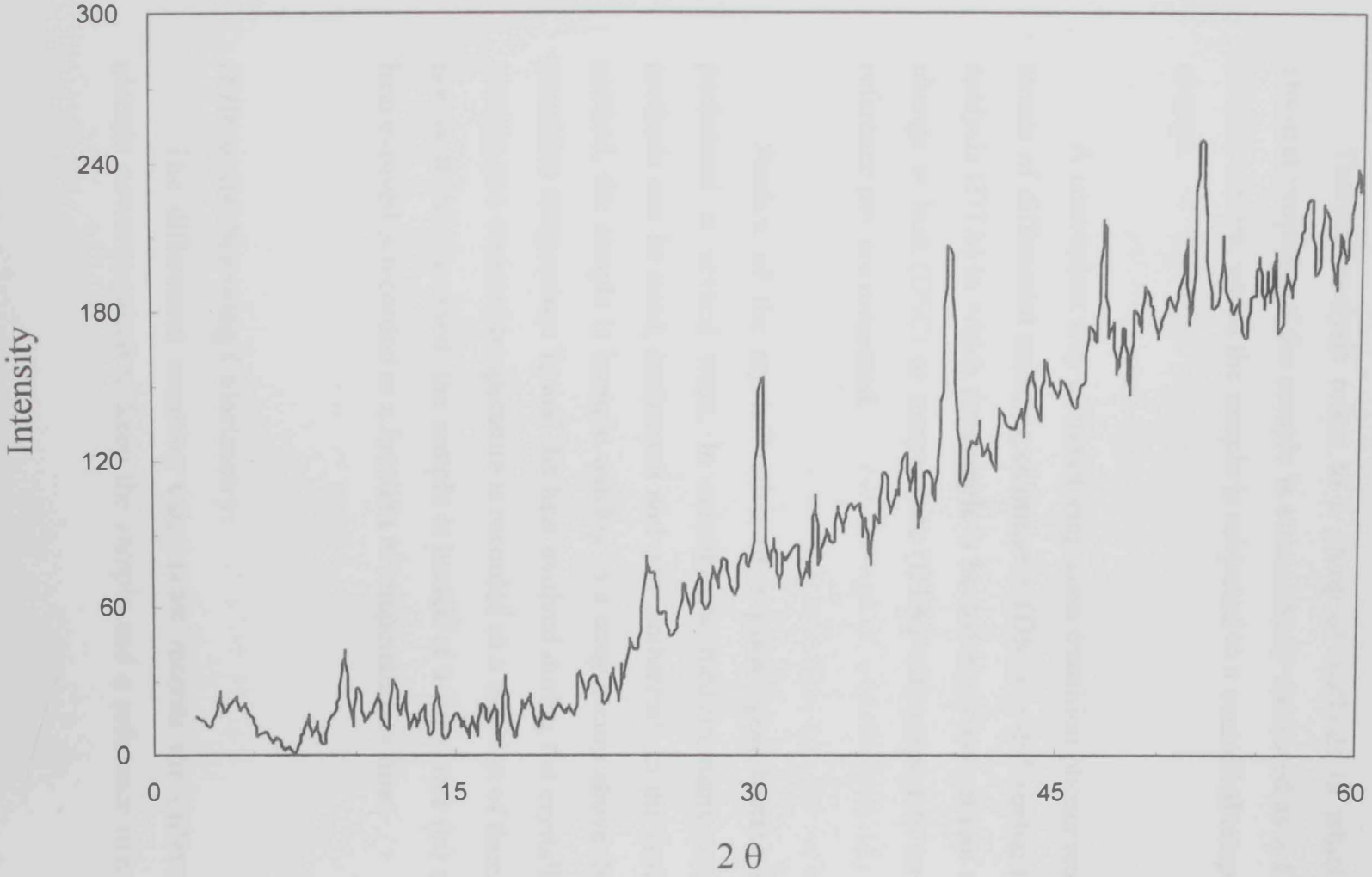

Fig. 3.15 X-ray diffraction pattern of $Se_{70}Te_{20}Sn_{10}$ glassy alloy.

calorimetry (DSC) provides quantitative thermodynamic and kinetic information about the physical and chemical changes occurring in the material.

Thermal analysis refers to a group of methods in which some physical property of the sample is continuously measured as a function of temperature, whilst the sample is subjected to a controlled temperature change.

A convenient way of monitoring glass transition phenomena is by means of differential scanning calorimetry (DSC) or differential thermal analysis (DTA) in which the sample is heated at a constant rate and the change in heat (DSC) or temperature (DTA) with respect to an empty reference pan are measured.

Studies of the crystallization of a glass upon heating can be performed in several ways. In calorimetric measurements two basic methods can be used; isothermal and non-isothermal. In the isothermal method, the sample is brought quickly to a temperature above the glass transition temperature T_g and the heat evolved during the crystallization process at a constant temperature is recorded as a function of time. In the non-isothermal method, the sample is heated at a fixed rate (α) and the heat evolved is recorded as a function of temperature or time.

Differential Scanning Calorimetry:

The differential scanning calorimeter records the difference in electric power required to keep the sample and a reference material at

equal temperatures as they are heated (or cooled) at a constant rate. The power difference shows up during physical or chemical transitions in the sample and is equivalent to the thermal energy absorbed or released during the transition.

The DSC instrument used in our measurements was (Perkin-Elmer DSC7). It consists of a thermocouple, sample and reference holders, control and evaluation units and a series of measuring units (recorder, amplifier, controller, etc.). Fig. 3.16 shows a block diagram of the system. The programmer of this instrument is capable of giving a wide range of heating rates from 1 °C/min to 200 °C/min. The recorder system incorporates and amplifies the signals from temperature (T) sensor and heat flow sensor. Theses signals were recorded on a twin pen recorder in typical ease. Also the recorder has a range of sensitivity setting and of chart speeds, so that peak width as well as height can be varied. The curve obtained was registered on x-y recorder. Also it was possible to save the data digitally and could be used later in (MS-Excel and MatLab) programs to plot it.

Samples in the form of powder weighing about 7 mg were sealed in aluminum crucibles and placed inside the sample holder. The sample was heated from room temperature up to 500 °C with different heating rates ranging from 5 K/min to 50 K/min. Nitrogen was used as a purge gas with a flow rate of about 100 ml/min.

The temperature and energy calibration of the instrument were performed using a well known melting temperature and melting enthalpy of high purity indium, as shown in Fig 3.17.

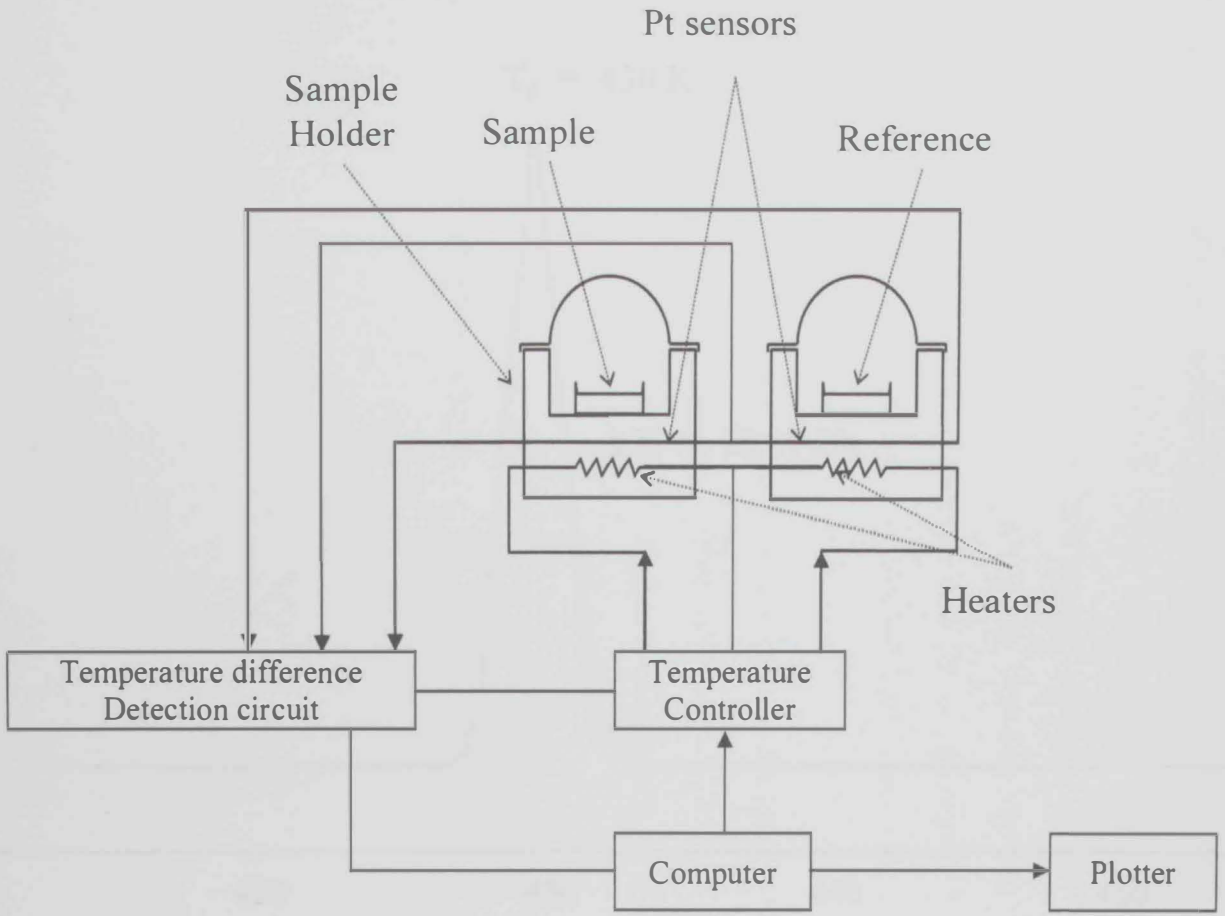

Fig. 3.16 Block diagram for the DSC instrument (T. Hatakeyama, et. al., 1999, Thermal Analysis Fundamentals and Applications to Polymer Science, John Wiley, second edition)

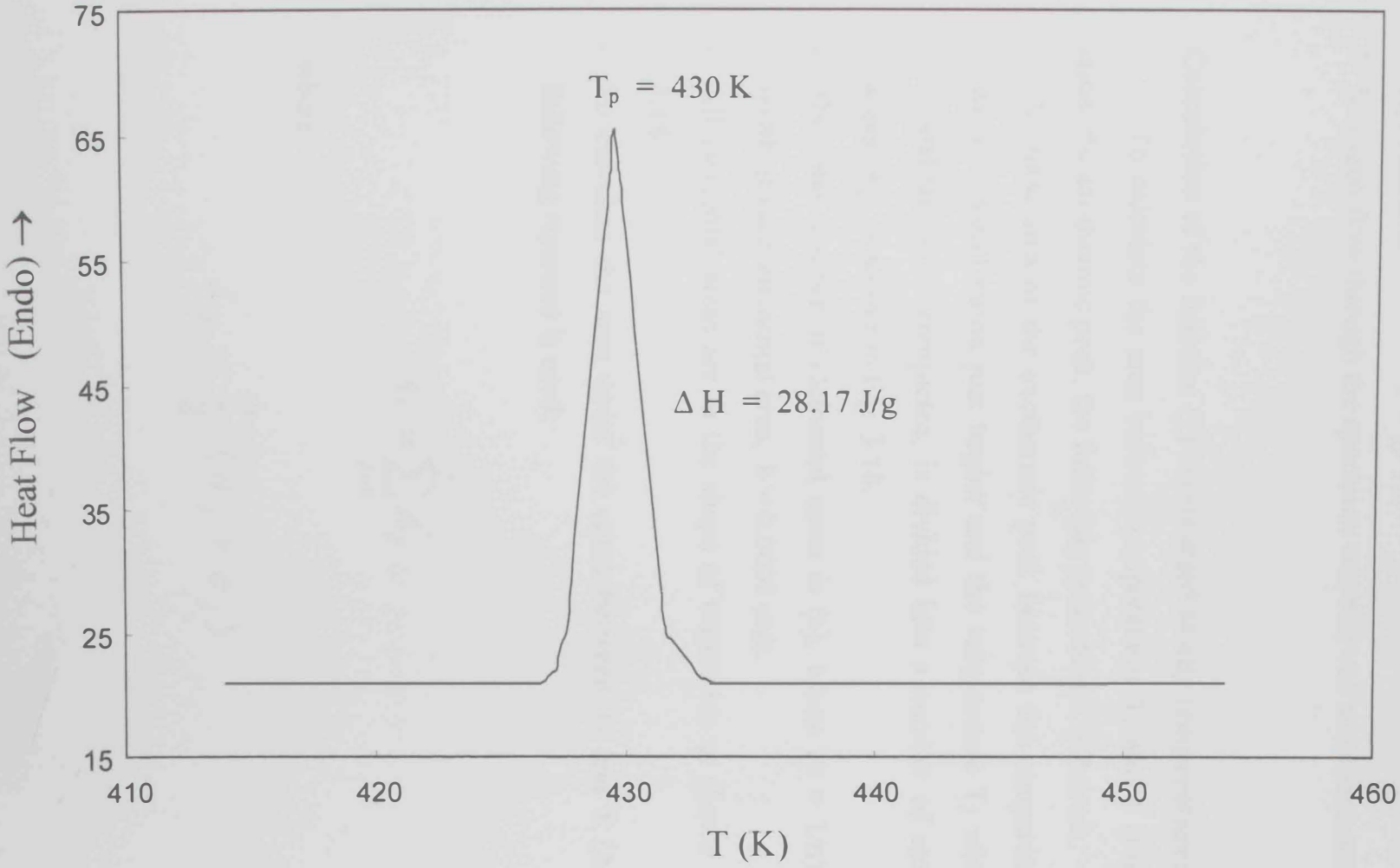

Fig 3.17 DSC diffraction pattern for Indium.

The following precautions were maintained in order to insure accurate results:

1- The heating rate was uniform over the whole temperature range and reproducible.

2- Nitrogen flow through the specimen was allowed at a constant rate.

Calculation of the fraction (χ) crystallized at any temperature:

To calculate the area between temperatures T_1 and T (Fig 3.18) under the exothermic peak, the following procedure is followed:

- The total area of the exothermic peak between the temperature T_1, where crystallization just begins and the temperature T_2 where the crystallization is completed, is divided into a number of elemental areas (A_j), as shown in Fig. 3.18.
- The total number of elemental areas is (n), where (b = 1/n) is the width of each elemental area, b = 0.0001 unit.
- All elemental areas are in the shape of trapezoids as shown in Fig. 3.18.
- To calculate the area under the curve between T_1 and T (A_T), the following equation is used:

$$A_T = \sum_{j=1}^{T} A_j \qquad (3.2)$$

where

$$A_j = \frac{b}{2}(a_j + c_j)$$

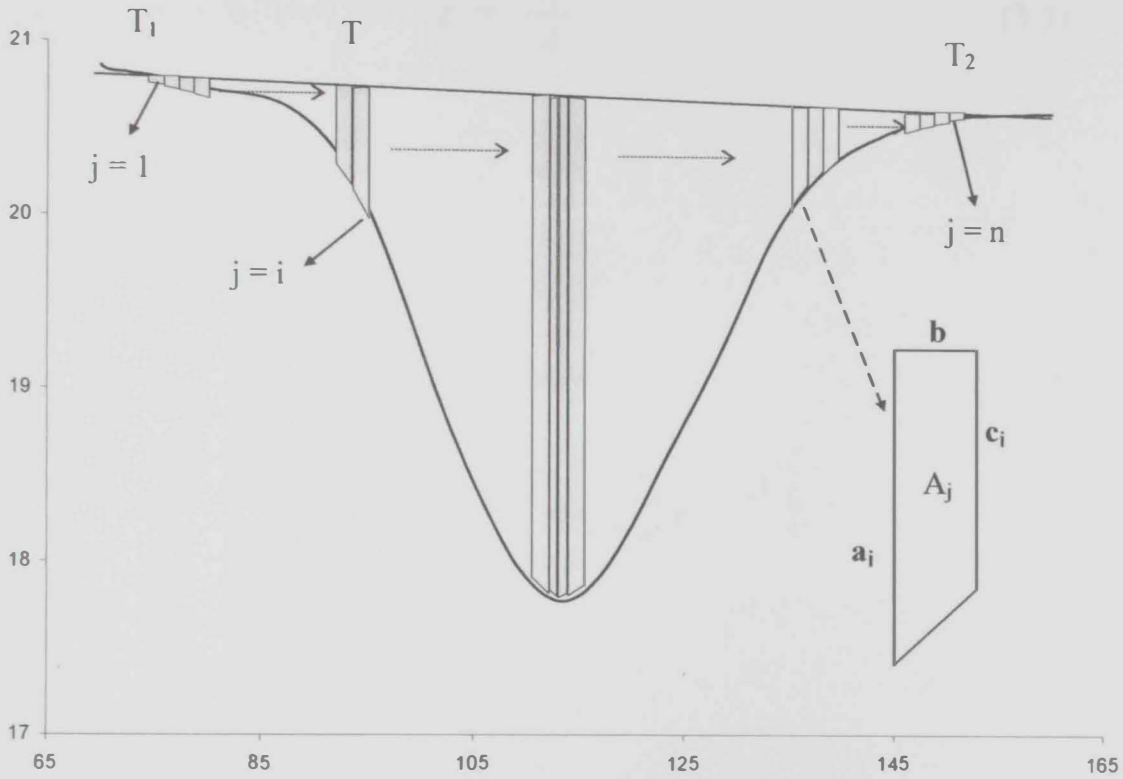

Fig. 3.18 Schematic diagram showing the method of discrete calculation of the area under the crystallization peak of DSC thermogram.

where b, a_j and c_j are as defined in Fig 3.18.

- The total area (A) is the summation of all elemental areas (A_j).
- The fraction (χ) crystallized at any temperature (i = T) is calculated from the following equation:

$$\chi = \frac{A_T}{A} \tag{3.3}$$

Chapter 4

Results and Discussion

The crystallization characteristics for glassy alloys in the Se-Te system were studied using a differential scanning calorimetric (DSC) measurements. The glassy alloys used for the present study are listed in Table 4.1. DSC thermograms of glassy systems have exhibited common features, which could be explained by considering (as an example) the DSC thermogram of $Se_{80}Te_{20}$ alloy that shows three characteristic features, in the temperature range of investigation (Fig. 4.1).

1- An endothermic peak corresponding to the glass transition temperature. This endothermic peak is usually observed in DSC curves as a result of a change in specific heat. Also the endothermic peak may be expected when the glassy spectrum relaxes quickly at the glass transition temperature due to a decrease in viscosity [45]. This peak is caused by a rapid increase in enthalpy due to structural relaxation.

2- An exothermic peak due to crystallization.

3- An endothermic peak due to melting or softening of the alloy.

Four characteristic transition temperatures are indicated in Fig. 4.1, which are typical for glass-crystalline transformation. These temperatures are:

1- The glass transition temperature (T_g), which is defined from the DSC thermograms as the temperature which corresponds to the point of intersection of the tangent lines of baseline of the onset temperature of the first endothermic peak.

	Alloy
System 1	Se_{80} Te_{20}
	Se_{80} Te_{16} Sb_4
	Se_{80} Te_{14} Sb_6
	Se_{80} Te_{12} Sb_8
	Se_{80} Te_{10} Sb_{10}
System 2	Se_{70} Te_{28} Sb_2
	Se_{70} Te_{24} Sb_6
	Se_{70} Te_{22} Sb_8
	Se_{70} Te_{20} Sb_{10}
	Se_{80} Te_{16} Cd_4

Table 4.1 Glassy alloys investigated in this study.

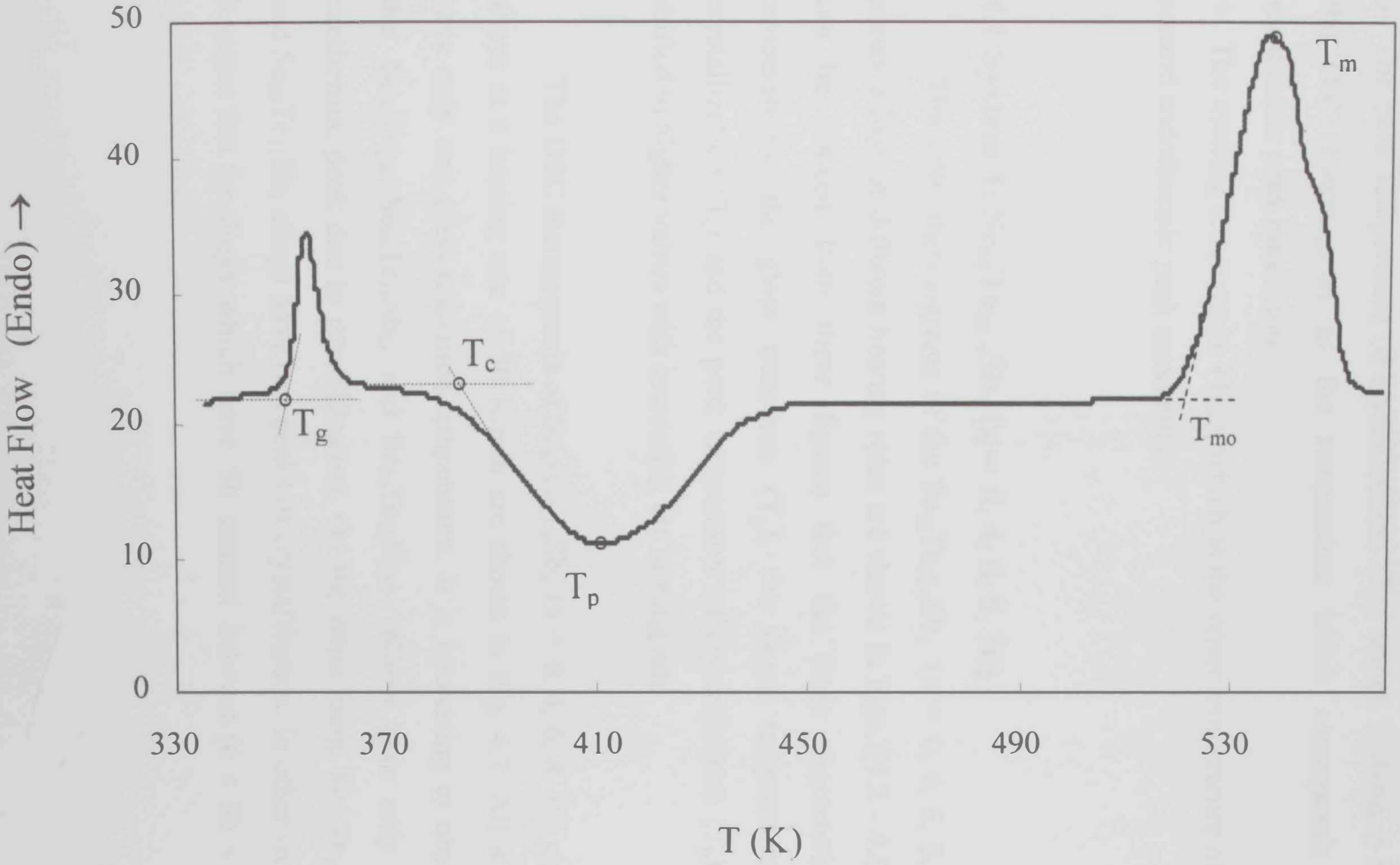

Fig. 4.1 Typical DSC thermogram for $Se_{80}Te_{20}$ at a heating rate of 50 K/min

2- The extrapolated onset crystallization temperature (T_c), which is defined from the DSC scan as the temperature which corresponds to the point of intersection of the tangent lines of the first side of the exothermic peak and the extrapolated base line.

3- The peak temperature of crystallization (T_p), which is defined from the DSC thermogram as the temperature which corresponds the exothermic peak maximum.

4- The melting temperature (T_{mo}), which is the onset temperature of the second endothermic peak maximum.

4.1 System 1: $Se_{80}Te_{20-x}Sb_x$ (x = 0, 4, 6, 8, 10)

The DSC thermograms of the $Se_{80}Te_{20-x}Sb_x$ (x = 0, 4, 6, 8, 10) glassy alloys at different heating rates are shown in Figs. (4.2 - 4.6). It can be noticed from these figures that the three characteristics temperatures; the glass transition (T_g), the onset temperature of crystallization (T_c) and the peak temperature of crystallization (T_p) are shifted to higher values with increasing the heating rate.

The DSC thermograms of $Se_{80}Te_{20-x}Sb_x$ (x = 0, 4, 6, 8, 10) glassy alloys at a heating rate of 30 K/min are shown in Fig. 4.7. All alloys have only one glass transition temperature. It is interesting to observe that $Se_{80}Te_{20}$, $Se_{80}Te_{16}Sb_4$, and $Se_{80}Te_{10}Sb_{10}$ alloys have only one exothermic peak due to crystallization. On the other hand, $Se_{80}Te_{14}Sb_6$ and $Se_{80}Te_{12}Sb_8$ alloys have two peaks of crystallization. In other words, it seems that for alloys which have Sb content between (4 < Sb < 10)

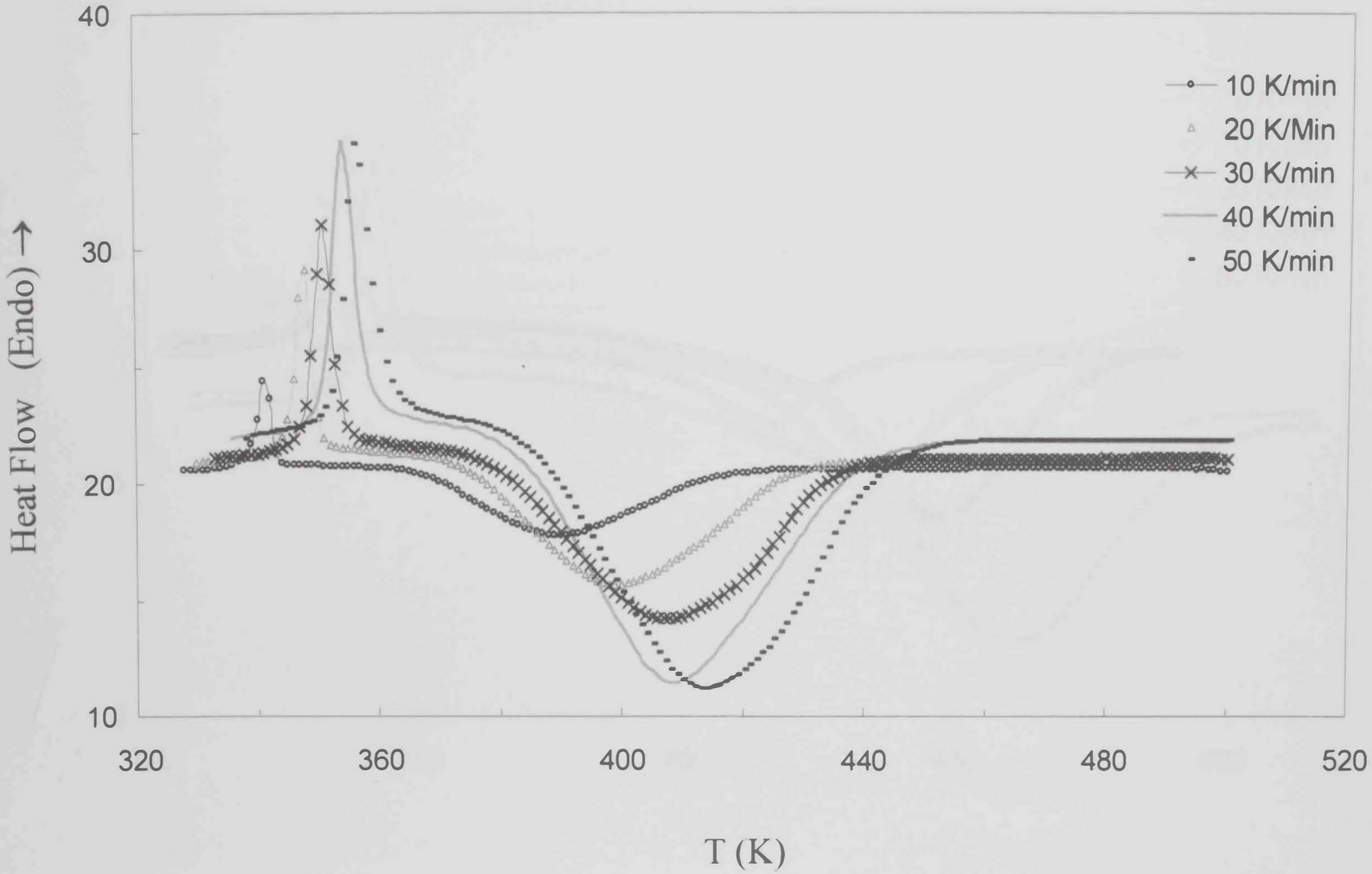

Fig. 4.2 DSC thermograrms for $Se_{80}Te_{20}$ glassy alloy at different heating rates.

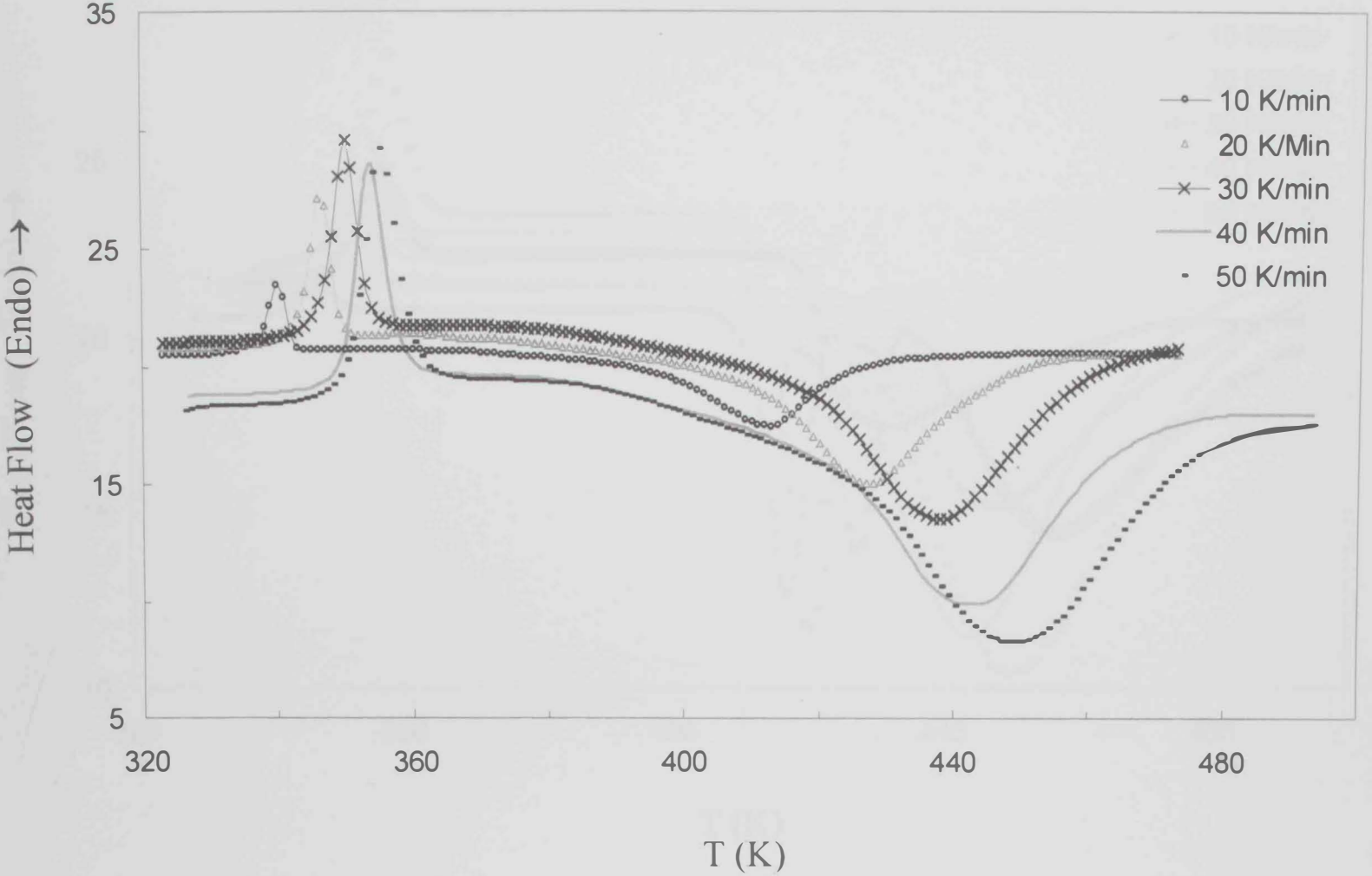

Fig. 4.3 DSC thermograrms for $Se_{80}Te_{16}Sb_4$ glassy alloy at different heating rates.

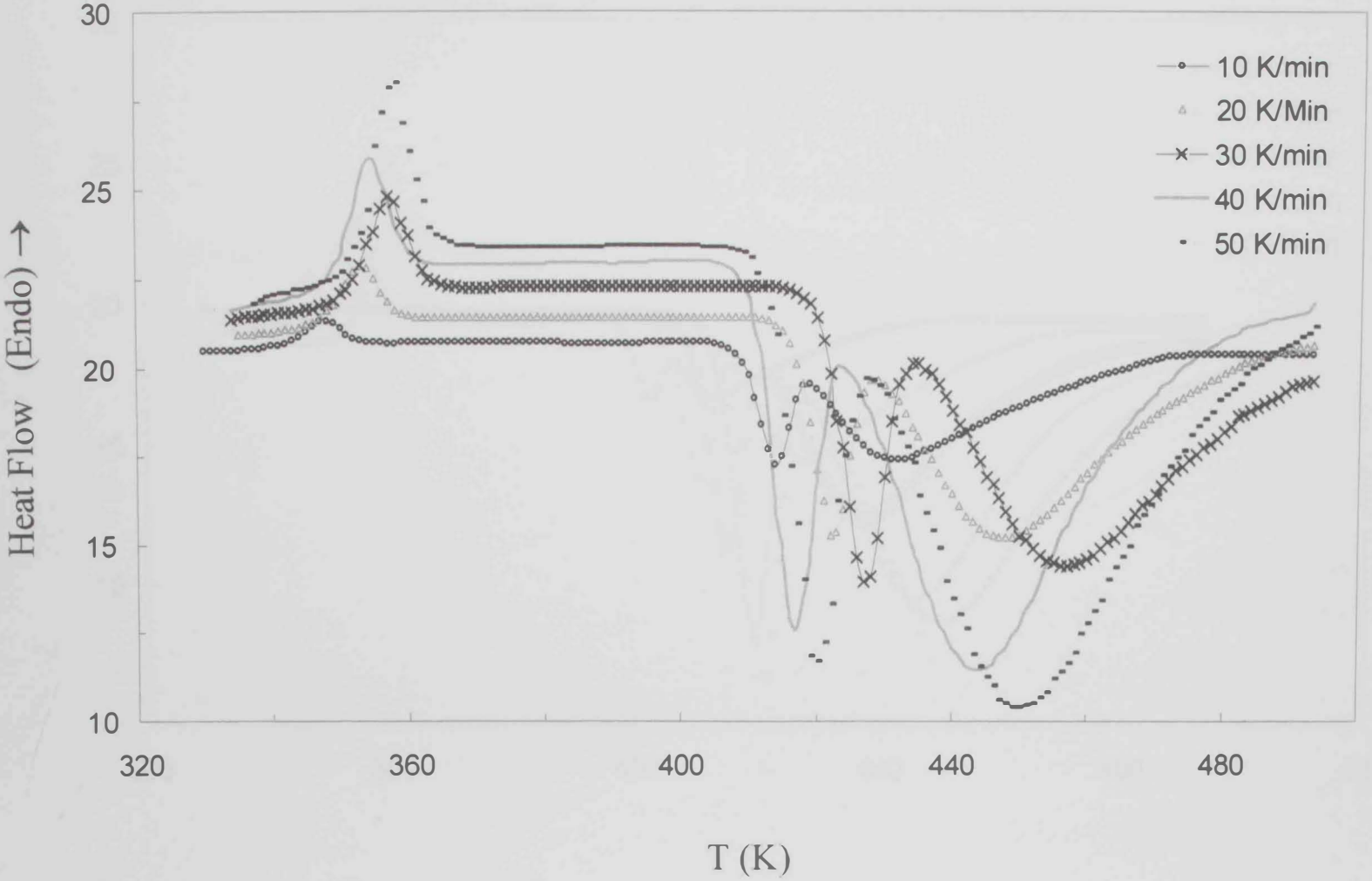

Fig. 4.4 DSC thermograrms for $Se_{80}Te_{14}Sb_6$ glassy alloyat different heating rates.

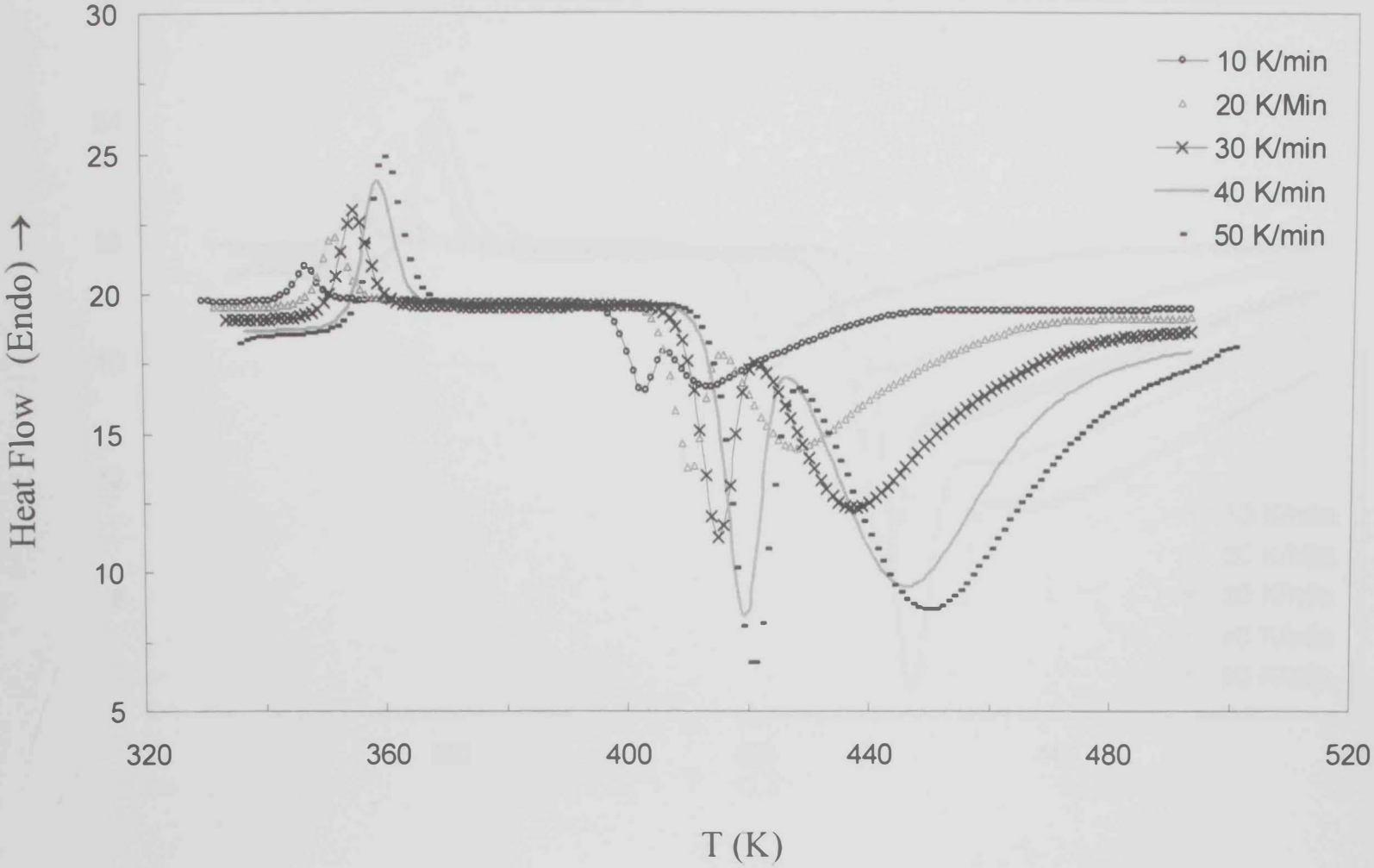

Fig. 4.5 DSC thermograrms for $Se_{80}Te_{12}Sb_8$ glassy alloy at different heating rates.

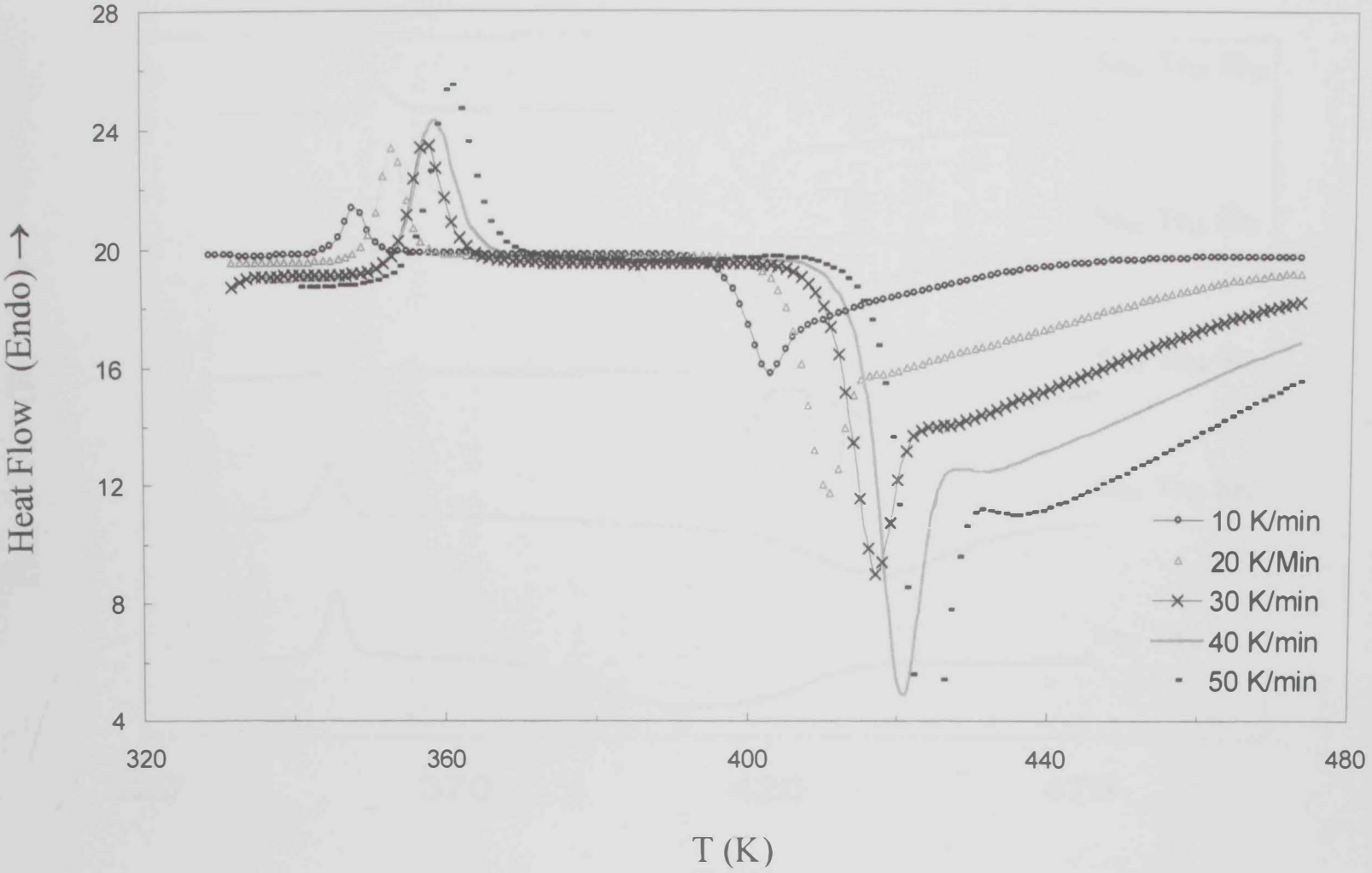

Fig. 4.6 DSC thermograrms for $Se_{80}Te_{10}Sb_{10}$ glassy alloy at different heating rates.

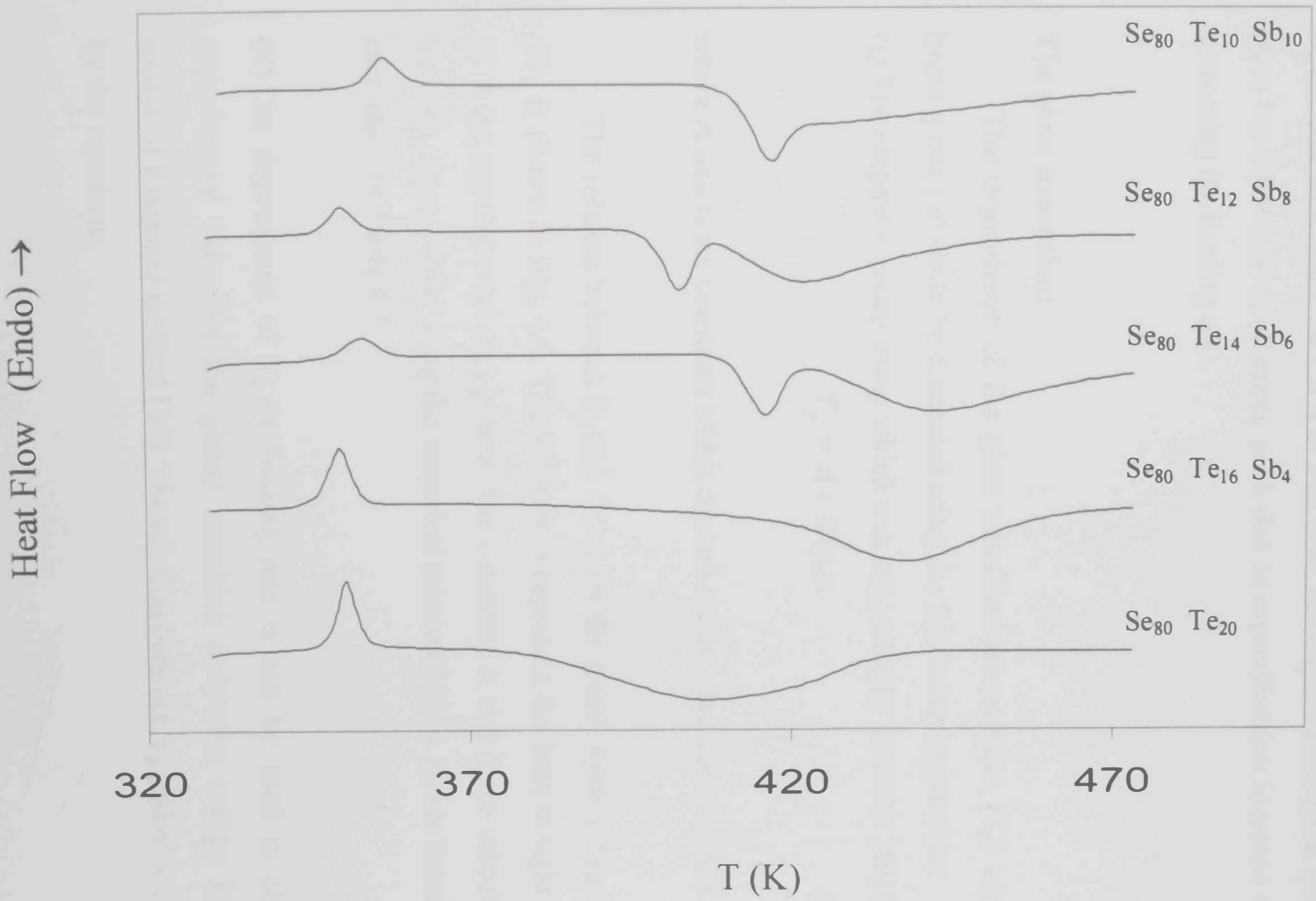

Fig.4.7 DSC thermograrms for $Se_{80}Te_{20-x}Sb_x$ glassy system at a heating rate of 30 K/min.

there are two peaks of crystallization. This is the case for all other heating rates as well. The existence of two peaks of crystallization may indicate that such an alloy has two glassy phases and crystallization takes place in these two phases. The existence of overlapping phases was observed in other chalcogenide glasses such as $Se_{60}Ge_{20}Sb_{20}$ [46]. It can be noticed from Figs. (4.2 – 4.6) that both the endothermic peak due to glass transition and exothermic peak due to crystallization increase with increasing the heating rate.

The glass transition:

The dependence of the glass transition temperature (T_g) on the heating rate (α) could be discussed using the following approaches:

(i) The empirical relationship which was suggested by Lasocke [40] is:

$$T_g = A + B \ln \alpha \qquad (4.1)$$

where A and B are constants which depend on the glass composition.

The relation between T_g and $\ln(\alpha)$ for the glassy system $Se_{80}Te_{20-x}Sb_x$ is shown in Fig. 4.8. The solid lines represent the best straight line fit to the experimental data points. The constants A and B are calculated for each glassy alloy, using the empirical relationship (4.1), are listed for each alloy in Table 4.2.

(ii) The dependence of T_g on heating rate α can be used to obtain experimental value for the glassy transition activation energy E_t by means of Kissinger method [38]. The relation between T_g and α is given by the equation:

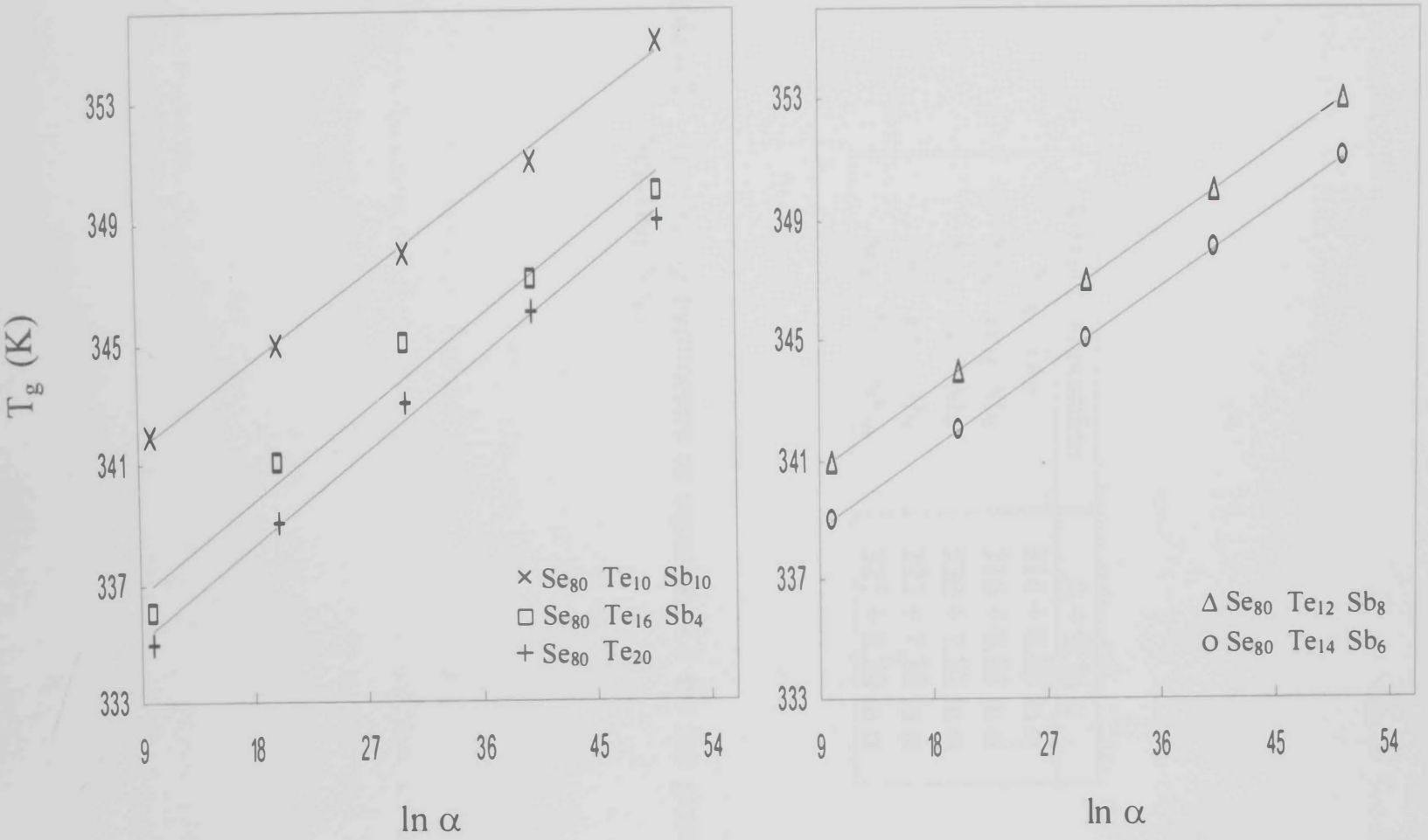

Fig. 4.8 T_g versus $\ln \alpha$ for $Se_{80}Te_{20-x}Sb_x$ glassy system.

Glass Composition	A + B ln α
Se_{80} Te_{20}	314 + 8.69 ln α
Se_{80} Te_{16} Sb_4	316 + 8.55 ln α
Se_{80} Te_{14} Sb_6	320 + 7.32 ln α
Se_{80} Te_{12} Sb_8	323 + 7.30 ln α
Se_{80} Te_{10} Sb_{10}	321 + 8.30 ln α

Table 4.2 The fitting parameters to equation 4.1 for the glassy system $Se_{80}Te_{20-x}Sb_x$.

$$ln\left(\frac{\alpha}{T_g^2}\right) = -\frac{E_t}{RT_g} + Constant \qquad (4.2)$$

where R is the gas constant. Although originally derived for the crystallization process, it was suggested that the expression is valid in a very general case [43] and has been often used to calculate E_t [41, 42, 44].

The variation of $\ln(\alpha/T_g^2)$ with $(1/T_g)$ is shown in Fig. 4.9 for the glassy system $Se_{80}Te_{20-x}Sb_x$. The solid lines represent the best straight lines fit to the experimental data points. The activation energy for the glass transition (E_t) was calculated from the slope of each line.

(iii) Mahadevan et.al. approximation [30] could be used. The variation of $\ln(1/T_g^2)$ with $\ln\alpha$ is considered to be less than that of $(1/T_g)$ with $\ln\alpha$. Therefore eq. (4.2) could be approximated by

$$ln(\alpha) = -\frac{E_t}{RT_g} + Constant \qquad (4.3)$$

The variation of $\ln\alpha$ with $(1/T_g)$ is shown in Fig. 4.10 for the glassy system $Se_{80}Te_{20-x}Sb_x$. The best fitting straight lines are also shown, where the activation energy for the glass transition was calculated from the slope. The values of E_t calculated from the slope of Fig. 4.9 and Fig. 4.10 are listed in Table 4.3. It is clear that the two deduced values of E_t for each alloy are in good agreement with each other. This implies that either eq.(4.2) or eq.(4.3) could be used to calculate the glass transition activation energy. The average value of E_t is also listed in Table 4.3 for each glassy alloy. It could be observed from

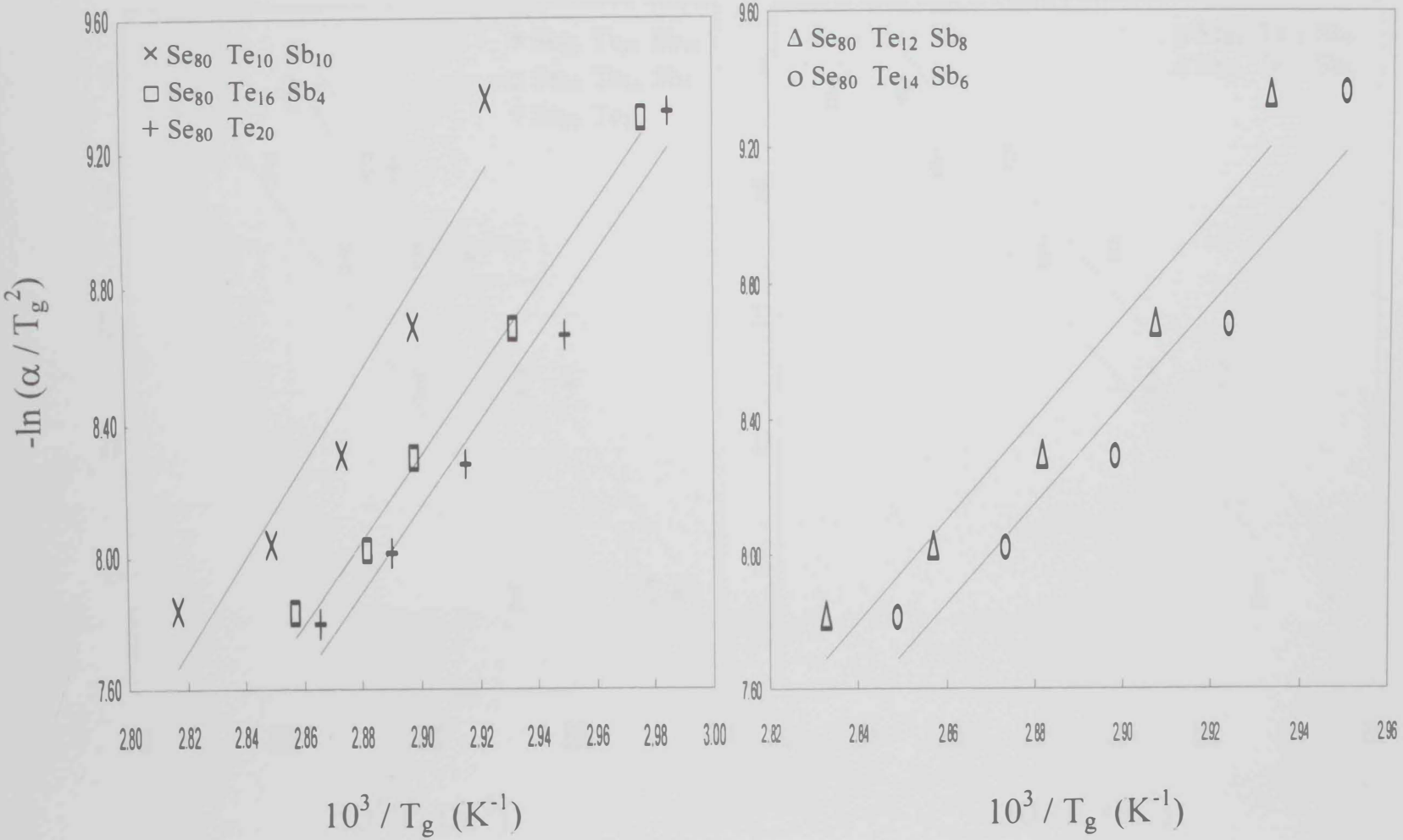

Fig 4.9 $-\ln(\alpha/T_g^2)$ versus $(10^3/T_g)$ for $Se_{80}Te_{20-x}Sb_x$ glassy system.

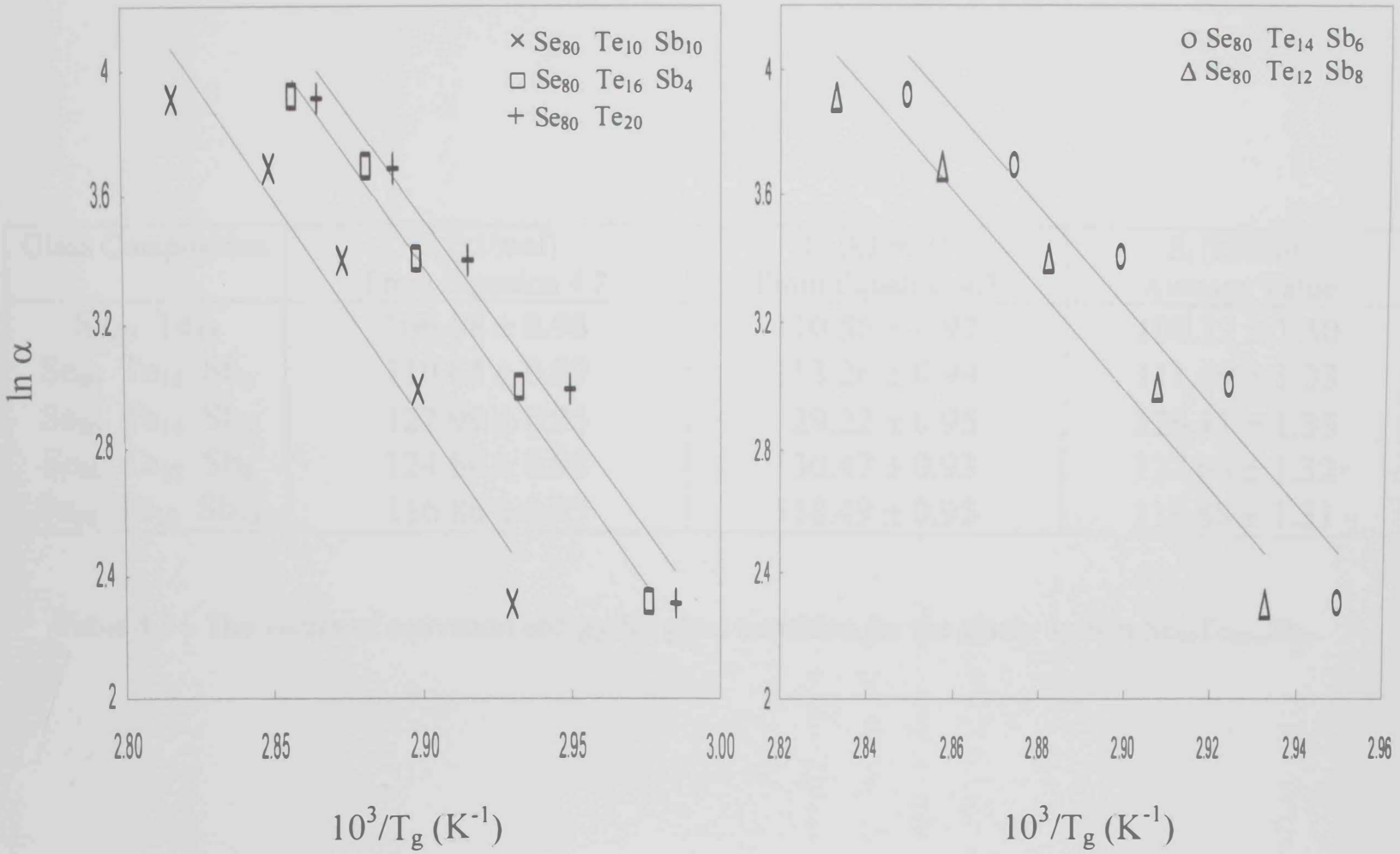

Fig 4.10 ln α versus $(10^3/T_g)$ for $Se_{80}\ Te_{20-x}\ Sb_x$ glassy system.

Glass Composition	E_t (kJ/mol) From Equation 4.2	E_t (kJ/mol) From Equation 4.3	E_t (kJ/mol) Average Value
Se_{80} Te_{20}	106.68 ± 0.98	110.56 ± 0.97	108.12 ± 1.30
Se_{80} Te_{16} Sb_4	110.64 ± 0.99	113.26 ± 0.99	111.69 ± 1.33
Se_{80} Te_{14} Sb_6	122.99 ± 0.95	129.22 ± 0.95	126.11 ± 1.35
Se_{80} Te_{12} Sb_8	124.80 ± 0.98	130.47 ± 0.93	127.68 ± 1.32
Se_{80} Te_{10} Sb_{10}	116.86 ± 0.93	118.49 ± 0.95	118.88 ± 1.31

Table 4.3 The values of activation energy for glass transition for the glassy system $Se_{80}Te_{20-x}Sb_x$.

this table that increasing Sb content results in increasing the value of the activation energy of glass transition up to 8 at.% of Sb. When Sb content is increased to 10 at.%, E_c decreases.

It is interesting to observe the effect of Sb on the glass transition temperature for the glassy system $Se_{80}Te_{20-x}Sb_x$. This behavior is represented in Fig. 4.11. Increasing Sb content results in a linear increase of the glass transition temperature.

Crystallization kinetics:

The dependence of the crystallization temperature (T_c) on the heating rate (α) could be discussed by using the following approaches:
(i) Kissinger formula [38], where it has been shown that for homogenous crystallization with spherical nucleation, the dependence of T_c and α is given by the following relation [42]:

$$ln\left(\frac{\alpha}{T_c^2}\right) = -\frac{E_c}{RT_c} + Constant \qquad (4.4)$$

where E_c is the activation energy for crystallization.

(ii) Mahadevan et.al. [30] have indicated that eq.(4.4) could be approximated by

$$ln(\alpha) = -\frac{E_c}{RT_c} + Constant \qquad (4.5)$$

since the variation of $(1/T_c^2)$ with $(\ln \alpha)$ is considered to be less than that of $1/T_c$ with $\ln \alpha$.

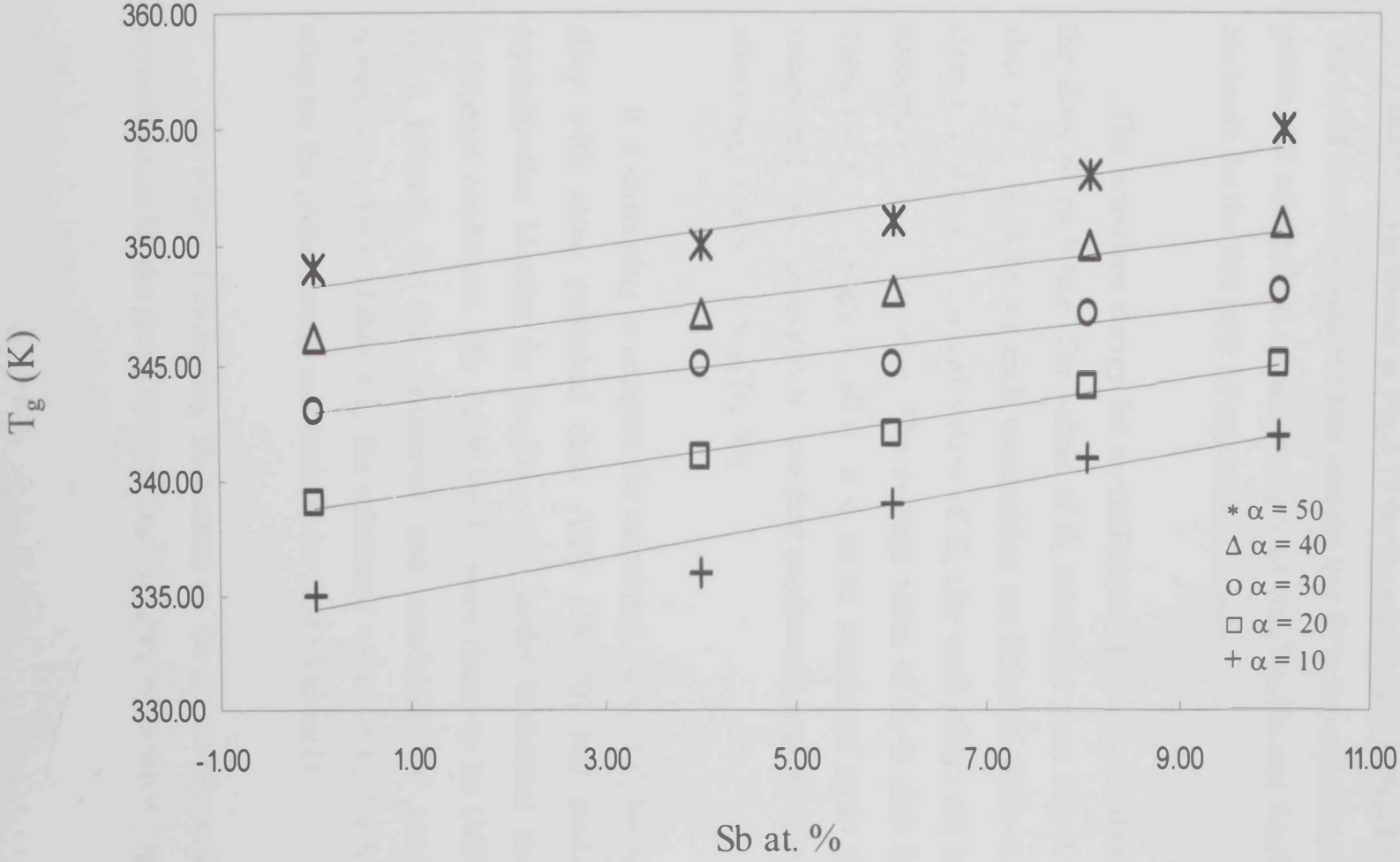

Fig. 4.11 Glass transition temperature as a function of Sb content for $Se_{80}Te_{20-x}Sb_x$ glassy system at different heating rates.

Equations (4.4) and (4.5) have been used by several authors [30, 47, 48] to calculate the activation energy of crystallization E_c. The relations 4.4 and 4.5 are represented in Figs. 4.12 and 4.13. The relation between $\ln(\alpha/T_c^2)$ and $(1/T_c)$ is shown in Fig. 4.12, while that between $\ln(\alpha)$ and $(1/T_c)$ is shown in Fig.4.13 for the glassy system $Se_{80}Te_{20-x}Sb_x$. The solid lines represent the best straight line fit to the experimental data points. All calculations for the glassy alloy $Se_{80}Te_{14}Sb_6$ and $Se_{80}Te_{12}Sb_8$ are made for the first peak of crystallization only.

The activation energy for crystallization (E_c) was calculated from the slope of each line. The values of E_c calculated from Fig. 4.12 and also from Fig. 4.13 for each composition are listed in Table 4.4. It is clear that the two deduced values of E_c (for each alloy) are in good agreement with each other. The average value of E_c is also listed in Table 4.4 for each glassy alloy. It is to be mentioned again that the values of E_c are calculated for the first exothermic peak for the glassy alloys $Se_{80}Te_{14}Sb_6$ and $Se_{80}Te_{12}Sb_8$.

It is interesting to compare the calculated value of E_c for $Se_{80}Te_{20}$ alloy with some published data. Afify [49, 50] had studied the crystallization kinetics for $Se_{80}Te_{20}$ alloy under isothermal and non-isothermal conditions. His value for E_c were found to be (160.8 and 123.5 kJ/mol) for the isothermal and non-isothermal conditions, respectively. From Table 4.3, the calculated value of E_c for $Se_{80}Te_{20}$ alloy for the present study was found to be (154.65 kJ/mol).

The effect of increasing Sb content on the on-set temperature of crystallization for the glassy system $Se_{80}Te_{20-x}Sb_x$ is shown in Fig. 4.14.

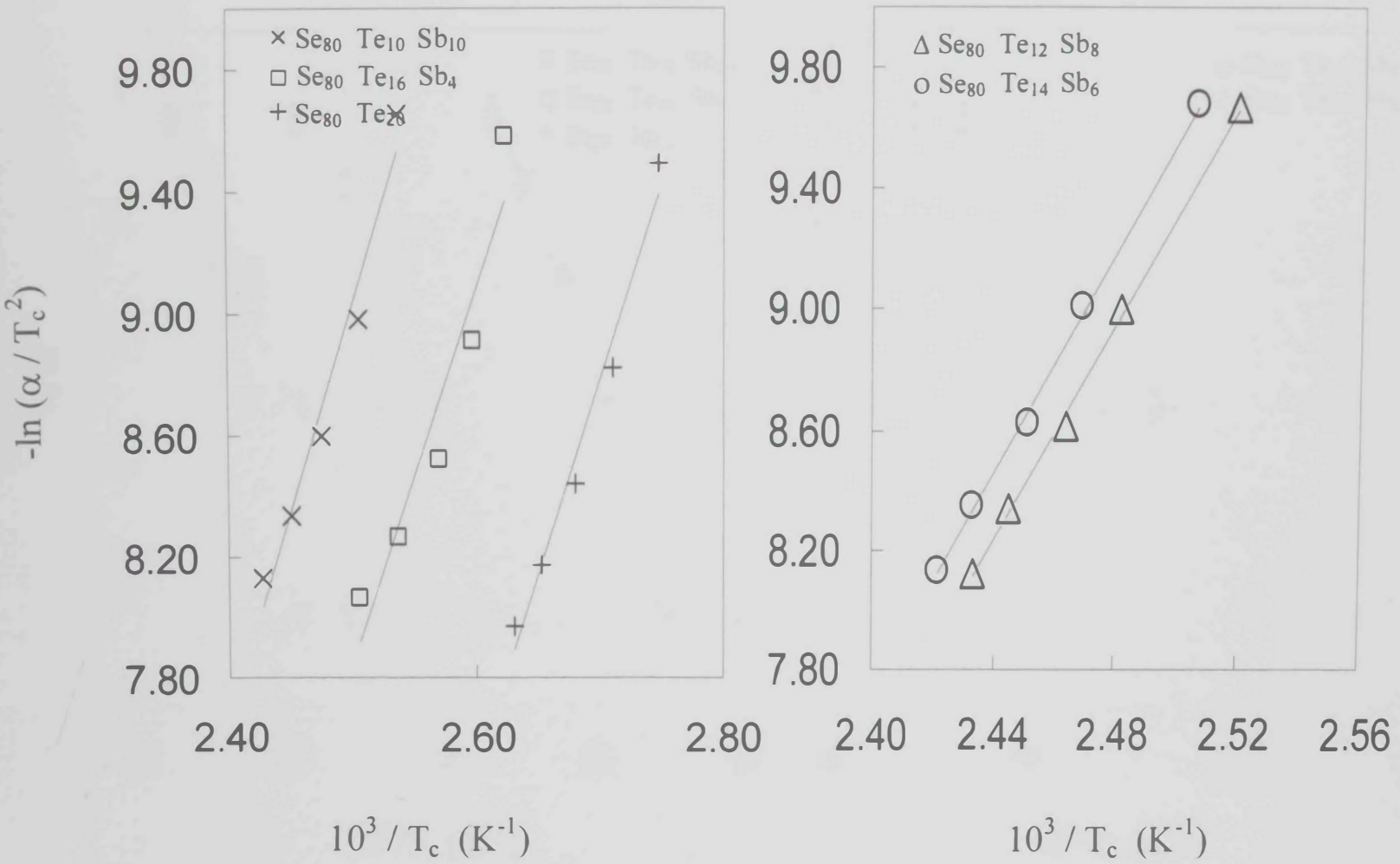

Fig 4.12 $-\ln(\alpha/T_c^2)$ versus $(10^3/T_c)$ for $Se_{80}Te_{20-x}Sb_x$ glassy system.

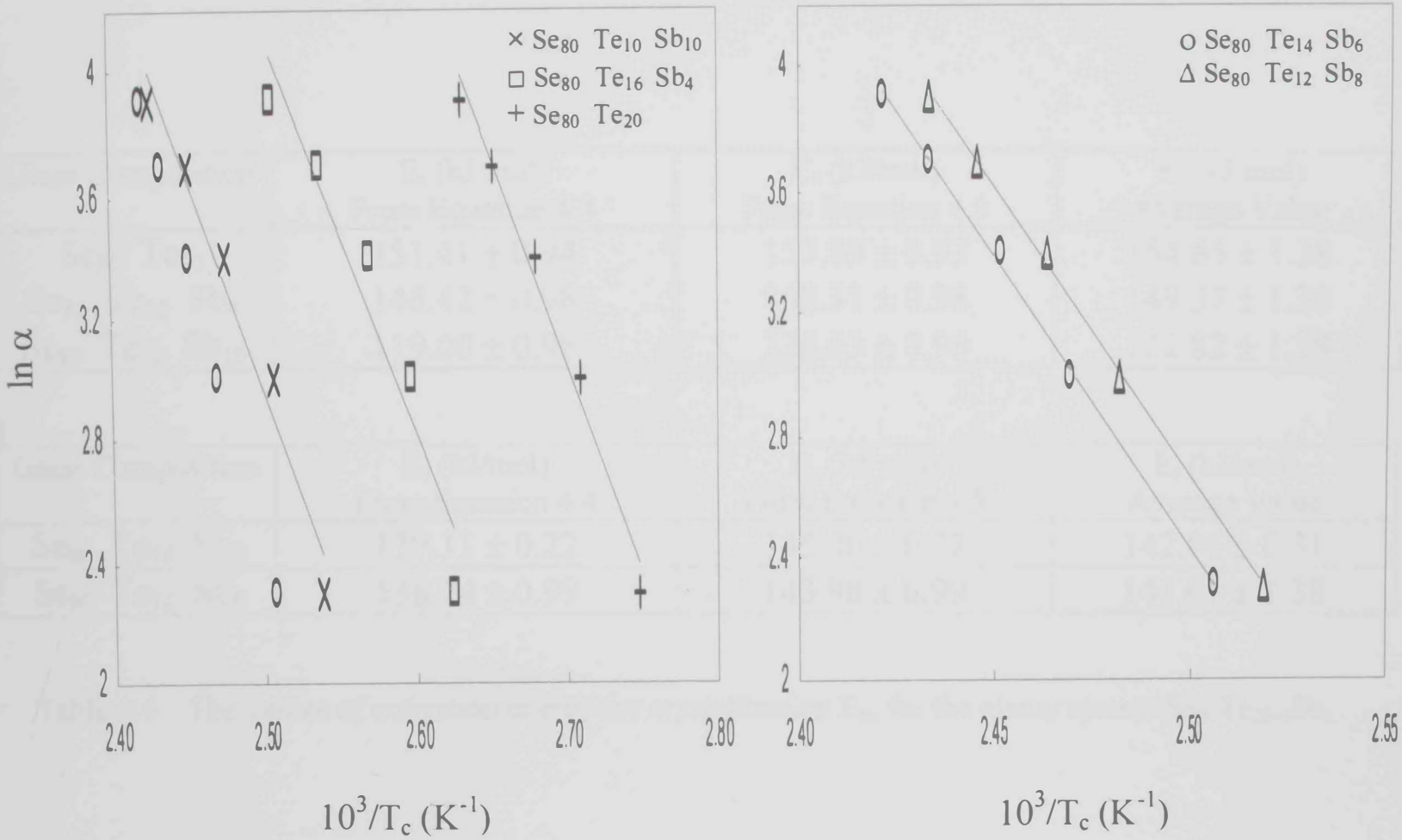

Fig 4.13 $\ln\alpha$ versus $(10^3/T_c)$ for $Se_{80}Te_{20-x}Sb_x$ glassy system.

a)

Glass Composition	E_c (kJ/mol) From Equation 4.4	E_c (kJ/mol) From Equation 4.5	E_c (kJ/mol) Average Value
Se_{80} Te_{20}	151.41 ± 0.94	157.89 ± 0.93	154.65 ± 1.38
Se_{80} Te_{16} Sb_4	146.42 ± 0.98	152.31 ± 0.98	149.37 ± 1.38
Se_{80} Te_{10} Sb_{10}	119.00 ± 0.96	126.63 ± 0.96	122.82 ± 1.38

b)

Glass Composition	E_c (kJ/mol) From Equation 4.4	E_c (kJ/mol) From Equation 4.5	E_c (kJ/mol) Average Value
Se_{80} Te_{14} Sb_6	139.11 ± 0.22	145.00 ± 0.22	142.06 ± 0.31
Se_{80} Te_{12} Sb_8	138.24 ± 0.99	143.98 ± 0.99	141.01 ± 1.38

Table 4.4 The values of activation energy for crystallization E_{co} for the glassy system $Se_{80}Te_{20-x}Sb_x$.

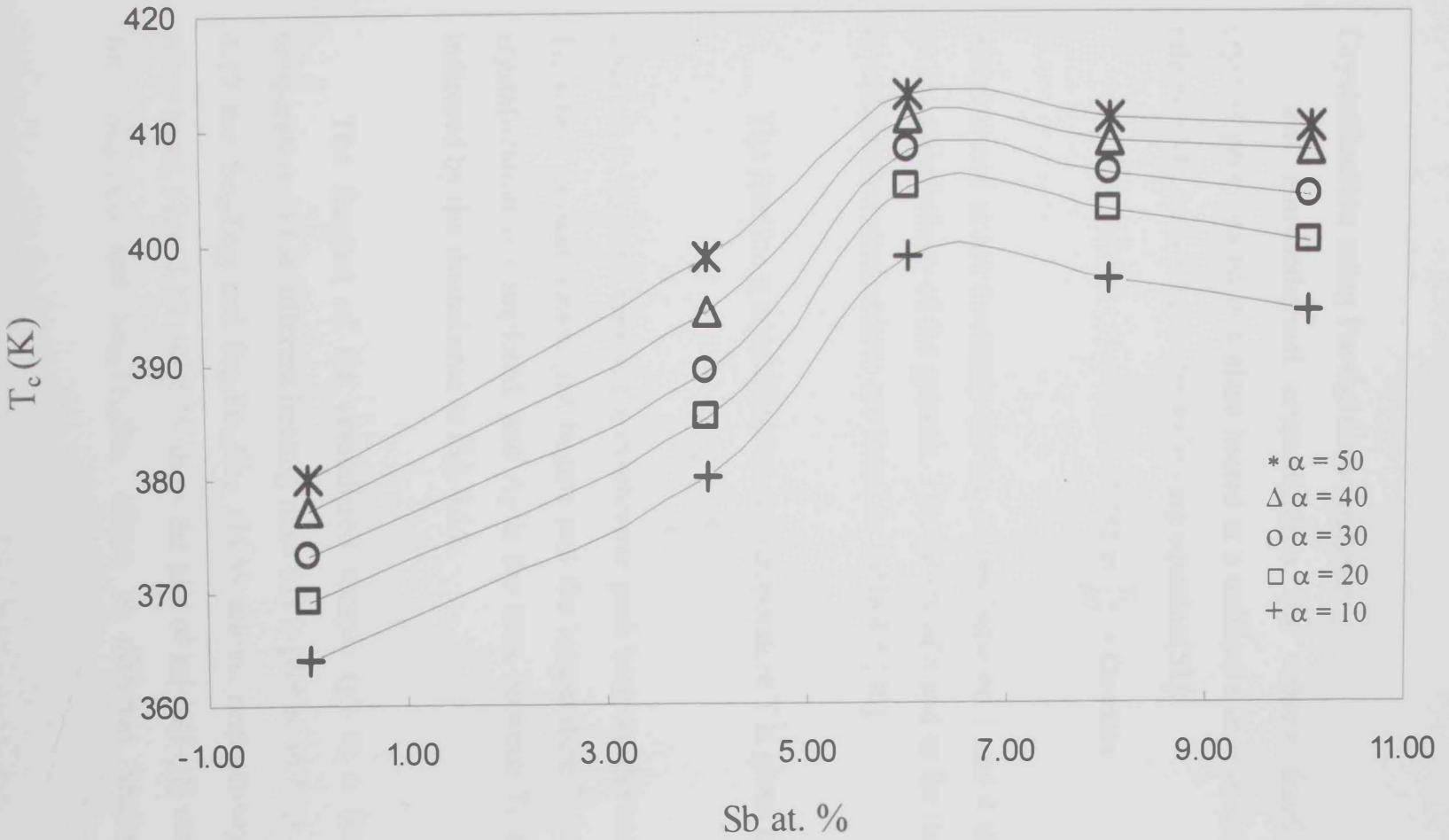

Fig.4.14 Onset temperature of crystallization as a function of Sb content for $Se_{80}Te_{20-x}Sb_x$ glassy system at different heating rates.

It is interesting to notice that increasing Sb at.% up to 6% results in noticeable increase in the value of T_c. Further increase of Sb at.% up to 10% results in a slight decrease in the value of T_c.

Crystallization using Partial area analysis:

For non-isothermal crystallization, the volume fraction χ of crystals precipitated in a glass heated at a uniform rate α is found to be related to E_c according to the following equation[51]:

$$\ln[-\ln(1-\chi)] = -n \ln \alpha - 1.052\, m \frac{E_c}{RT} + Constant \qquad (4.6)$$

where n and m are constants having values between 1 and 4 depending on the morphology of the growth. The values of n and m for the various crystallization mechanisms are listed in Table 4.5 [30].

The fraction χ crystallized at any temperature T is given by:

$$\chi = \frac{A_T}{A}$$

where A is the total area of the exothermic peak between the temperature T_1, where crystallization just begins and the temperature T_2 where the crystallization is completed, and A_T is the area between T_1 and T, as indicated by the shaded area in Fig. 4.15.

The fraction of the crystallized sample (χ) as a function of temperature (T) at different heating rates (α) is plotted in Figs. 4.16 and 4.17 for $Se_{80}Te_{20}$ and $Se_{80}Te_{16}Sb_4$ glassy alloys, respectively. On the other hand, Figs. 4.18 and 4.19 show the plot of $\ln[-\ln(1-\chi)]$ versus (1/T) for $Se_{80}Te_{20}$ and $Se_{80}Te_{16}Sb_4$ alloys at different heating rates,

Mechanism	m	n
Bulk nucleation		
• Three dimensional growth	3	4
• Two dimensional growth	2	3
• One dimensional growth	1	2
Surface nucleation	1	1

Table 4.5 Values of n and m for various crystallization mechanism

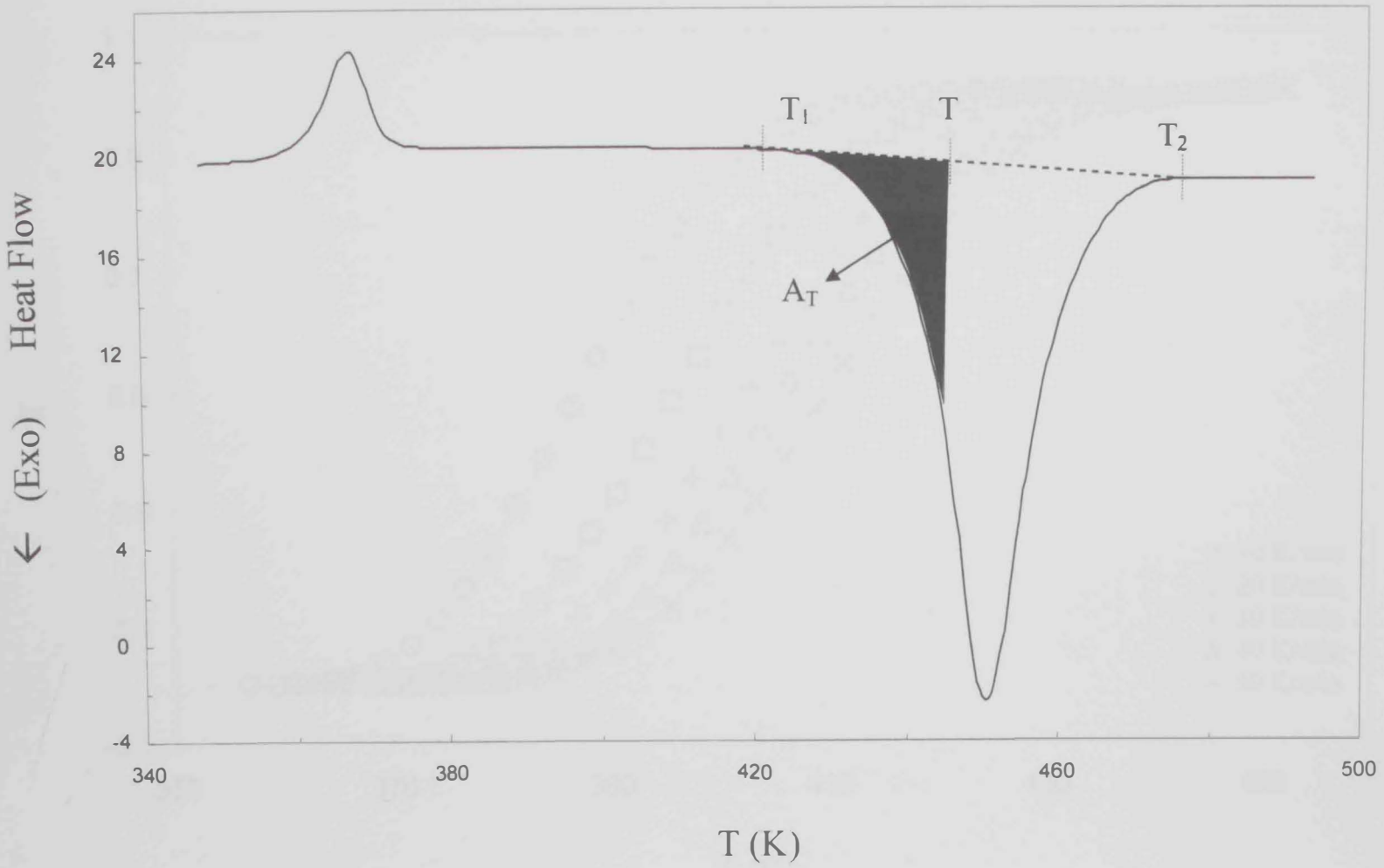

Fig. 4.15 Illustrating the calculation of the fraction of crystallized sample.

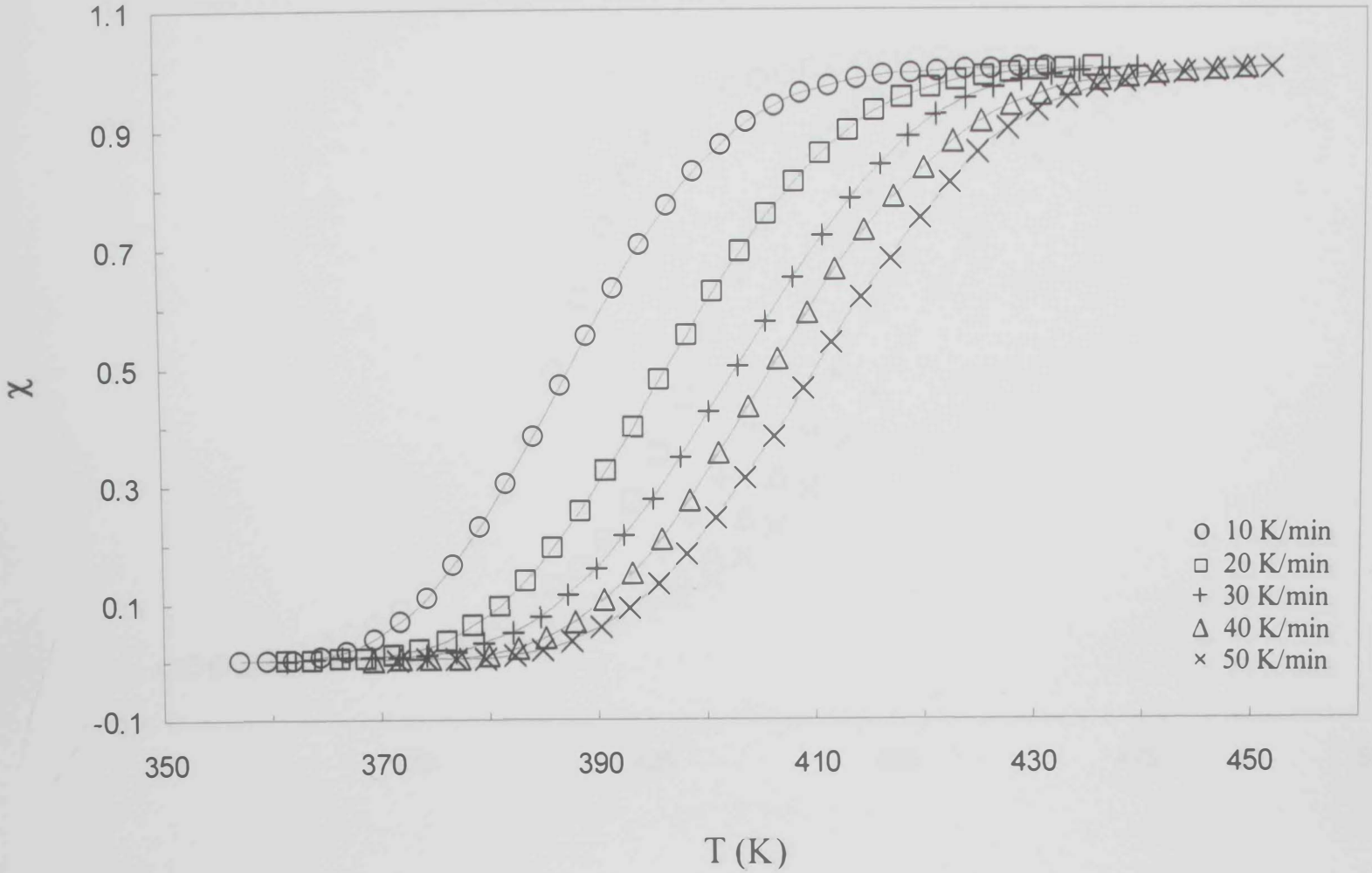

Fig. 4.16 The fraction of crystallization as a function of temperature at different heating rates for $Se_{80}Te_{20}$ glassy alloy.

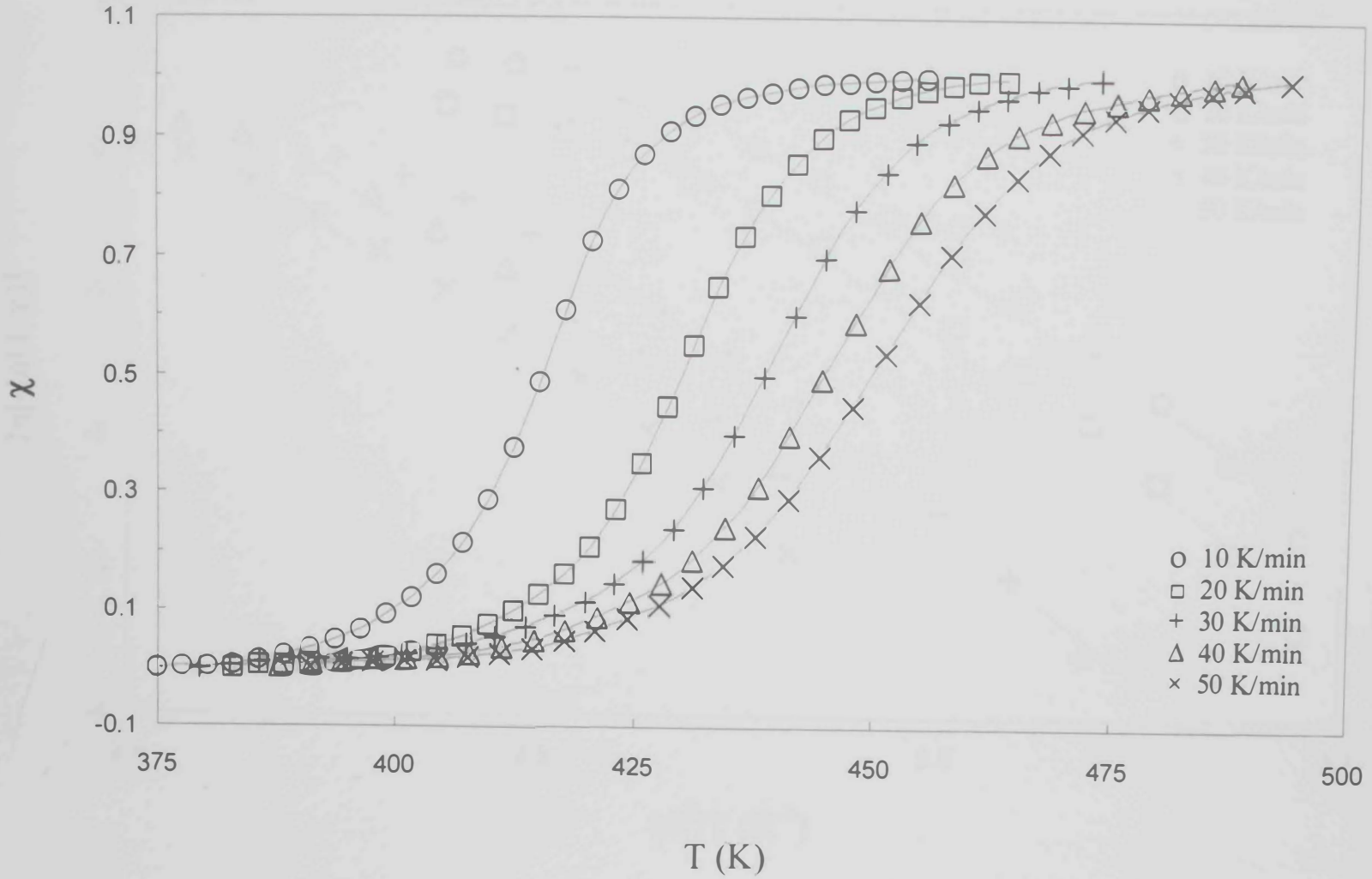

Fig. 4.17 The fraction of crystallization as a function of temperature at different heating rates for $Se_{80}Te_{16}Sb_4$ glassy alloy.

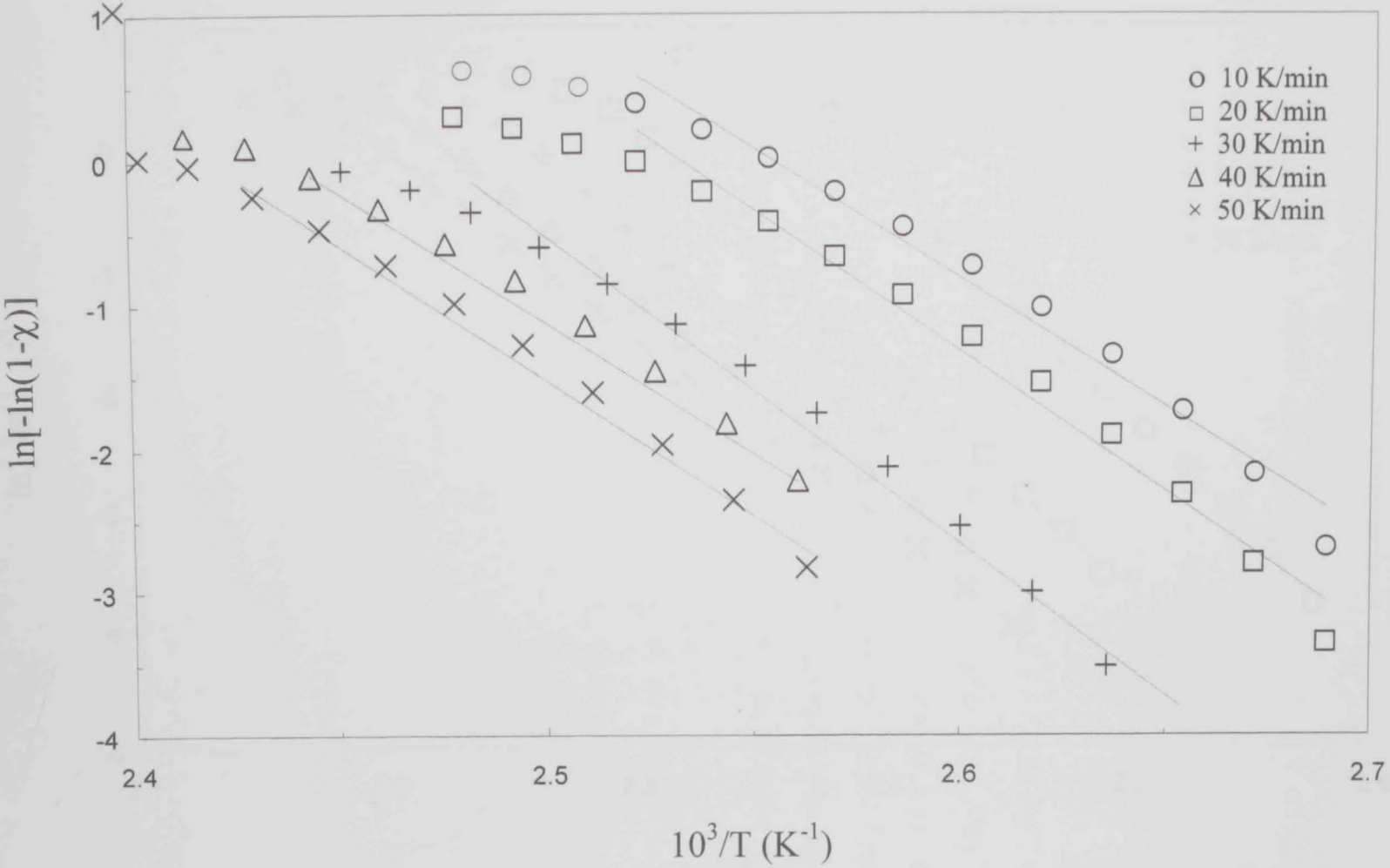

Fig. 4.18 $\ln[-\ln(1-\chi)]$ versus $(10^3/T)$ for $Se_{80}Te_{20}$ glassy alloy.

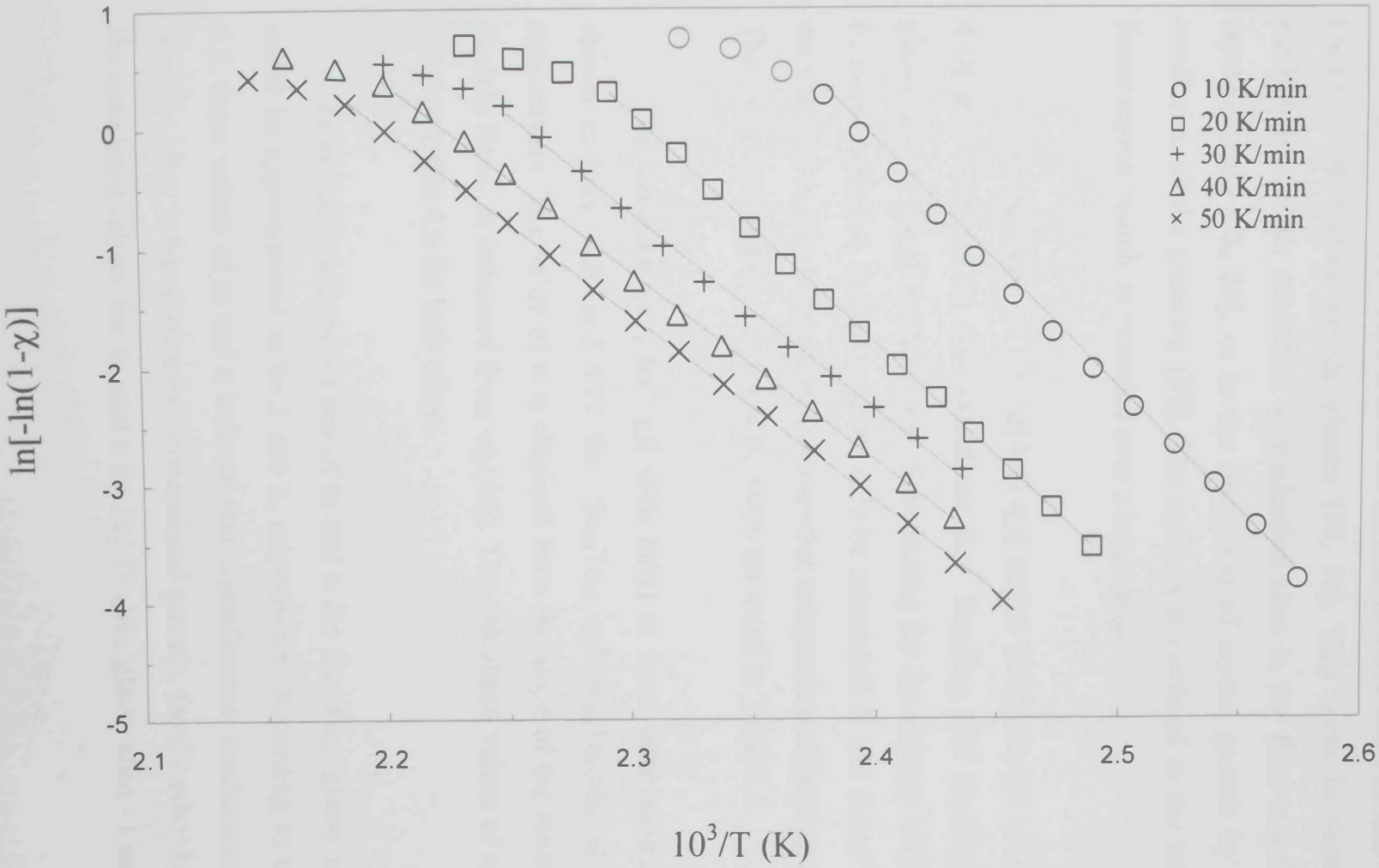

Fig. 4.19 ln[-ln(1-χ)] versus (10^3/T) for $Se_{80}Te_{16}Sb_4$ glassy alloy.

respectively. From these figures. it can be noticed that the plot is linear over most of the temperature range. At high temperatures, or in regions of large crystallized fractions, a break in the linearity, or rather a lowering of the initial slope is seen for all heating rates. Such breaks was found in other chalcogenide glasses [52, 53]. This break in slope is attributed to either saturation in nucleation sites in the final stages of crystallization [53, 54], or to the restriction of crystal growth by the small size of the particles [53]. The analysis is confined to the initial linear region, which is extended over a large range.

From the slope of the $\ln[-\ln(1-\chi)]$ versus $(1/T)$, shown in Figs. 4.18 and 4.19, $(m E_c)$ was calculated for $Se_{80}Te_{20}$ and $Se_{80}Te_{16}Sb_4$ glassy alloys, for all heating rates. Substituting for the average value of E_c from Table 4.4, the value of m could be calculated. It was found that the value of m , for both alloys, is somewhat independent of heating rate. The calculated values of m for both alloys are listed in Table 4.6.

The variation of $[-\ln(1-\chi)]$ with $\ln(\alpha)$ at fixed temperatures is shown in Figs. 4.20 and 4.21 for $Se_{80}Te_{20}$ and $Se_{80}Te_{16}Sb_4$ alloys, respectively. The value of n is obtained from the slope of the resulting straight lines, as indicated from eq.(4.6). The calculated values of n are listed in Table 4.6 for both alloys

From table 4.6, the values of m and n for $Se_{80}Te_{20}$ glassy alloy could be approximated to be 2 and 3, respectively. According to table 4.5, these values of m and n indicate that crystallization mechanism for $Se_{80}Te_{20}$ alloy is based on a two-dimensional growth. On the other hand, the calculated values for m and n for $Se_{80}Te_{16}Sb_4$ glassy alloy (1 and 2,

Glass Composition	m	n
Se_{80} Te_{20}	1.78± 0.13	2.67 ± 0.21
Se_{80} Te_{16} Sb_4	1.00 ± 0.11	2.05 ± 0.22

Table 4.6 The values of m and n for the glassy alloys $Se_{80}Te_{20}$ and $Se_{80}Te_{16}Sb_4$

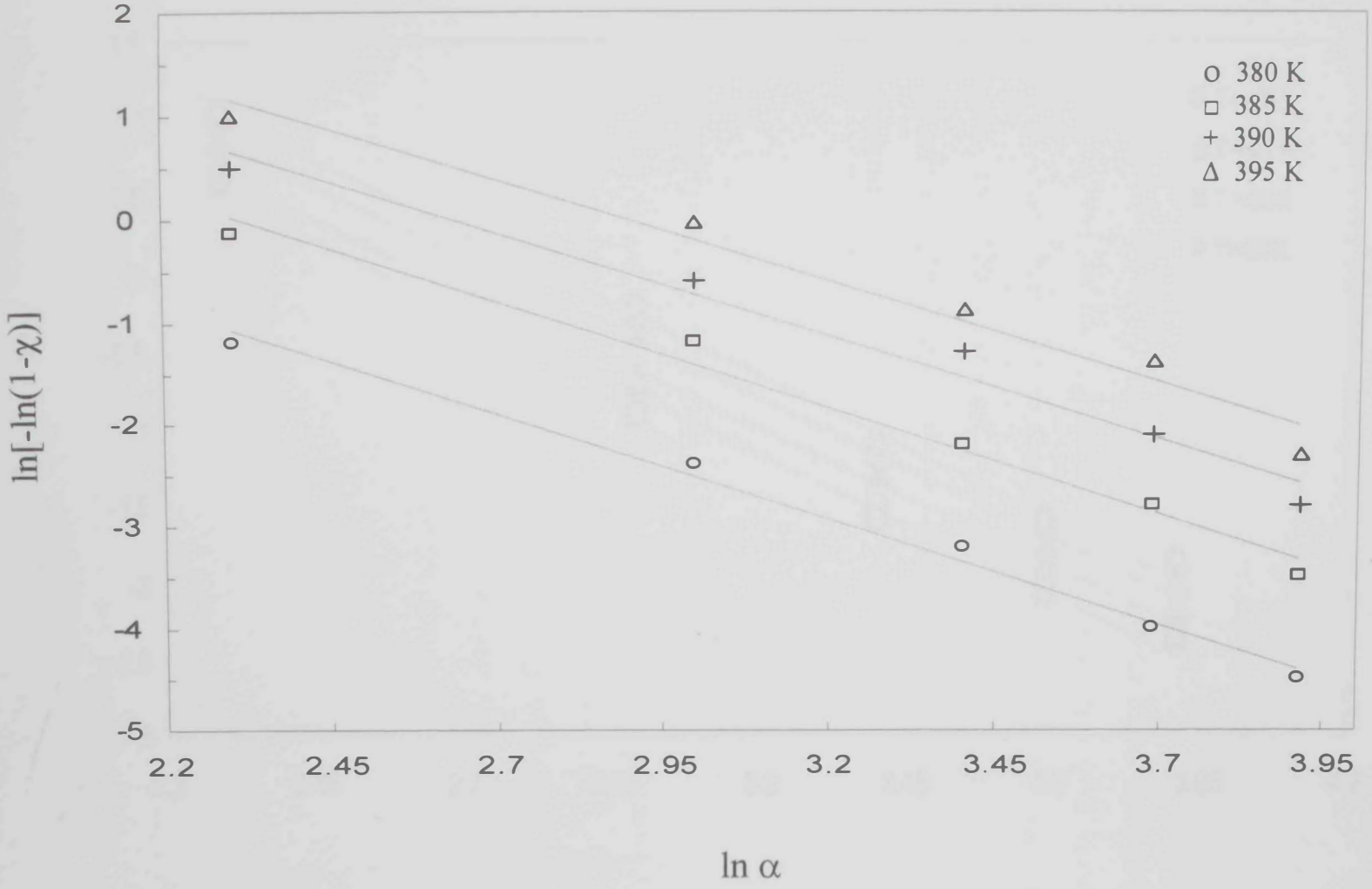

Fig. 4.20 $\ln[-\ln(1-\chi)]$ versus $\ln\alpha$ at constant temperatures for $Se_{80}Te_{20}$ glassy alloy.

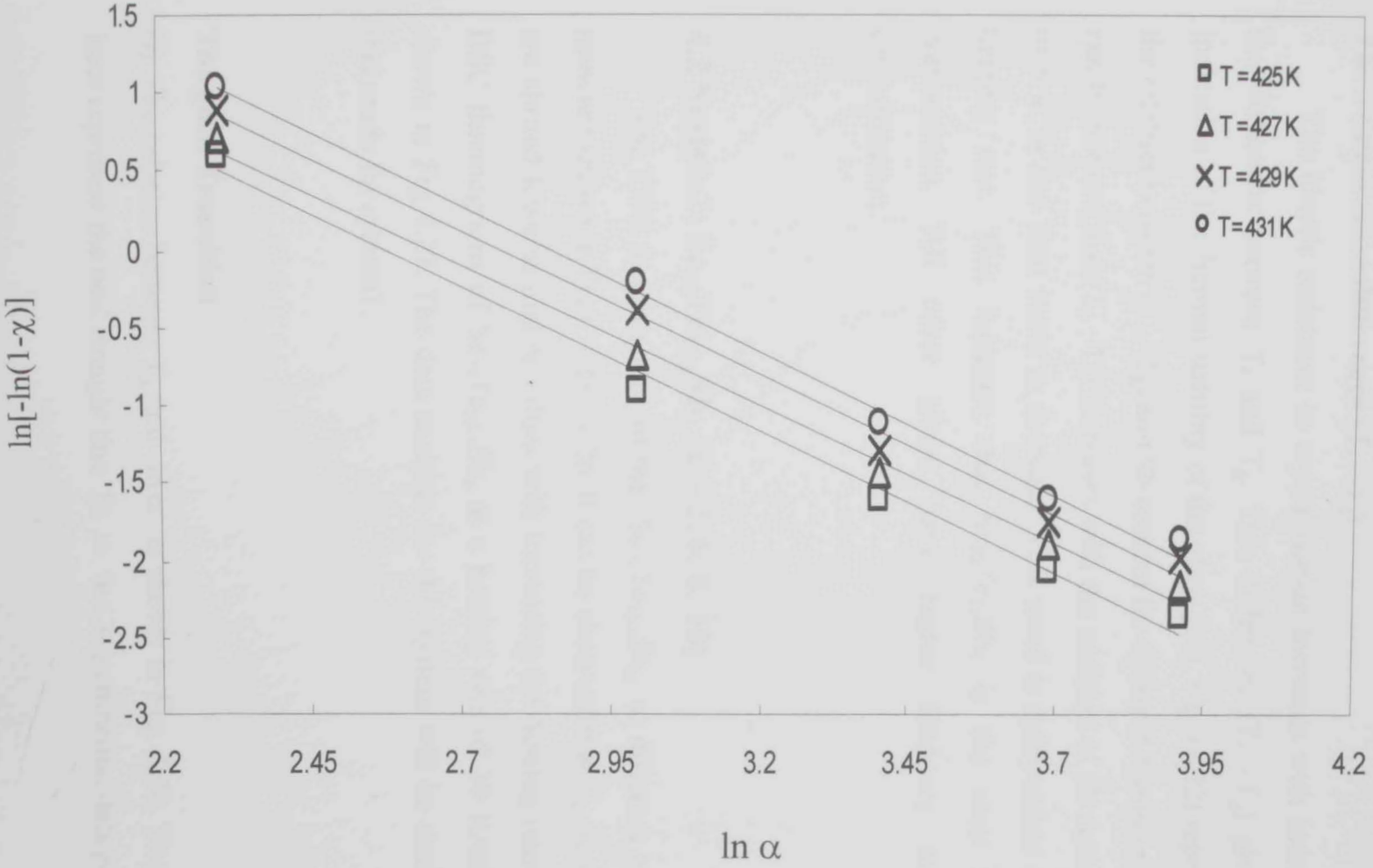

Fig. 4.21 $\ln[-\ln(1-\chi)]$ versus $\ln\alpha$ at constant temperatures for $Se_{80}Te_{16}Sb_4$ glassy alloy.

respectively) indicate that the crystallization mechanism for $Se_{80}Te_{16}Sb_4$ alloy is based on a one-dimensional growth.

The Temperature difference ($T_c - T_g$)

The kinetic resistance to crystallization increases with increasing the difference between T_c and T_g. This difference ($T_c - T_g$) gives an indication of the thermal stability of the glass [30]. Fig. (4.22) represents the relation between ($T_c - T_g$) and Sb content for different heating rates. It can be noticed that ($T_c - T_g$) increases with the addition of Sb content up to 6 at.% and then starts to decrease. This trend is independent of the heating rate. This indicates that $Se_{80}Te_{14}Sb_6$ is the most stable composition. All other alloys have higher tendency towards crystallization.

4.2 System2: $Se_{70}Te_{30-x}Sb_x$ (x = 2, 6, 8, 10)

The DSC thermograms of the $Se_{70}Te_{30-x}Sb_x$ at different heating rates are shown in Figs. 4.23 - 4.26. It can be observed that T_g, T_c and T_p are shifted towards higher values with increasing the heating rates. The DSC thermograms of $Se_{70}Te_{30-x}Sb_x$ at a heating rate of 30 K/min are shown in Fig 4.27. The data analysis for this system will be similar to that made for system1.

The glass Transition

(i) The relation between T_g and $\ln \alpha$ is shown in Fig. 4.28. The solid lines represent the best straight line fit to the experimental data points.

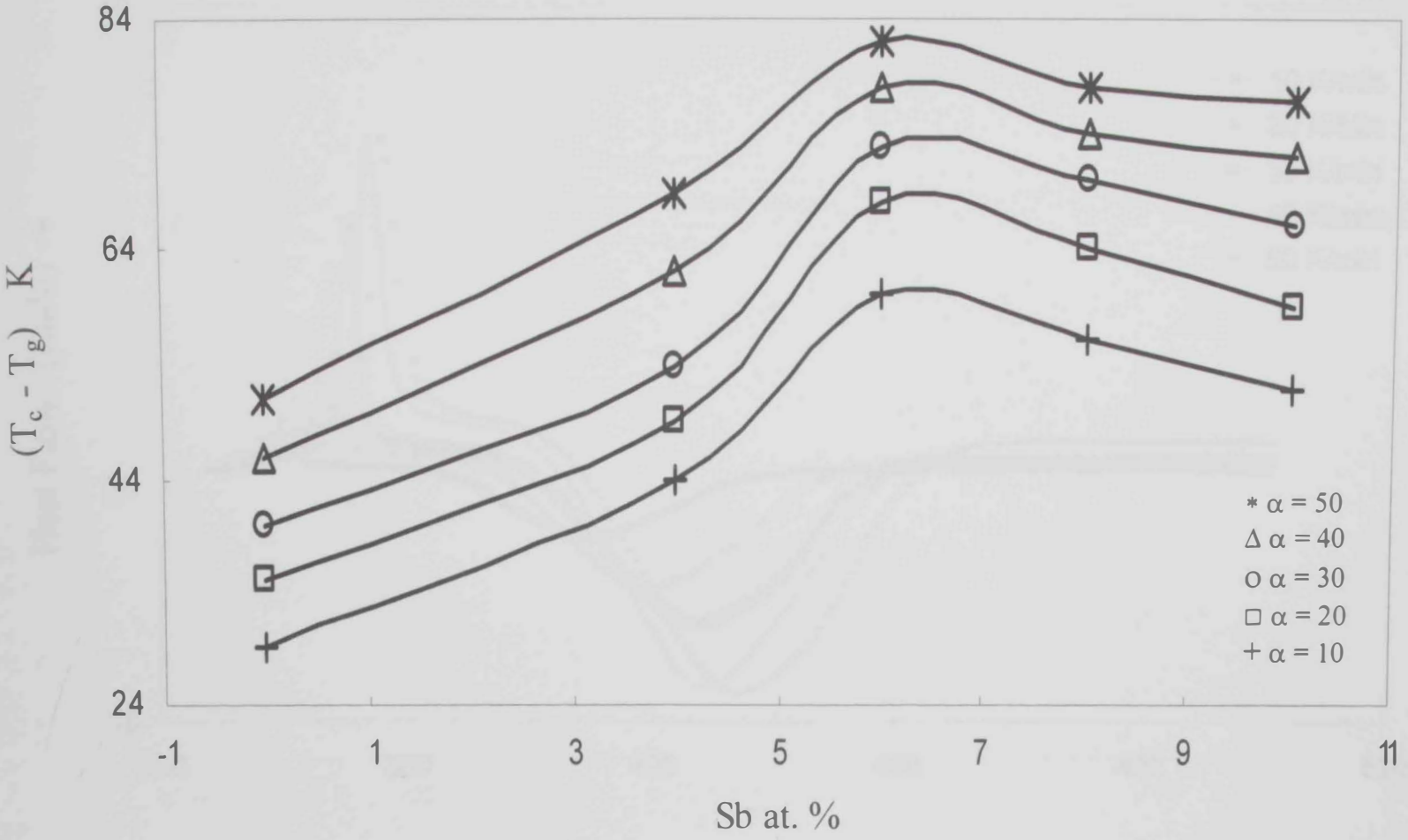

Fig. 4.22 $(T_c - T_g)$ as a function of Sb content for $Se_{80}Te_{20-x}Sb_x$ glassy system at different heating rates.

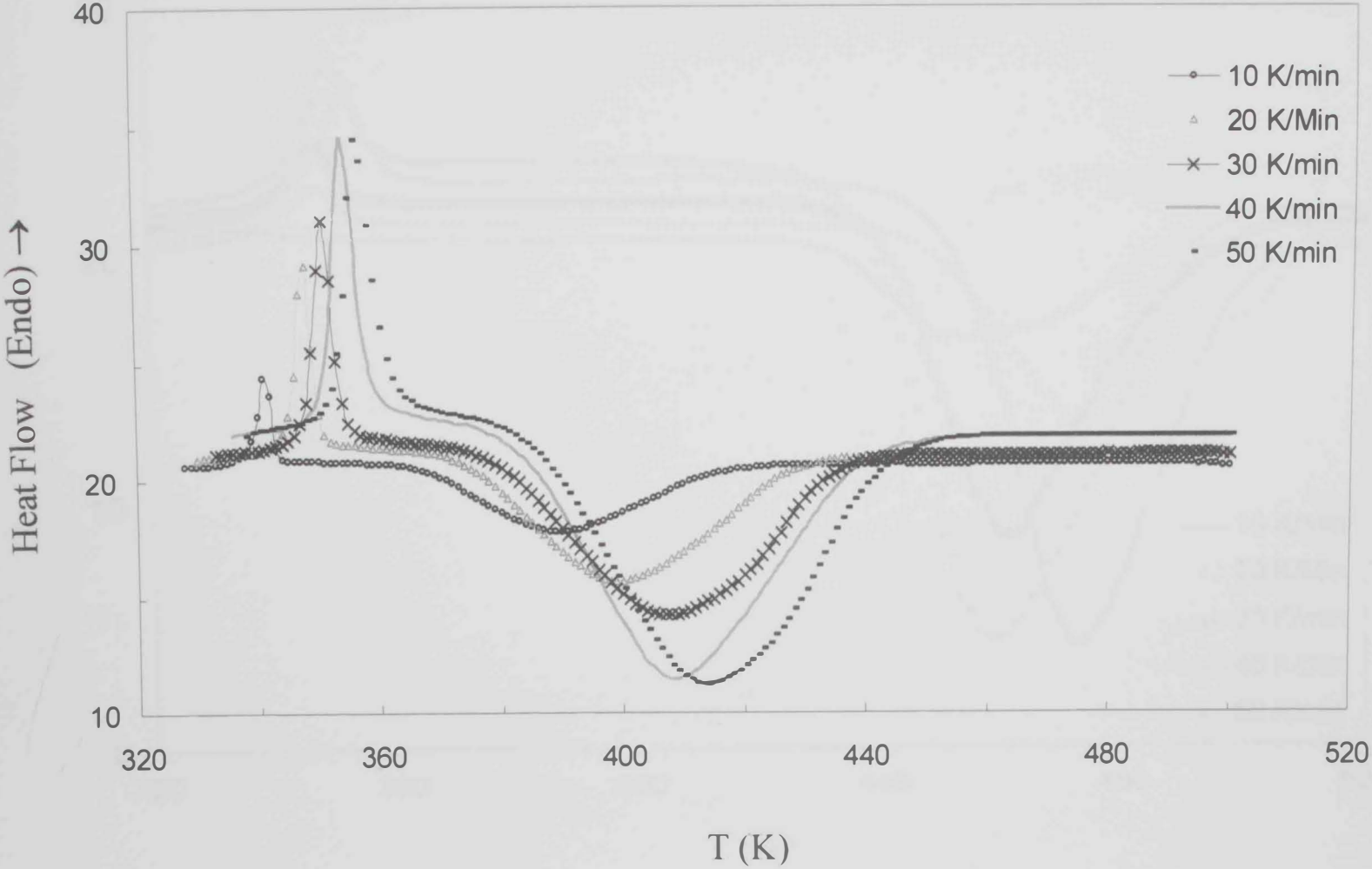

Fig. 23 DSC thermograrms for $Se_{70}Te_{28}Sb_2$ glassy alloy at different heating rates.

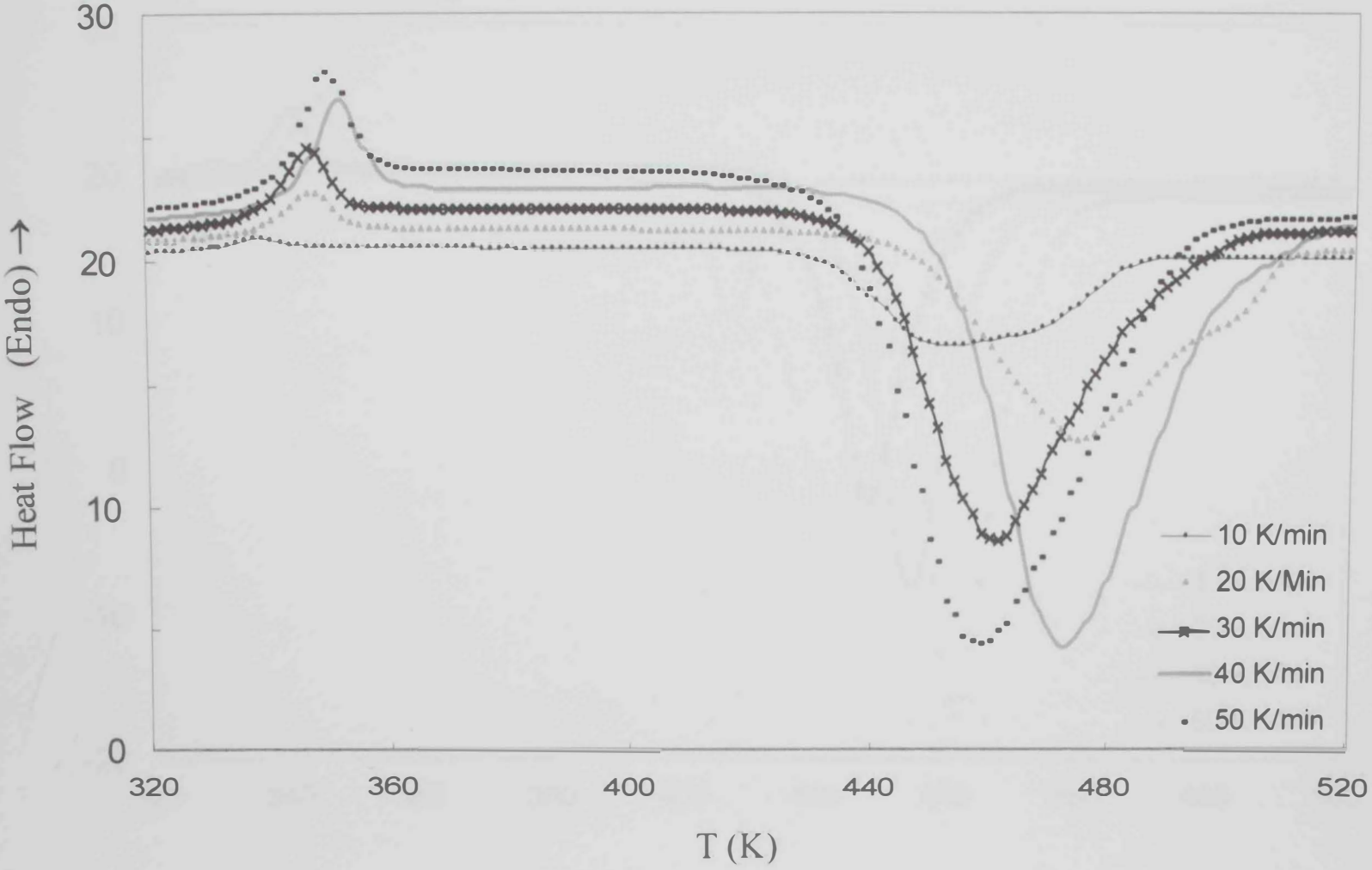

Fig. 4.24 DSC thermograrms for $Se_{70}Te_{24}Sb_6$ glassy alloy at different heating rates.

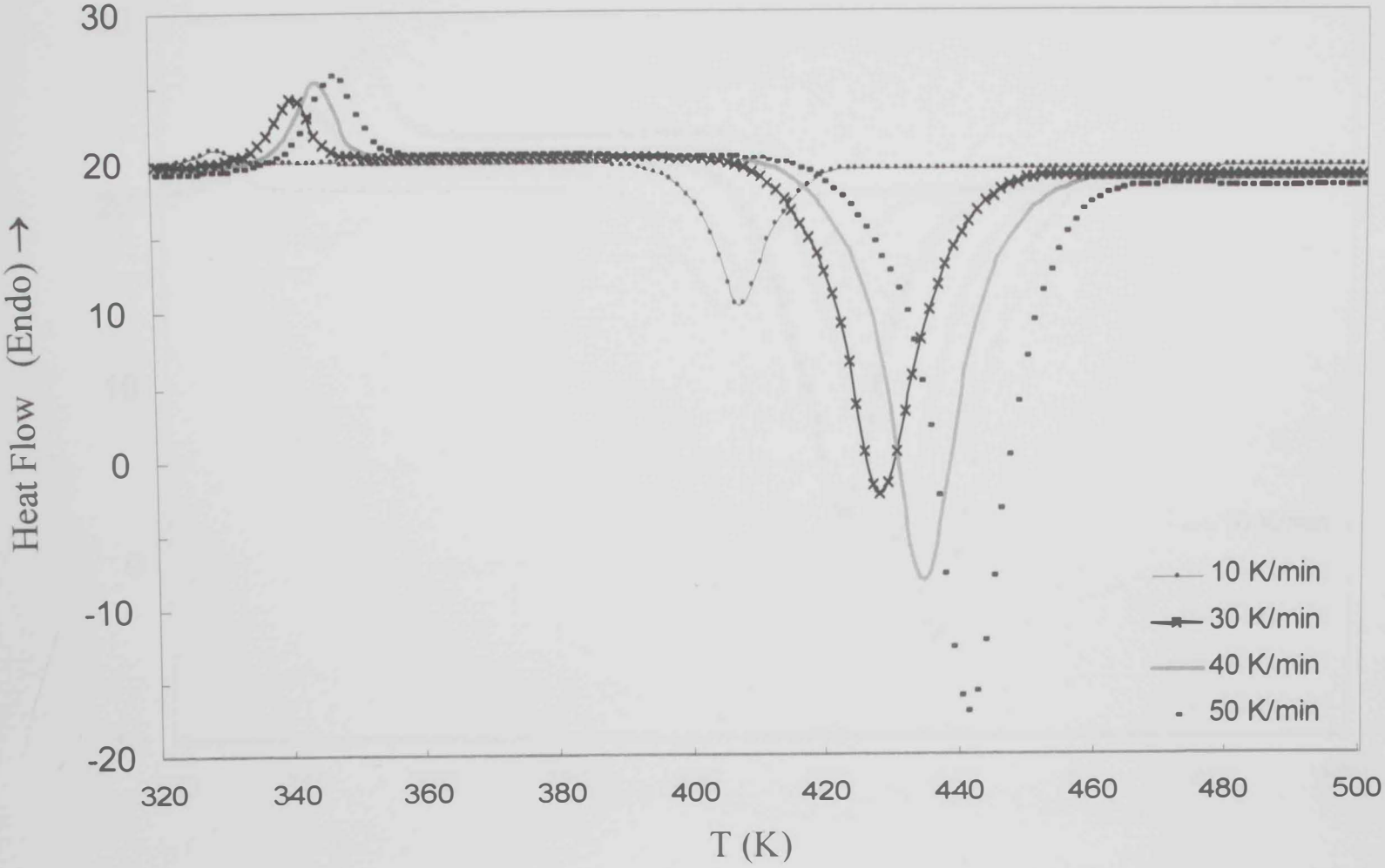

Fig. 4.25 DSC thermograrms for $Se_{70}Te_{22}Sb_8$ glassy alloy at different heating rates.

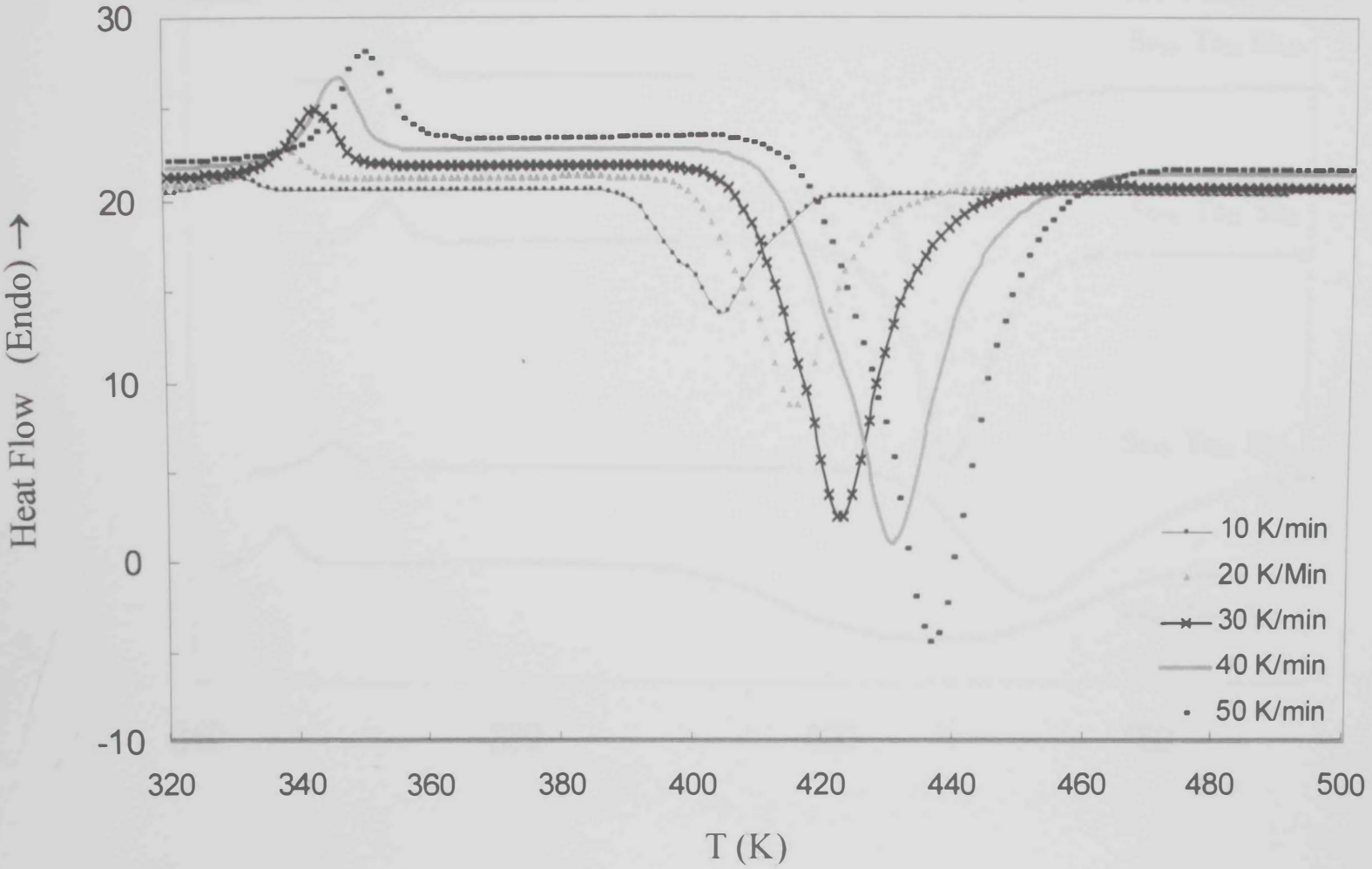

Fig. 4.26 DSC thermograrms for $Se_{70}Te_{20}Sb_{10}$ glassy alloy at different heating rates.

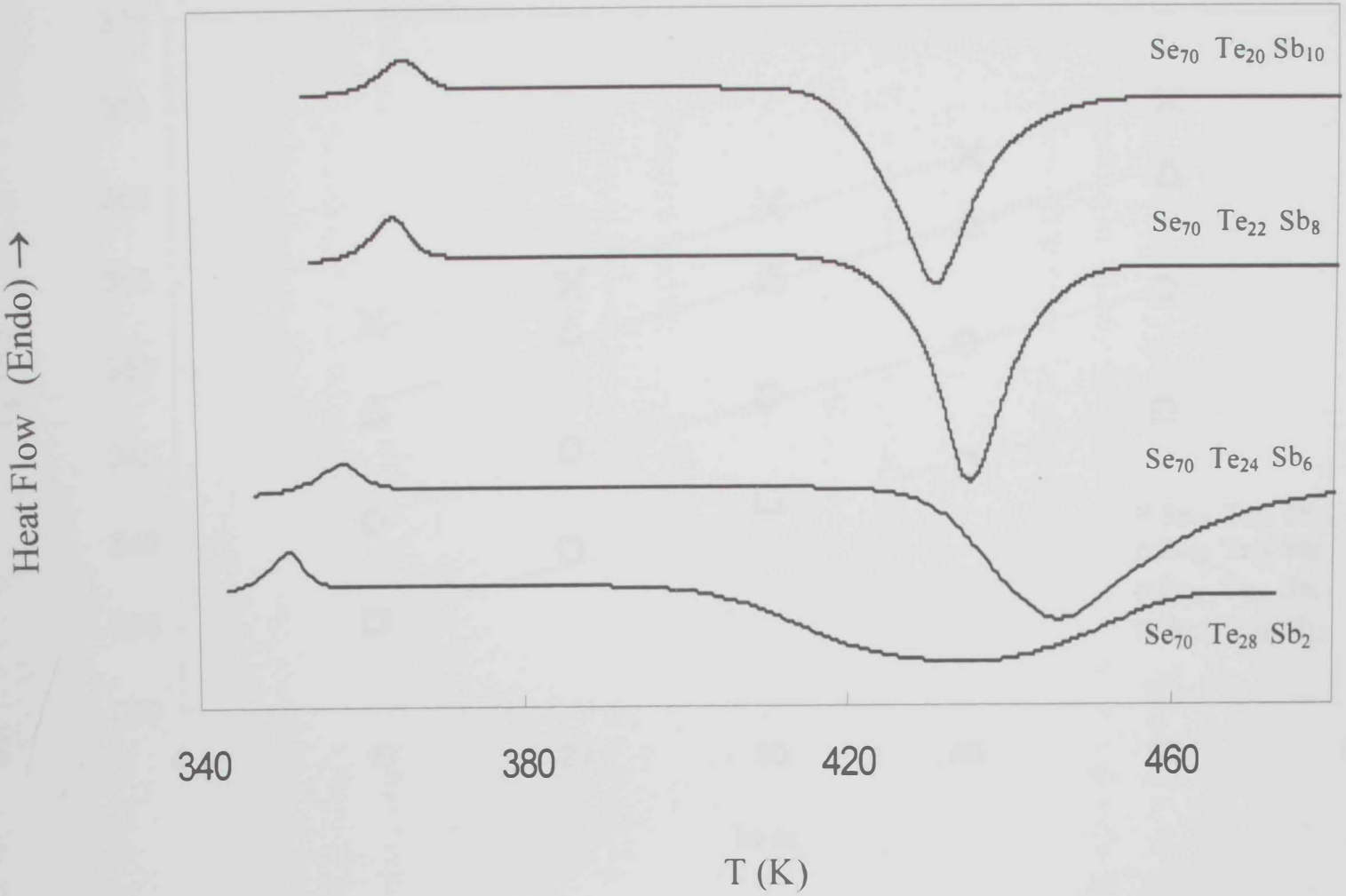

Fig. 4.27 DSC thermograrms for $Se_{70}Te_{30-x}Sb_x$ glassy system at a heating rate of 30 K/min.

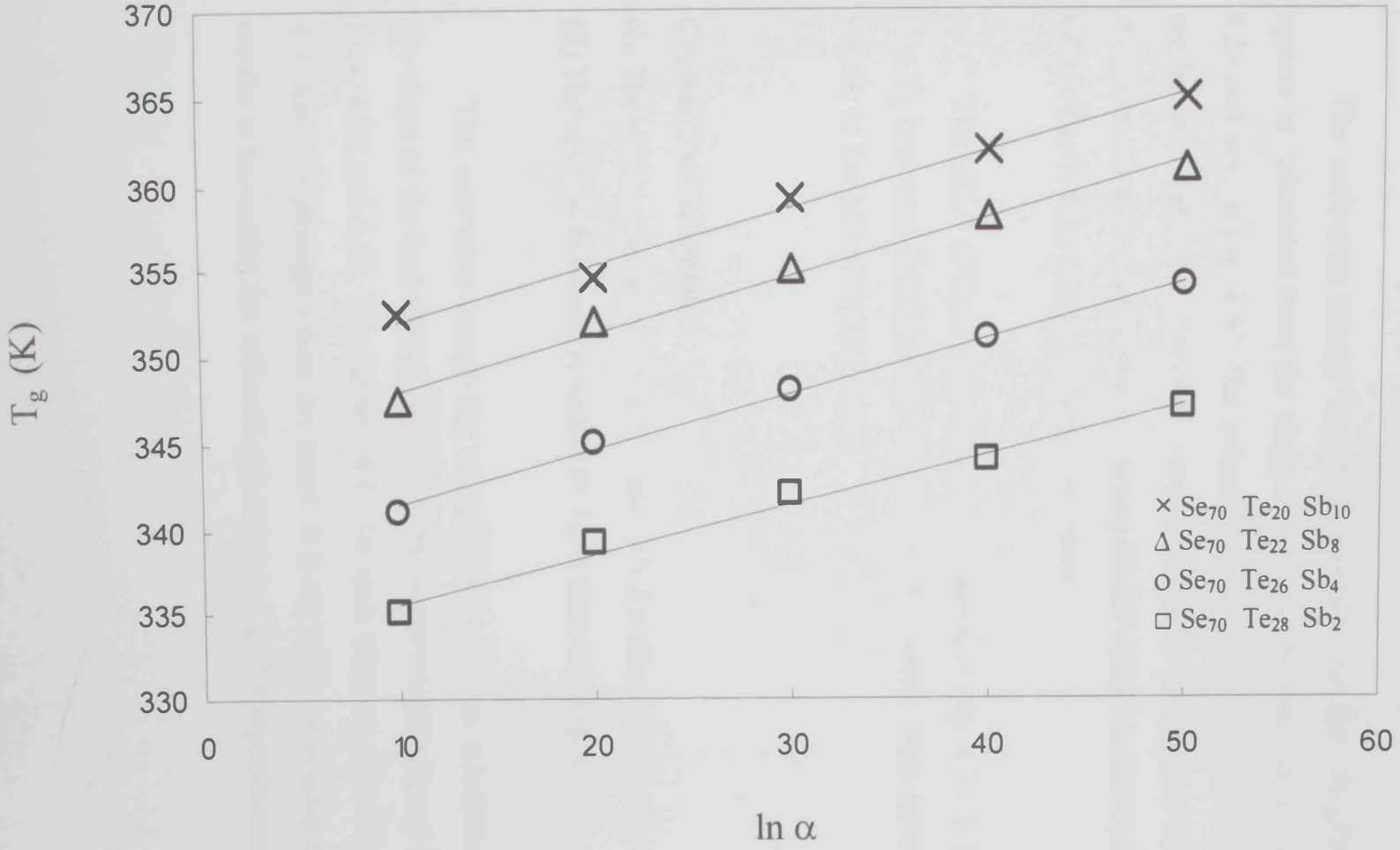

Fig. 4.28 T_g versus $\ln \alpha$ for $Se_{70}Te_{30-x}Sb_x$ glassy system.

The constants A and B are calculated for each glassy alloy, using eq. (4.1), and they are listed in Table 4.7 for each alloy.

(ii) The variation of $\ln(\alpha/T_g^2)$ with $(1/T_g)$ is shown in Fig. 4.29.

(iii)The variation of $\ln\alpha$ with $(1/T_g)$ is given in Fig 4.30.

The activation energy for glass transition for the $Se_{70}Te_{30-x}Sb_x$ system is calculated from the slope of the straight lines shown in Fig. 4.29 and also in Fig. 4.30. The values of E_t calculated from both figures are listed in Table 4.8. Also the average values are included in the table. It is interesting to observe that increasing Sb at.% result in decreasing the value of activation energy for glass transition.

The effect of increasing Sb on T_g is shown in Fig. 4.31. It is clear that T_g increases linearly with increasing Sb content. This behavior is similar to the behavior of system1.

Crystallization kinetics

(i) The relation between $\ln(\alpha/T_c^2)$ and $(1/T_c)$ is shown in Fig. 4.32.

(ii) The relation between $(\ln\alpha)$ and $(1/T_c)$ is shown in Fig. 4.33

The activation energy for crystallization E_c was calculated from the slope of the best straight line fit to the experimental data points for Figs. 4.32 and 4.33. The values of E_c for each alloy are listed in Table 4.9. Also the average values are listed. It is clear that increasing Sb at.% results in increasing the value of activation energy for crystallization.

Glass Composition	A + B ln α
Se_{70} Te_{28} Sb_2	333 + 0.28 ln α
Se_{70} Te_{24} Sb_6	338 + 0.37 ln α
Se_{70} Te_{22} Sb_8	345 + 0.41 ln α
Se_{70} Te_{20} Sb_{10}	349+ 0.52 ln α

Table 4.7 The fitting parameters to equation 4.1 for the glassy system $Se_{70}Te_{30-x}Sb_x$.

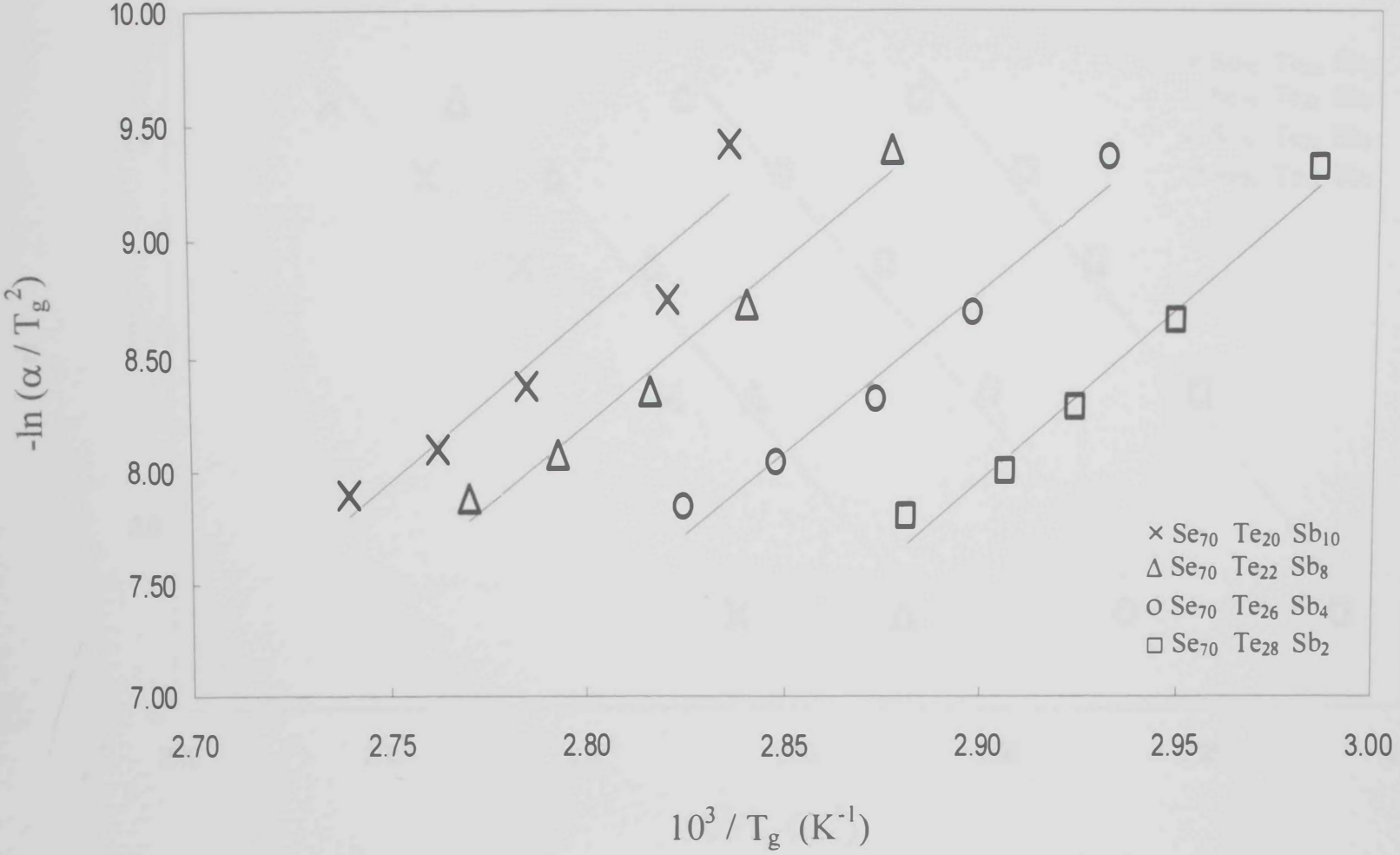

Fig 4.29 $-\ln(\alpha/T_g^2)$ versus $(10^3/T_g)$ for $Se_{70}Te_{30-x}Sb_x$ glassy system.

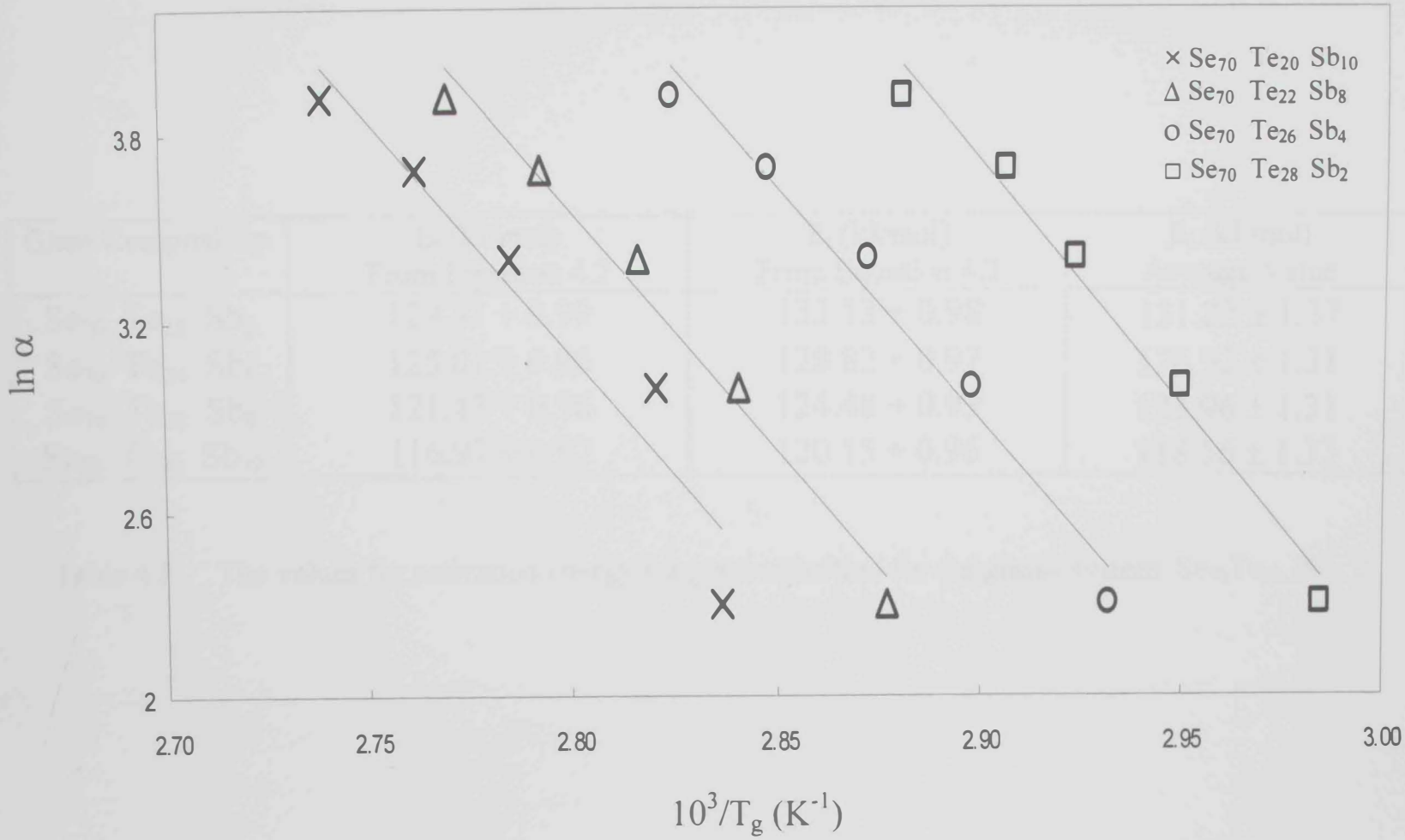

Fig 4.30 ln α versus $(10^3/T_g)$ for $Se_{70}Te_{30-x}Sb_x$ glassy system.

Glass Composition	E_t (kJ/mol) From Equation 4.2	E_t (kJ/mol) From Equation 4.3	E_t (kJ/mol) Average Value
Se_{70} Te_{28} Sb_2	129.31 + 0.99	133.13 + 0.98	131.22 ± 1.37
Se_{70} Te_{24} Sb_6	125.01 + 0.96	128.82 + 0.97	126.92 ± 1.31
Se_{70} Te_{22} Sb_8	121.43 + 0.96	124.48 + 0.93	123.96 ± 1.31
Se_{70} Te_{20} Sb_{10}	116.97 + 0.97	120.15 + 0.96	118.56 ± 1.33

Table 4.8 The values for activation energy for glass transition for the glassy system $Se_{70}Te_{30-x}Sb_x$.

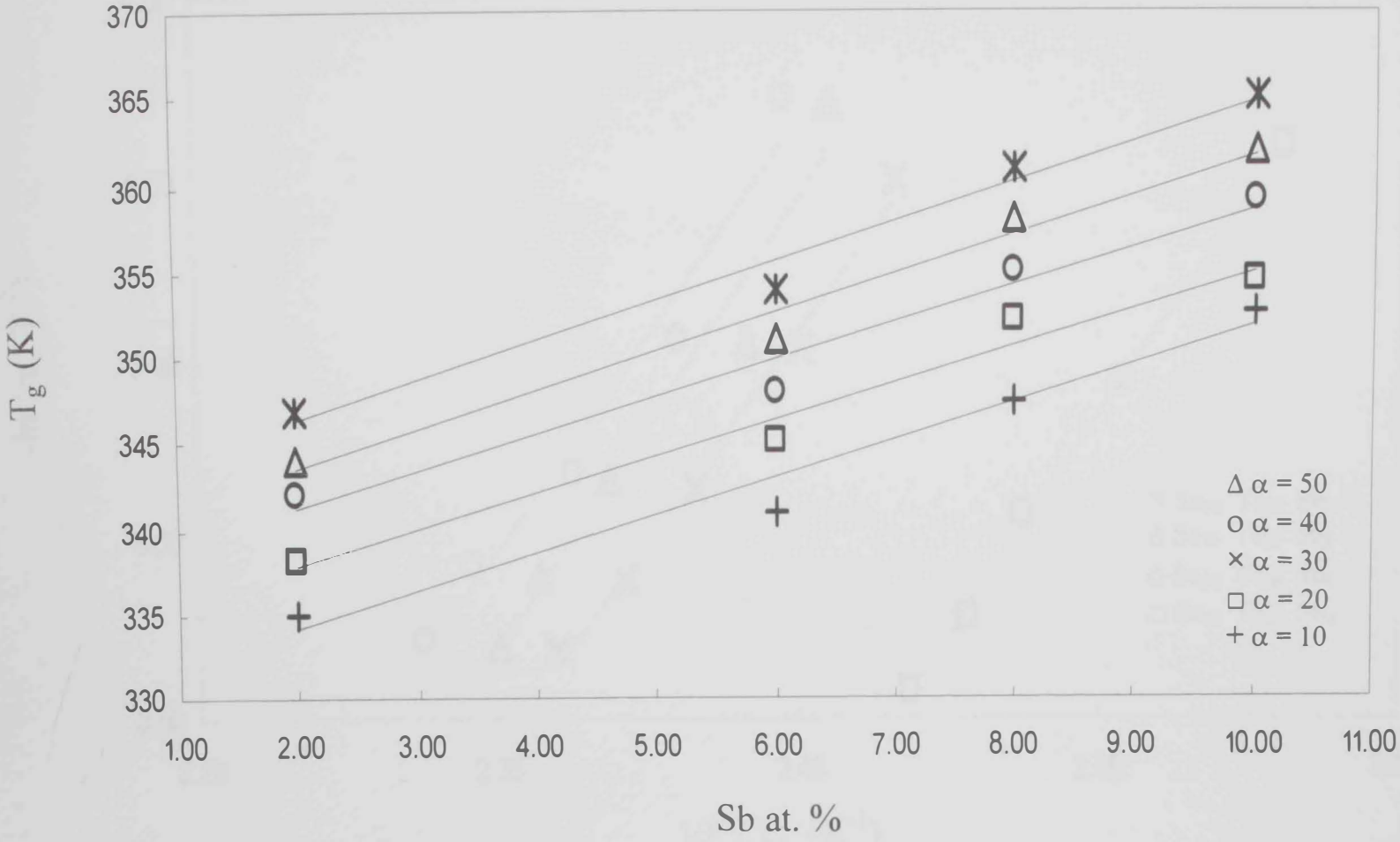

Fig. 4.31 Glass transition temperature for $Se_{70}Te_{30-x}Sb_x$ glassy system at different heating rates.

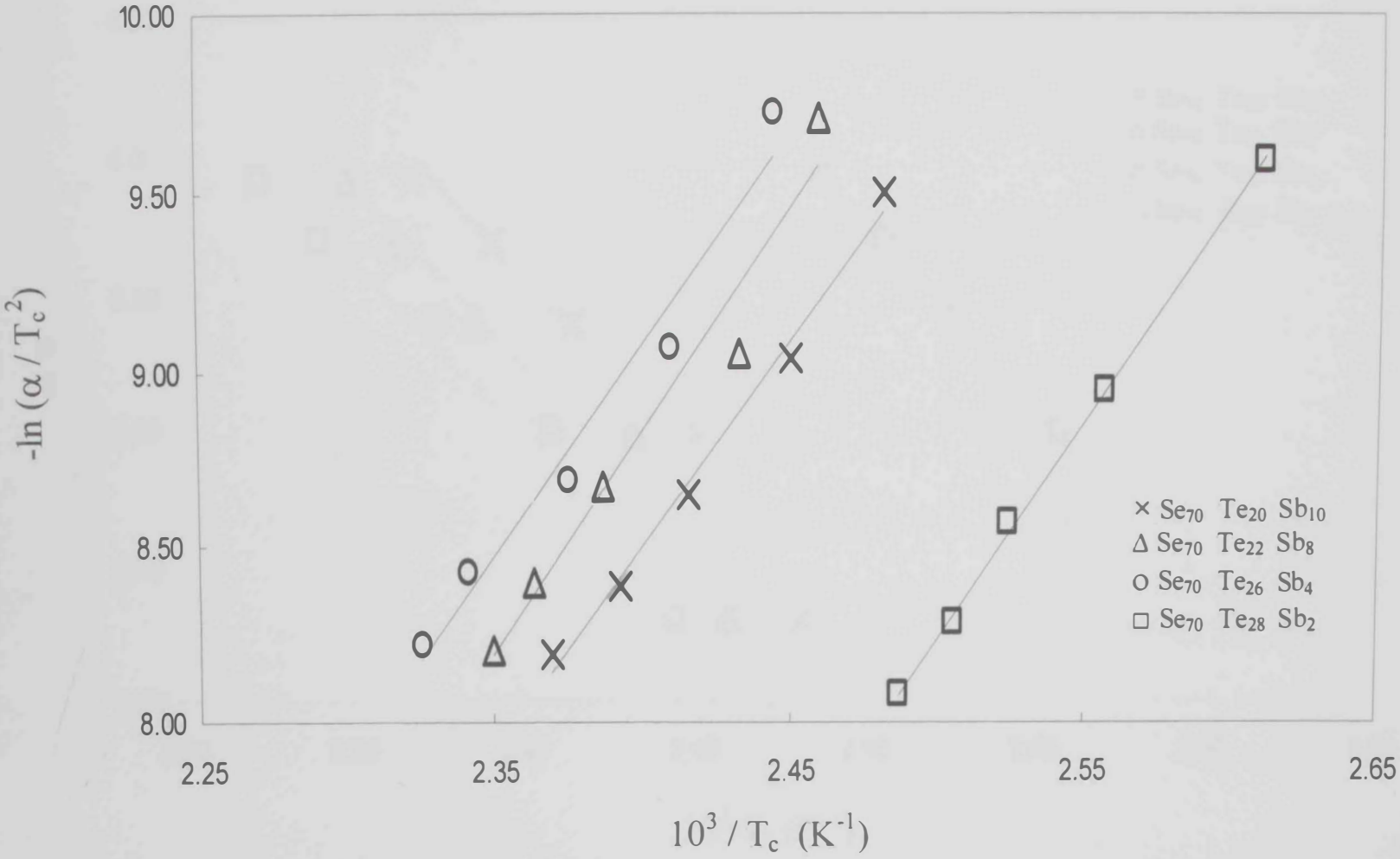

Fig 4.32 $-\ln(\alpha/T_c^2)$ versus $(10^3/T_c)$ for $Se_7Te_{3-x}Sb_x$ glassy system.

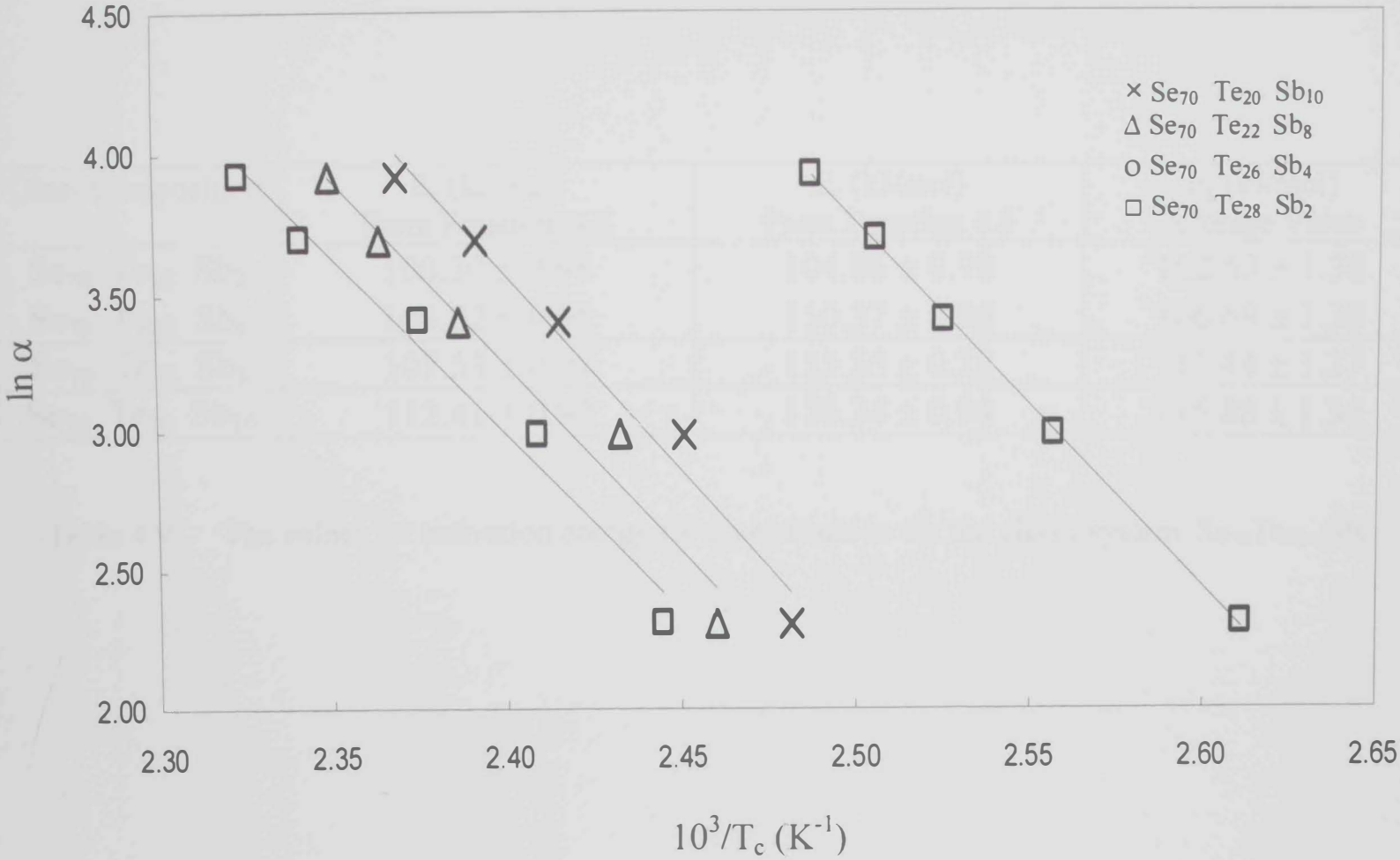

Fig 4.33 $\ln \alpha$ versus $(10^3/T_c)$ for $Se_{70}Te_{30-x}Sb_x$ glassy system.

Glass Composition	E_c (kJ/mol) From Equation 4.4	E_c (kJ/mol) From Equation 4.5	E_c (kJ/mol) Average Value
Se_{70} Te_{28} Sb_2	100.30 ± 0.98	104.86 ± 0.98	102.63 ± 1.38
Se_{70} Te_{24} Sb_6	103.02 ± 0.96	110.37 ± 0.96	106.69 ± 1.38
Se_{70} Te_{22} Sb_8	107.53 ± 0.97	115.35 ± 0.22	111.44 ± 1.37
Se_{70} Te_{20} Sb_{10}	112.41 ± 0.92	118.34 ± 0.94	115.88 ± 1.36

Table 4.9 The values for activation energy for crystallization for the glassy system $Se_{70}Te_{30-x}Sb_x$.

The effect of increasing the Sb at.% on T_c for the $Se_{70}Te_{30-x}Sb_x$ glassy system is shown in Fig 4.34. It is clear that increasing Sb content results in an increase in the value of T_c up to 6 at.% of Sb and then decreases slightly. Again the same trend was observed for $Se_{80}Te_{20-x}Sb_x$ glassy system.

Crystallization using partial area analysis

The fraction of the crystallized sample (χ) as a function of temperature (T) at different heating rates (α) are plotted in Figs 4.35 To 4.38 for the $Se_{70}Te_{30-x}Sb_x$ glassy system. The relation between $\ln[-\ln(1-\chi)]$ and (1/T) at different heating rates are shown in Figs. 4.39 To 4.42. It is clear that the plot is linear over most of the temperature range measured. At high temperatures, a break in the linearity is observed for all heating rates for all alloys. The analysis is confined to the lower linear region. From the slope, the value of m could be calculated for each heating rate and an average value is calculated for each alloy. The values of m are listed in Table 4.10.

The variation of $\ln[-\ln(1-\chi)]$ with $(\ln \alpha)$ at fixed temperature is shown in Figs. 4.43 To 4.46 for the $Se_{70}Te_{30-x}Sb_x$ glassy alloys. The value of n is obtained from the resulting straight lines. An average value for n was calculated for each glassy alloy and is listed in Table 4.10.

The crystallization mechanism for each glassy alloy could be predicted by comparing the calculated values for m and n, which are listed in Table 4.10 with those given in Table 4.5. It is interesting to observe that each alloy has a different crystallization mechanism:

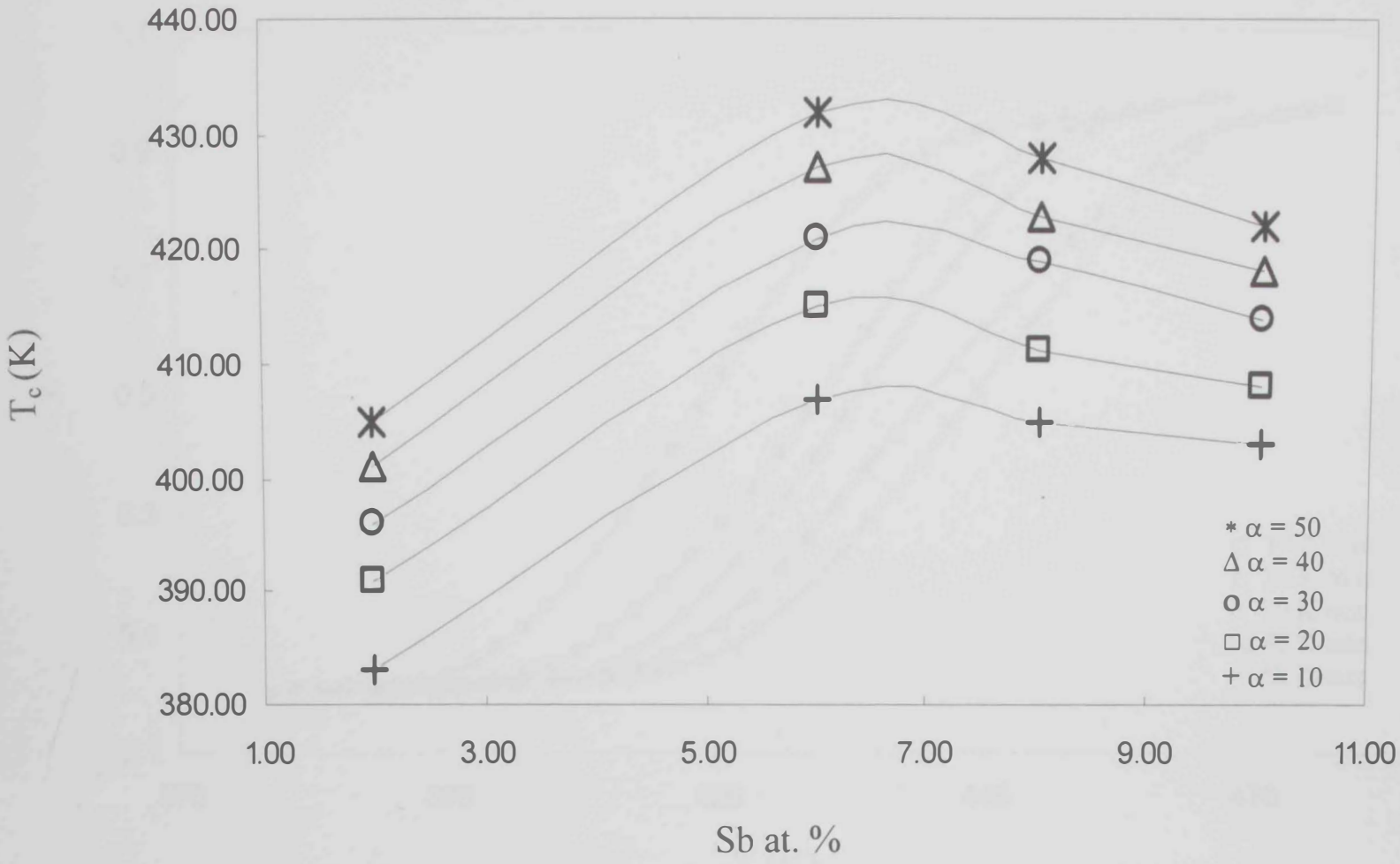

Fig. 4.34 Onset temperature of crystallization as a function of Sb content for $Se_{70}Te_{30-x}Sb_x$ glassy system at different heating rates.

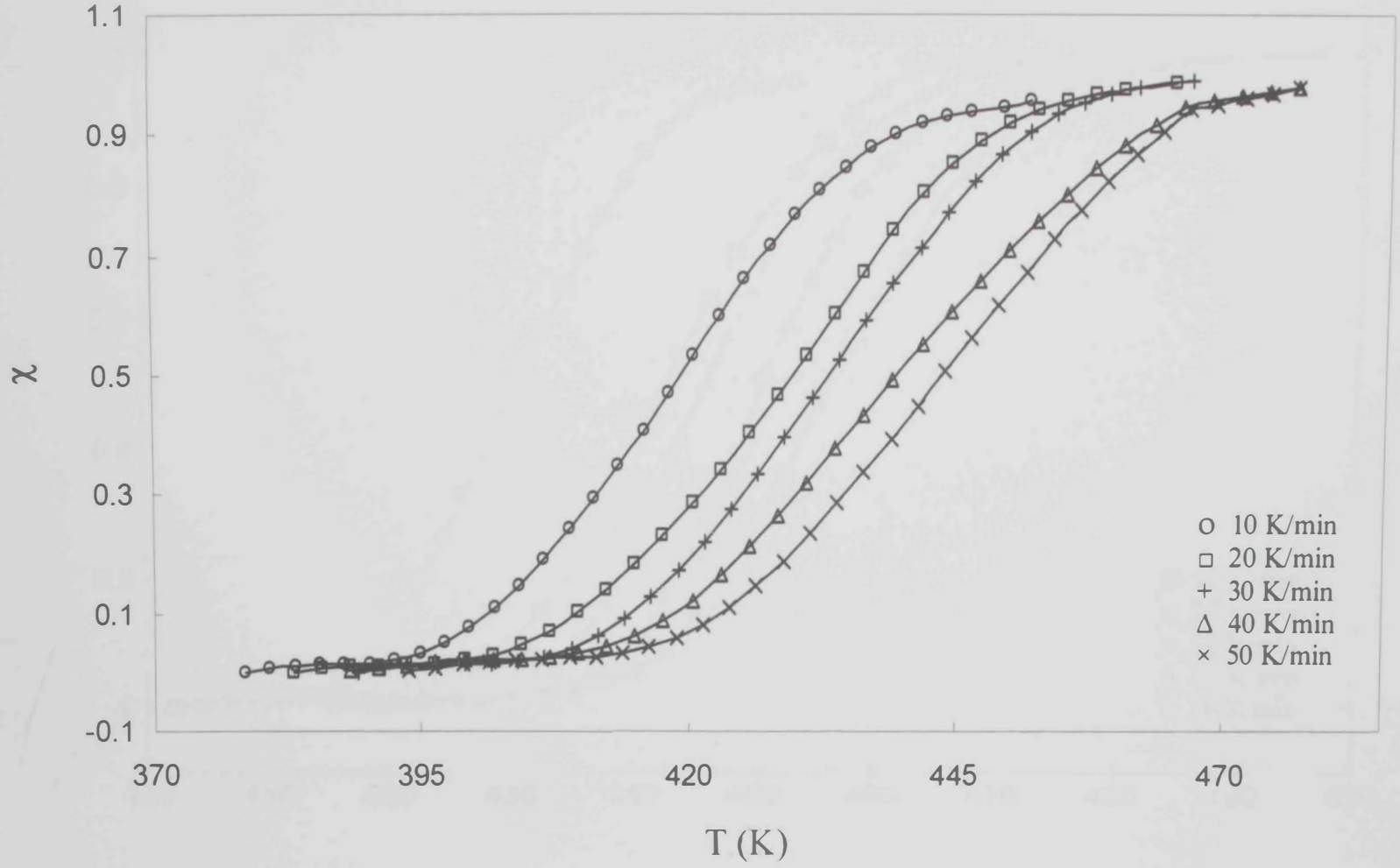

Fig. 4.35 The fraction of crystallization as a function of temperature at different heating rates for $Se_{70}Te_{28}Sb_2$ glassy alloy.

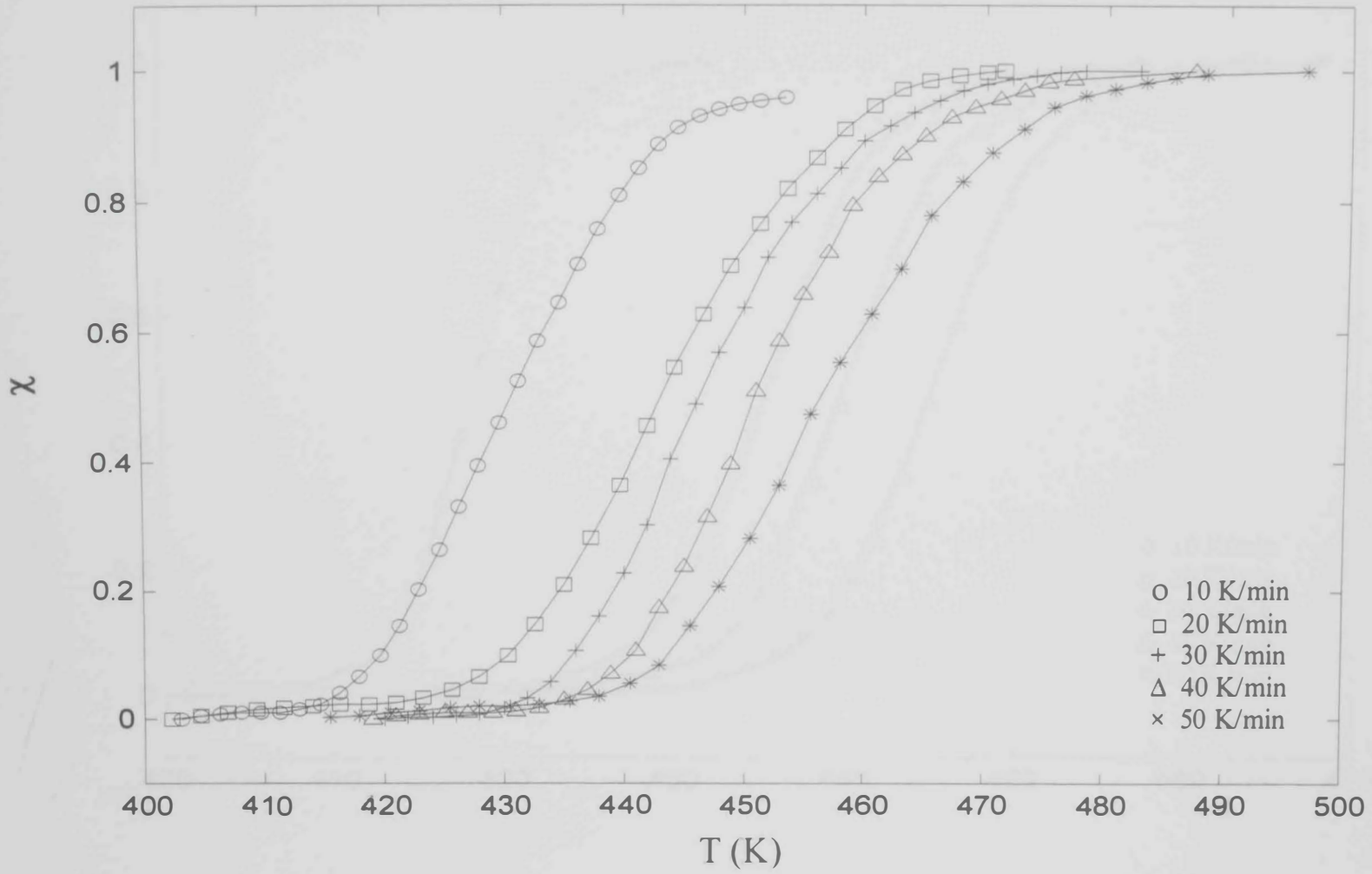

Fig. 4.36 The fraction of crystallization as a function of temperature at different heating rates for $Se_{70}Te_{24}Sb_6$ glassy alloy.

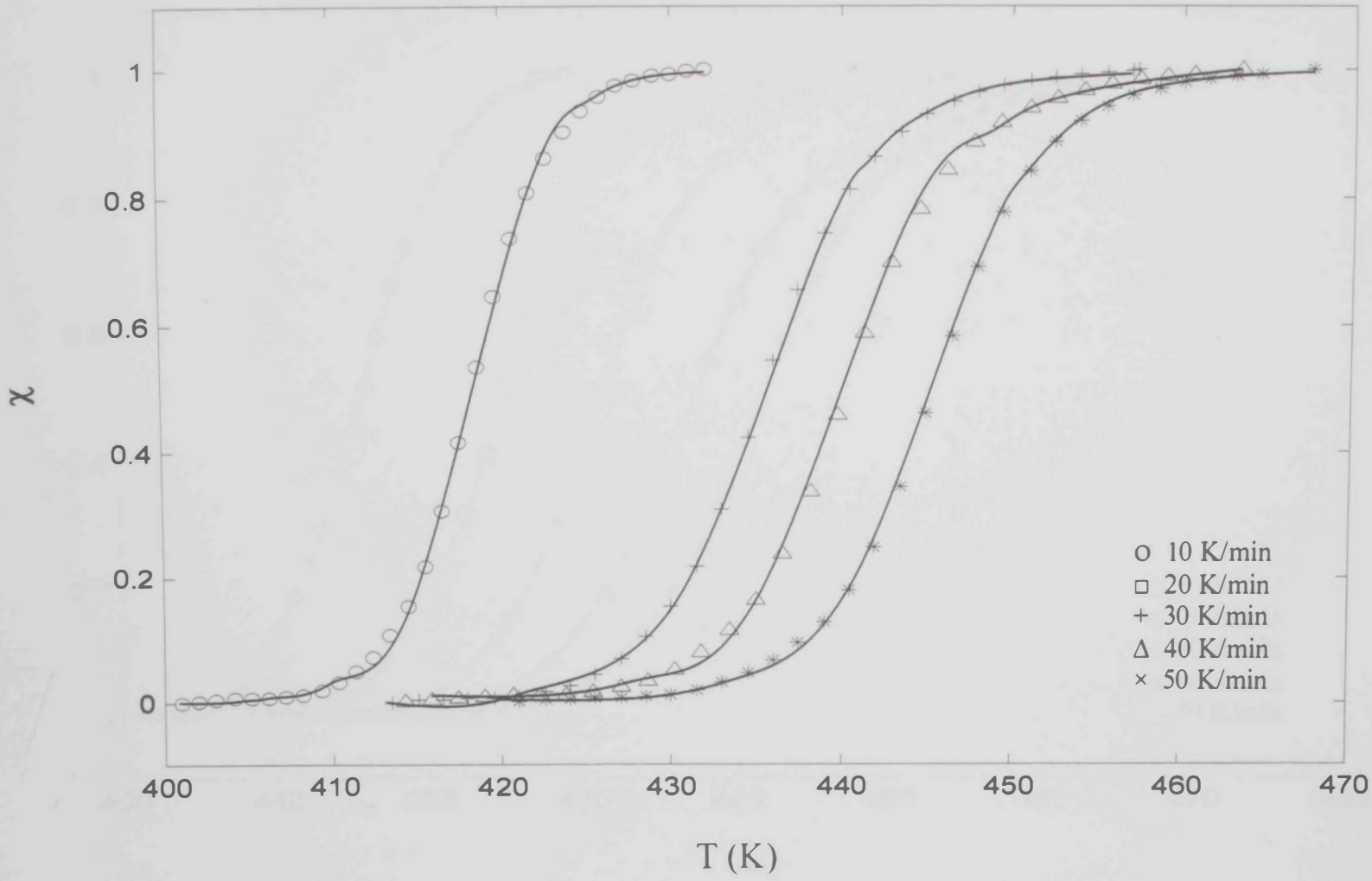

Fig. 4.37 The fraction of crystallization as a function of temperature at different heating rates for $Se_{70}Te_{22}Sb_8$ glassy alloy.

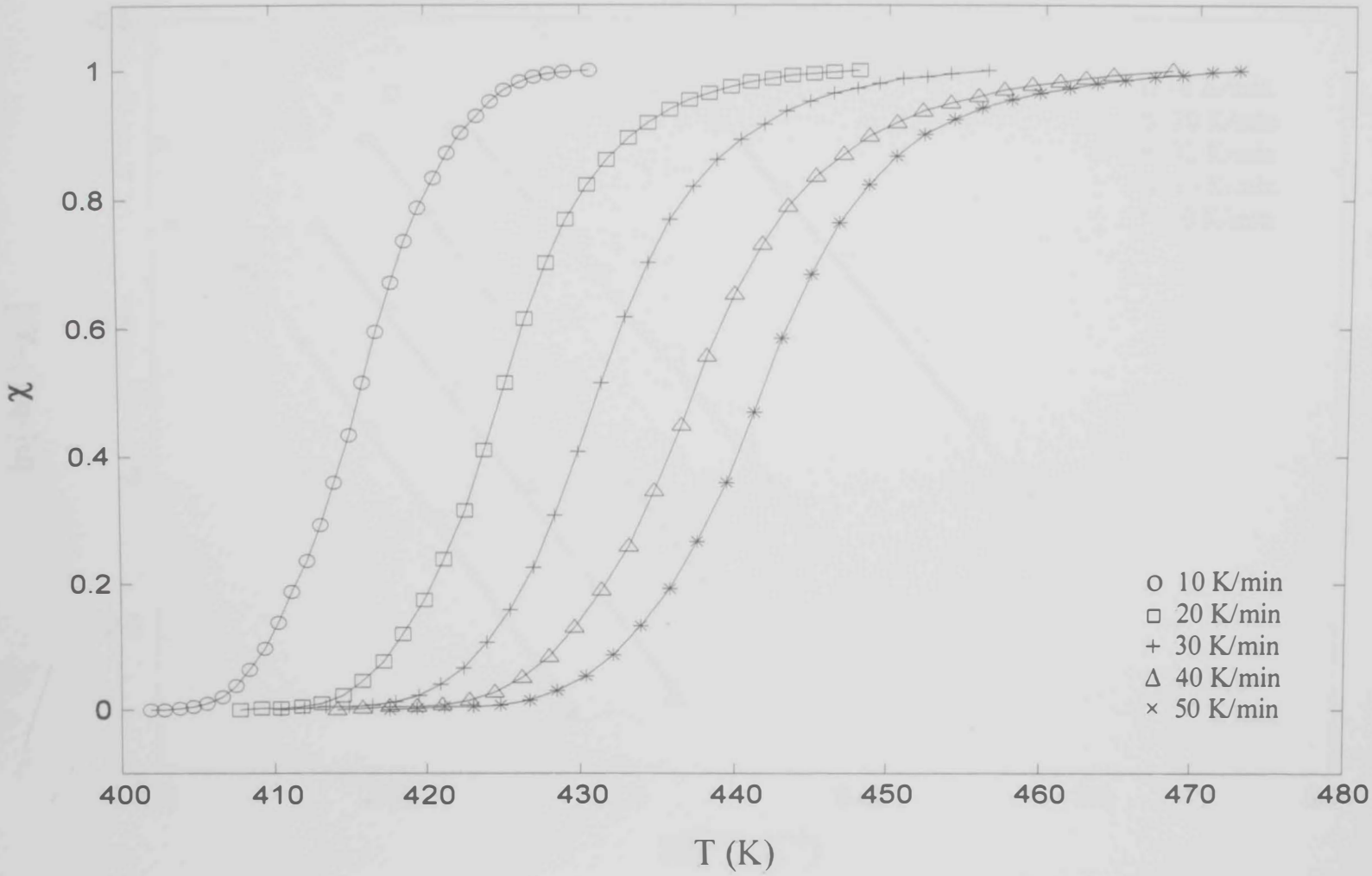

Fig. 4.38 The fraction of crystallization as a function of temperature at different heating rates for $Se_{70}Te_{20}Sb_{10}$ glassy alloy.

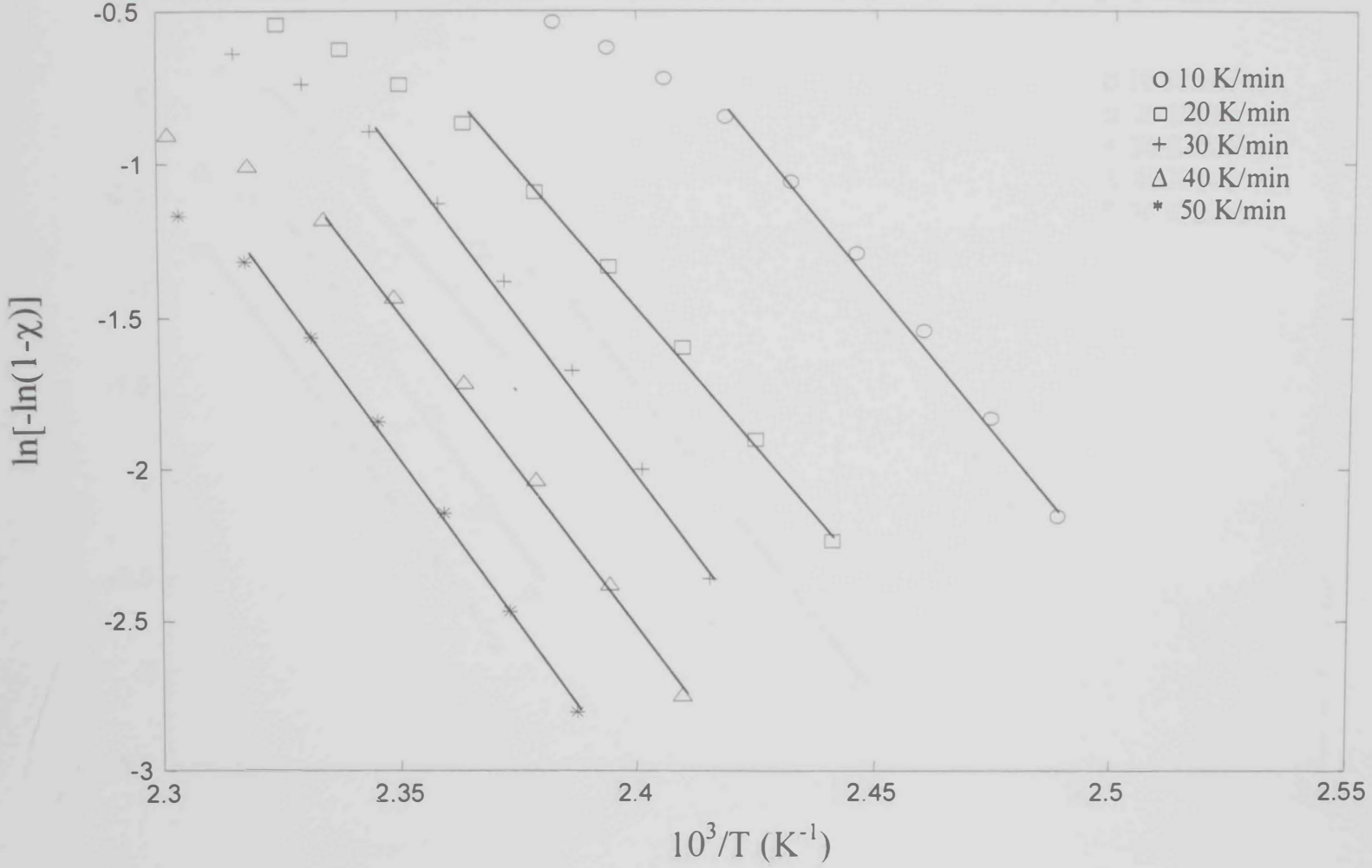

Fig. 4.39 $\ln[-\ln(1-\chi)]$ versus $(10^3/T)$ for $Se_{70}Te_{28}Sb_2$ glassy alloy.

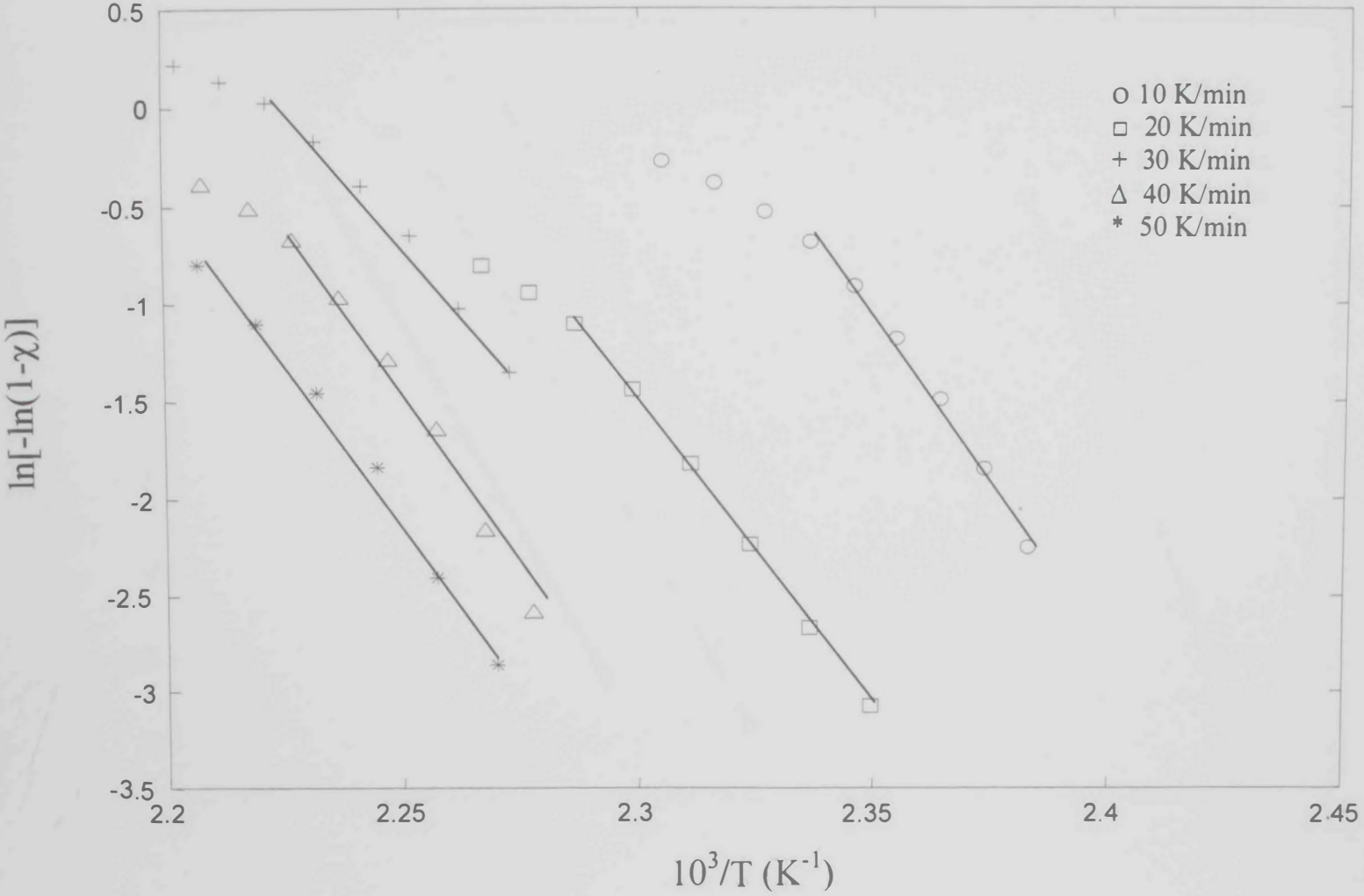

Fig. 4.40 ln[-ln(1-χ)] versus (10^3/T) for $Se_{70}Te_{24}Sb_6$ glassy alloy.

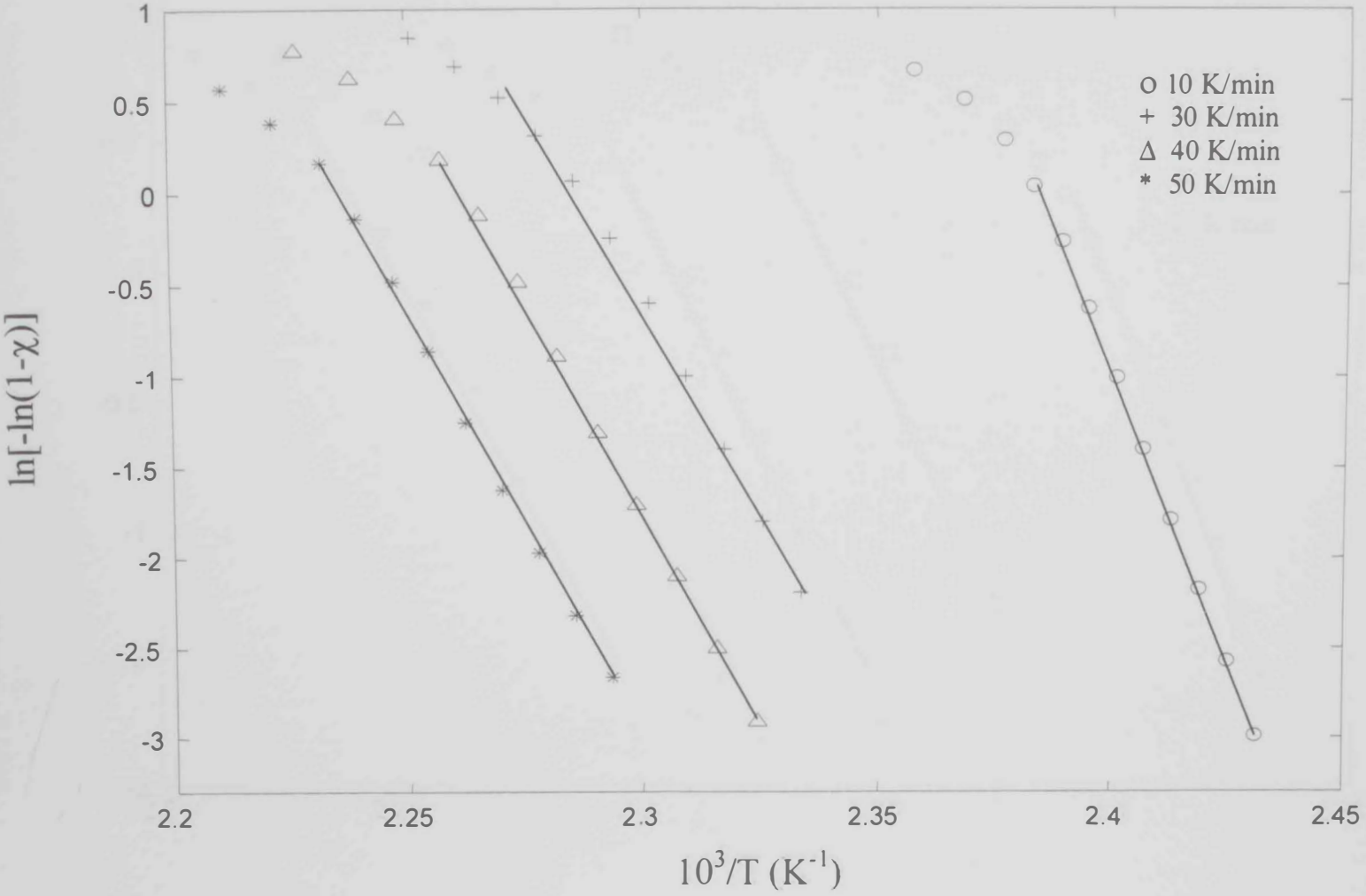

Fig. 4.41 $\ln[-\ln(1-\chi)]$ versus $(10^3/T)$ for $Se_{70}Te_{22}Sb_8$ glassy alloy.

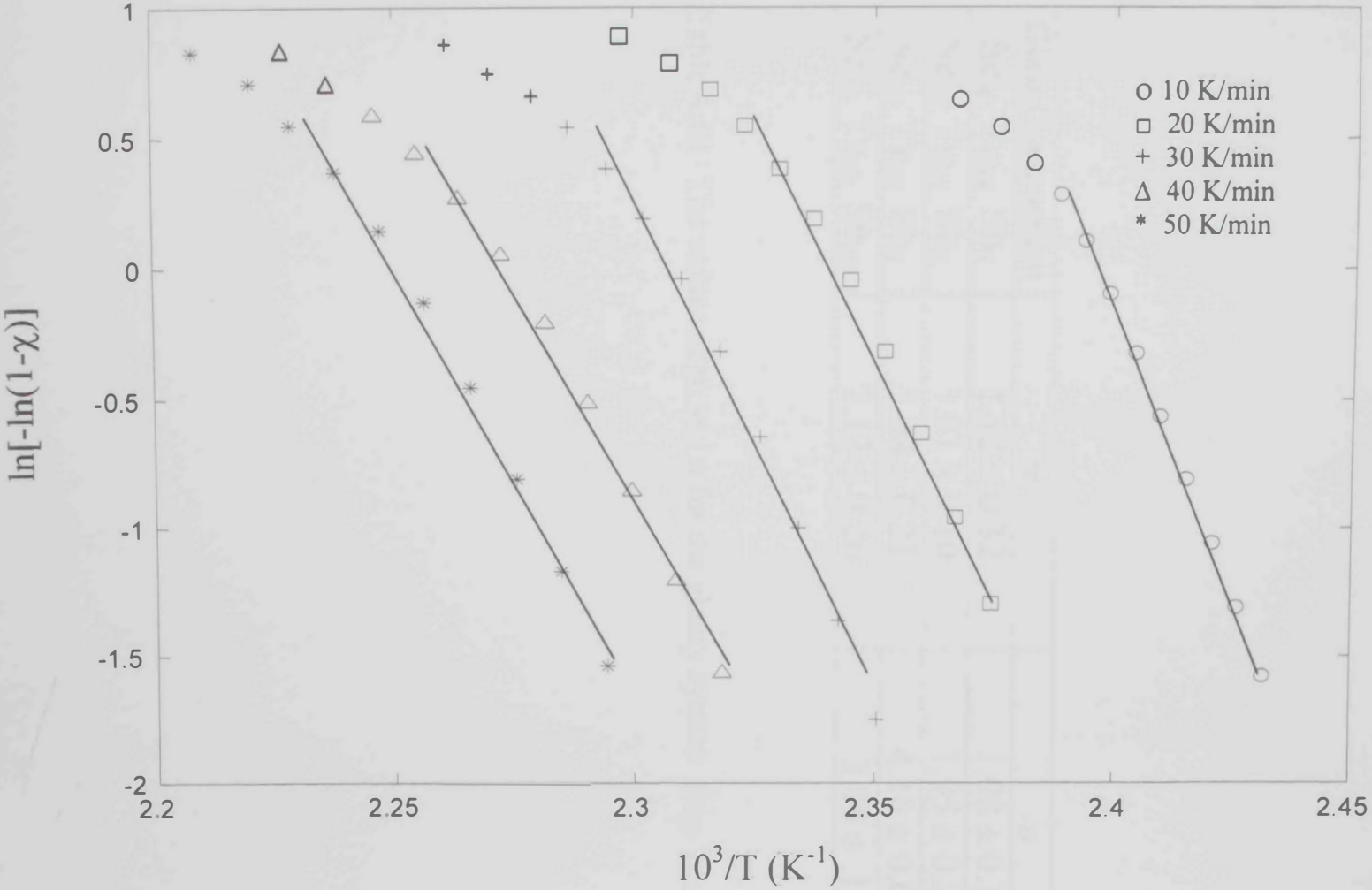

Fig. 4.42 ln[-ln(1-χ)] versus (10^3/T) for $Se_{70}Te_{20}Sb_{10}$ glassy alloy.

Glass Composition	m	n
Se_{70} Te_{28} Sb_2	1.12 ± 0.32	1.08 ± 0.18
Se_{70} Te_{24} Sb_6	1.01 ± 0.10	1.95 ± 0.26
Se_{70} Te_{22} Sb_8	3.08 ± 0.21	4.16 ± 0.07
Se_{70} Te_{20} Sb_{10}	2.12 ± 0.26	3.09 ± .15

Table 4.10 The values of m and n for the glassy system Se_{70} Te_{30-x} Sb_x.

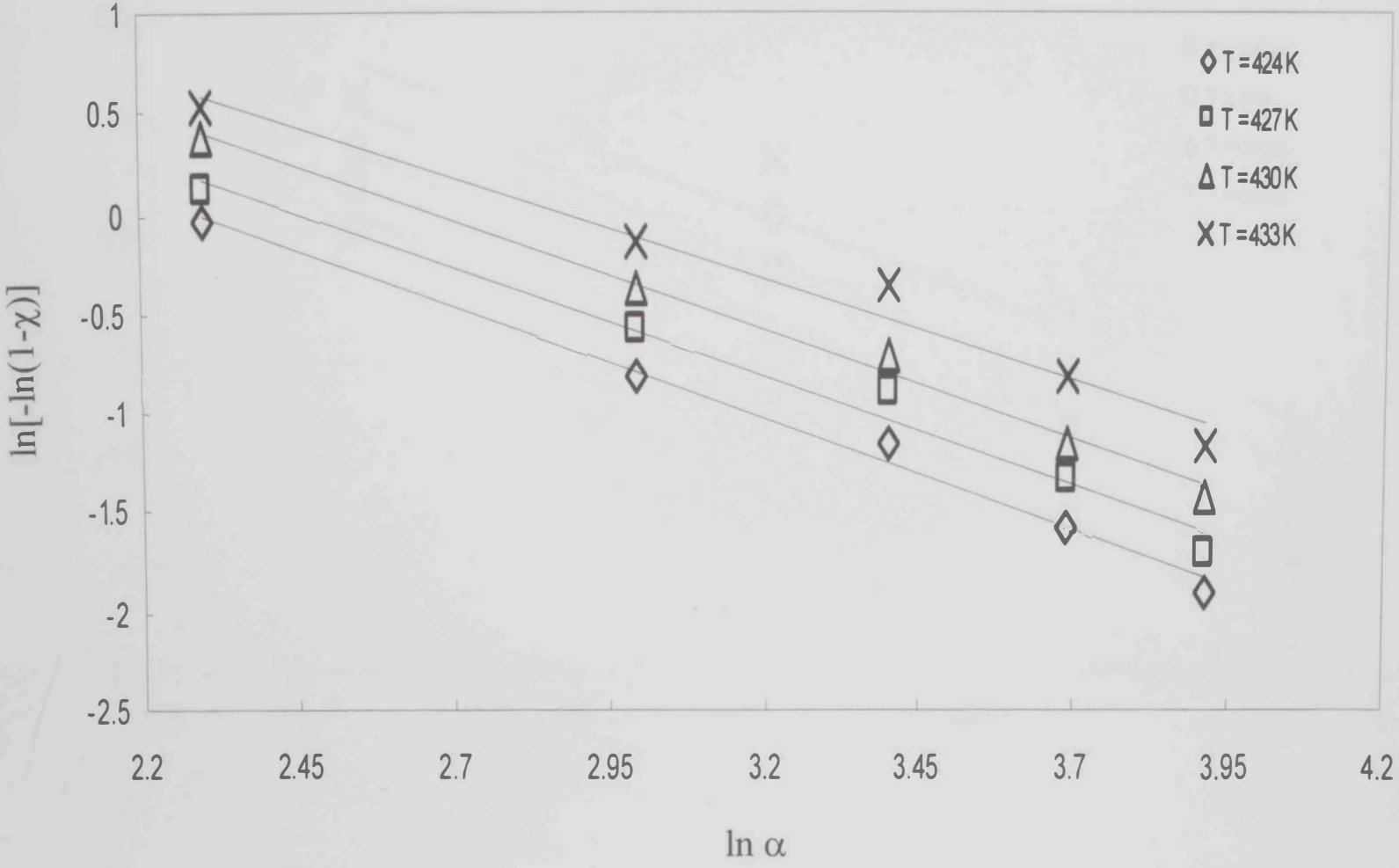

Fig. 4.43 $\ln[-\ln(1-\chi)]$ versus $\ln \alpha$ at constant temperatures for $Se_{70}Te_{28}Sb_2$ glassy alloy.

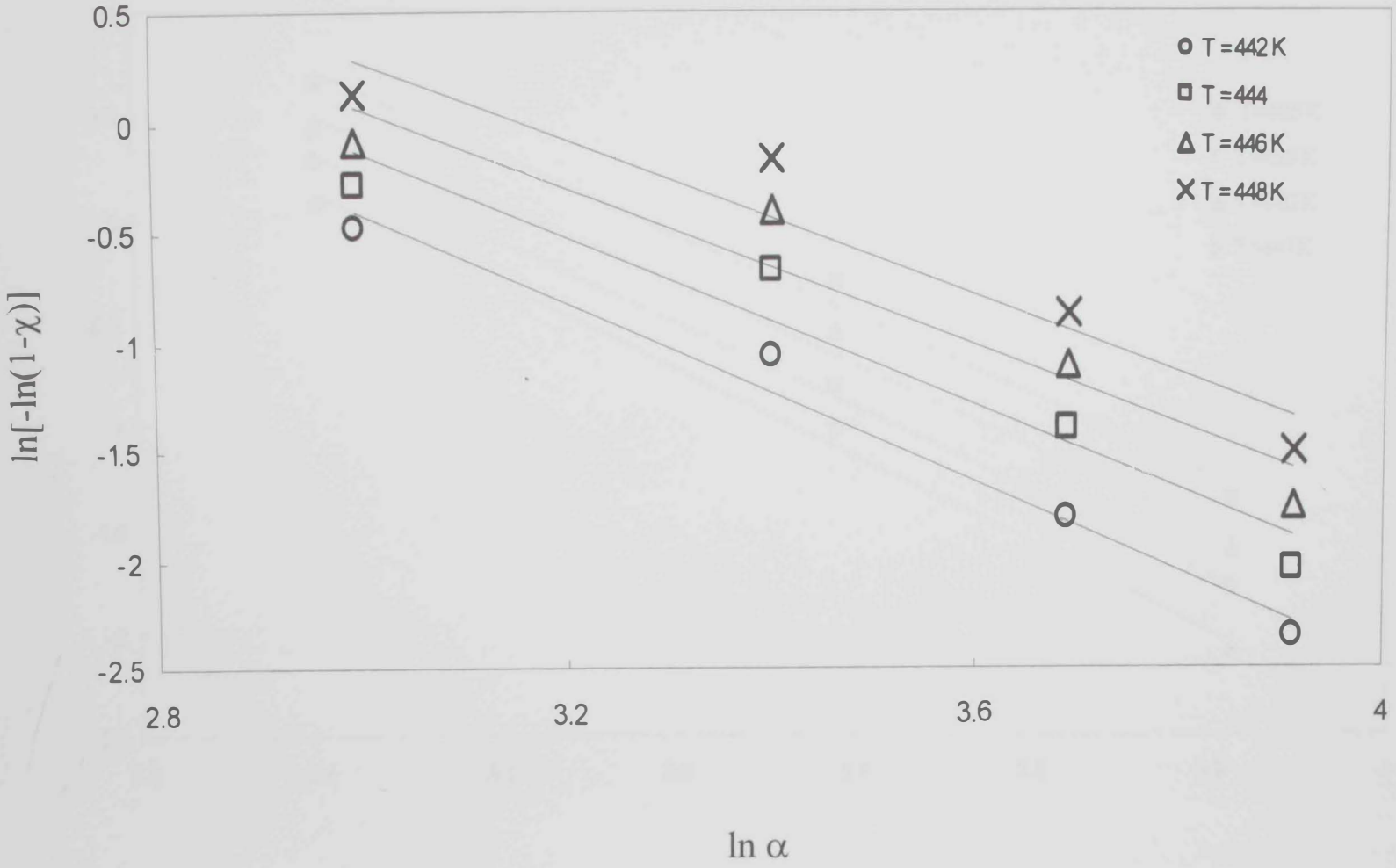

Fig. 4.44 $\ln[-\ln(1-\chi)]$ versus $\ln\alpha$ at constant temperatures for $Se_{70}Te_{24}Sb_6$ glassy alloy.

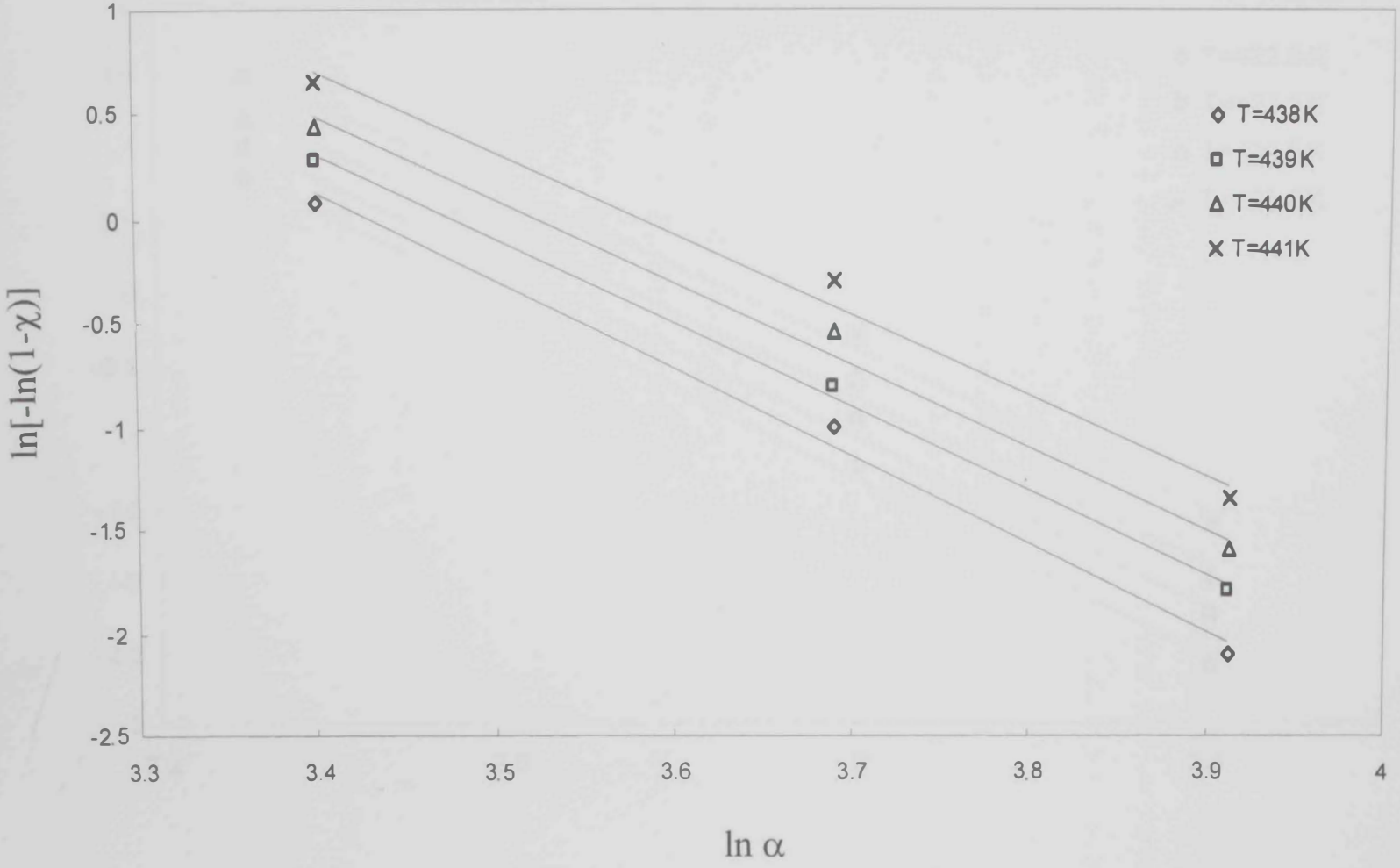

Fig. 4.45 $\ln[-\ln(1-\chi)]$ versus $\ln\alpha$ at constant temperatures for $Se_{70}Te_{22}Sb_8$ glassy alloy.

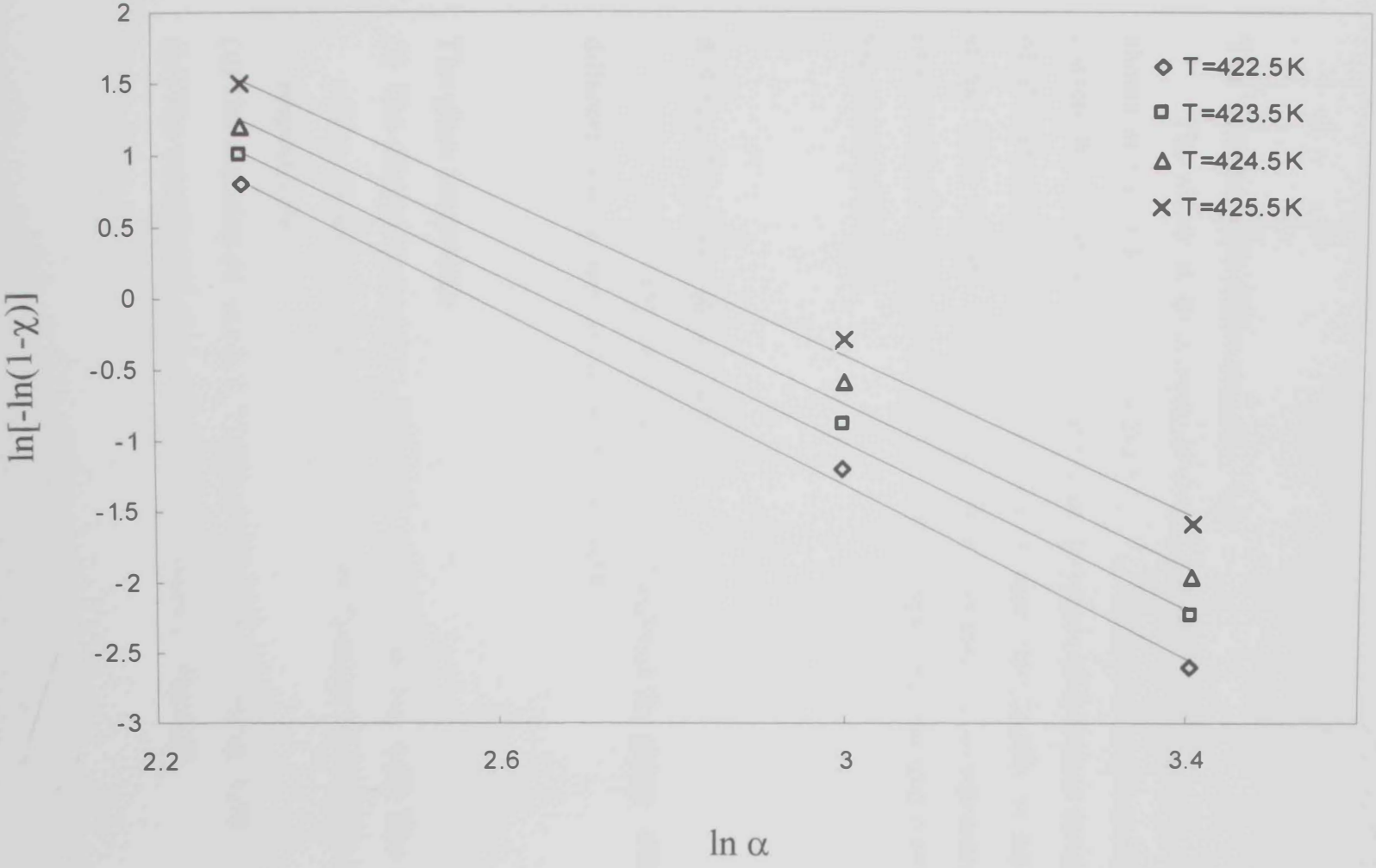

Fig. 4.46 $\ln[-\ln(1-\chi)]$ versus $\ln\alpha$ at constant temperatures for $Se_{70}Te_{20}Sb_{10}$ glassy alloy.

- $Se_{70}Te_{28}Sb_2$: surface nucleation
- $Se_{70}Te_{24}Sb_6$: one dimensional growth
- $Se_{70}Te_{22}Sb_8$: three-dimensional growth
- $Se_{70}Te_{20}Sb_{10}$: two dimensional growth

The Temperature difference ($T_c - T_g$)

The effect of Sb content on the temperature difference ($T_c - T_g$) is shown in Fig. 4.47. It is clear that ($T_c - T_g$) increases with increasing Sb content from 2 at.% to 6 at.% and then decreases with further increasing of Sb content up to 10 at.%. This indicates that $Se_{70}Te_{24}Sb_6$ is the most stable alloy in the $Se_{70}Te_{30-x}Sb_x$ glassy system. It is interesting to observe that the alloy with 6 at.% of Sb in both system1 and sytem2 is the most stable alloy.

4.3 $Se_{80}Te_{16}Cd_4$ glassy alloy:

The DSC thermograms for the $Se_{80}Te_{16}Cd_4$ glassy alloy at different heating rates are shown in Fig. 4.48.

The glass Transition

(i) The relation between T_g and $\ln \alpha$ is shown in Fig. 4.49. The value of the constants A and B in eq.(4.1) were found to be 303 and 10.76, respectively.

(ii) The variation of $\ln (\alpha/T_g^2)$ with $(1/T_g)$ is shown in Fig. 4.50.

(iii) The variation of $\ln \alpha$ with $(1/T_g)$ is shown in Fig 4.51.

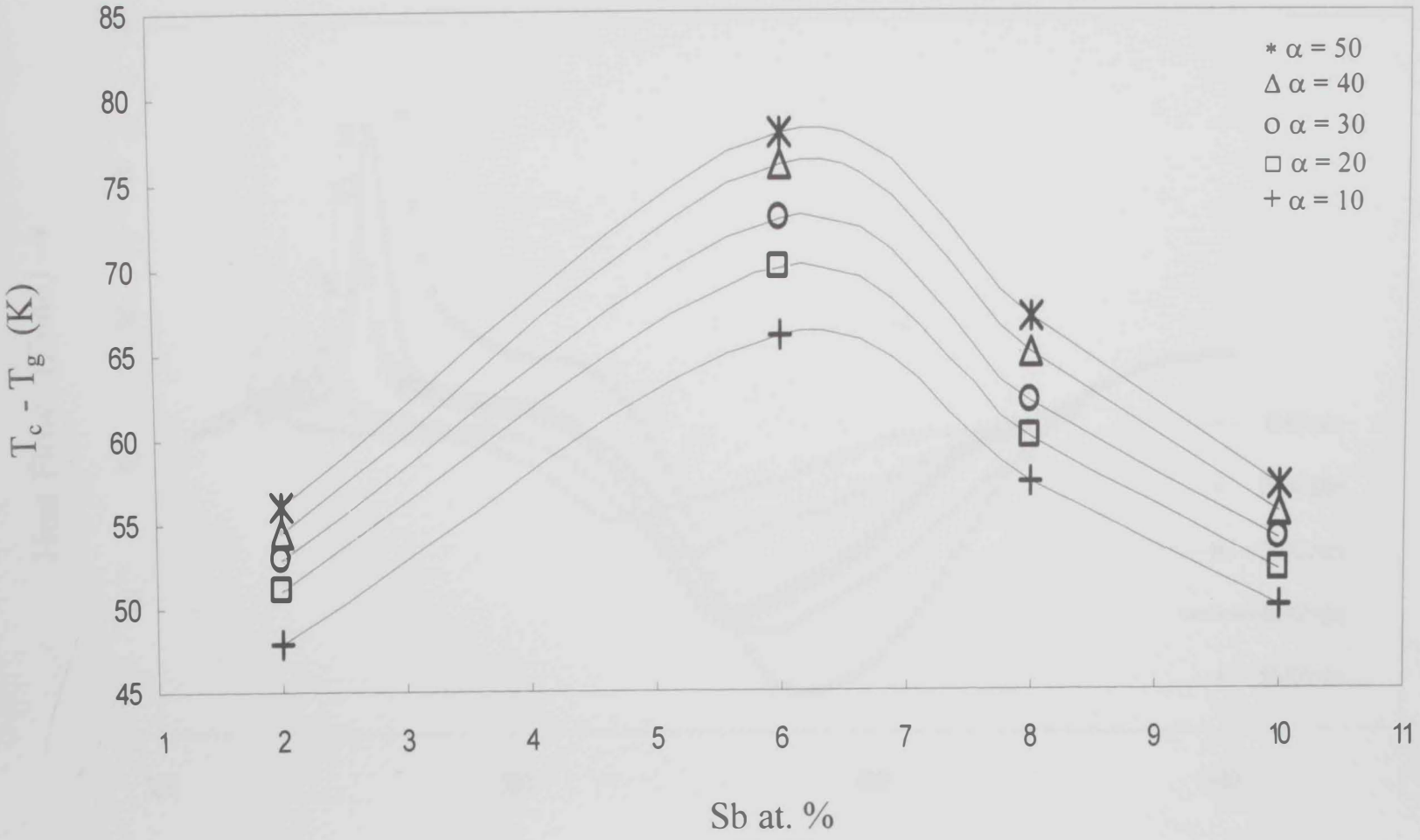

Fig. 4.47 $(T_c - T_g)$ as a function of Sb at.% for $Se_{70}Te_{30-x}Sb_x$ glassy system at different heating rates.

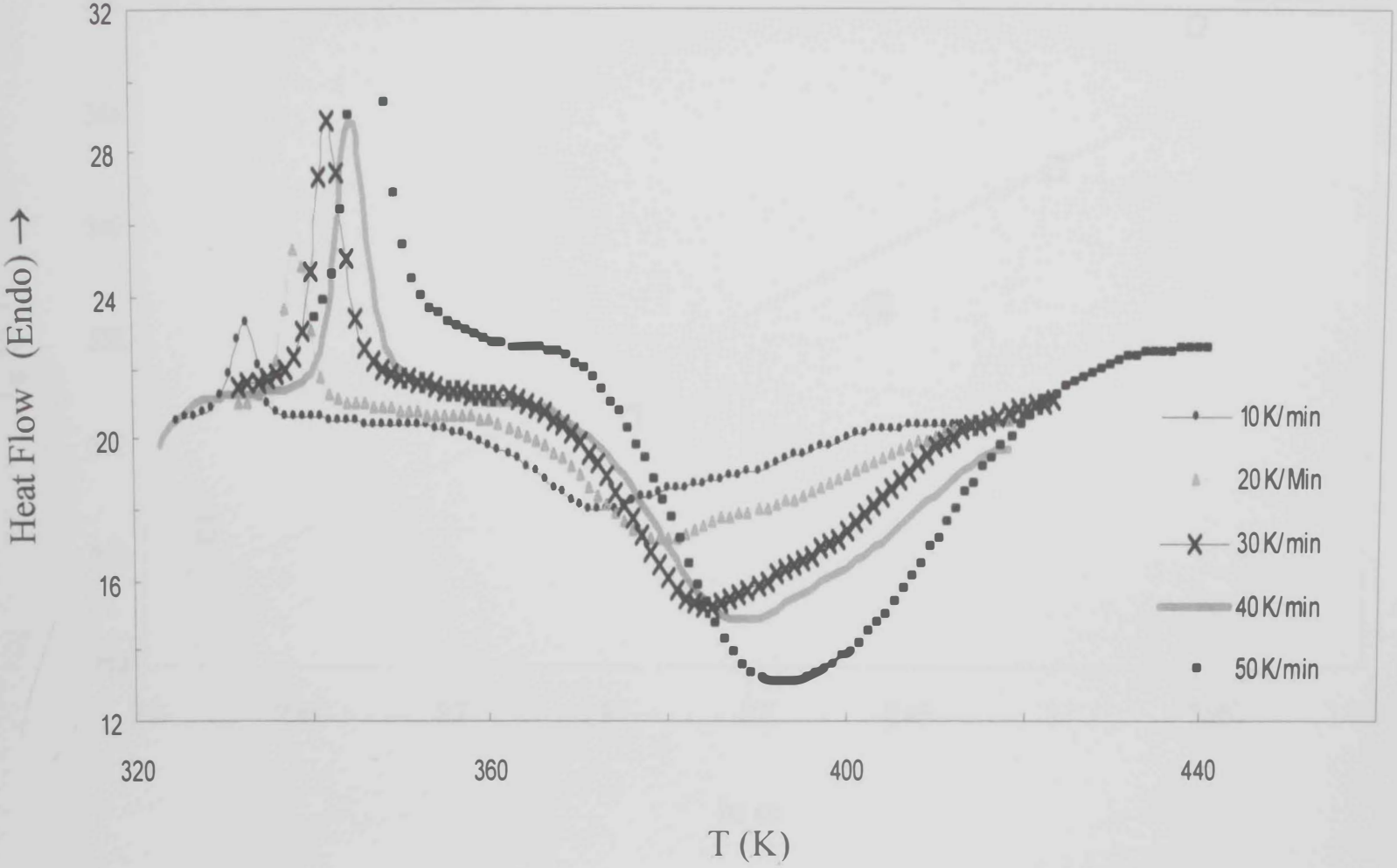

Fig. 4.48 DSC thermograrms for $Se_{80}Te_{16}Cd_4$ glassy alloy at different heating rates.

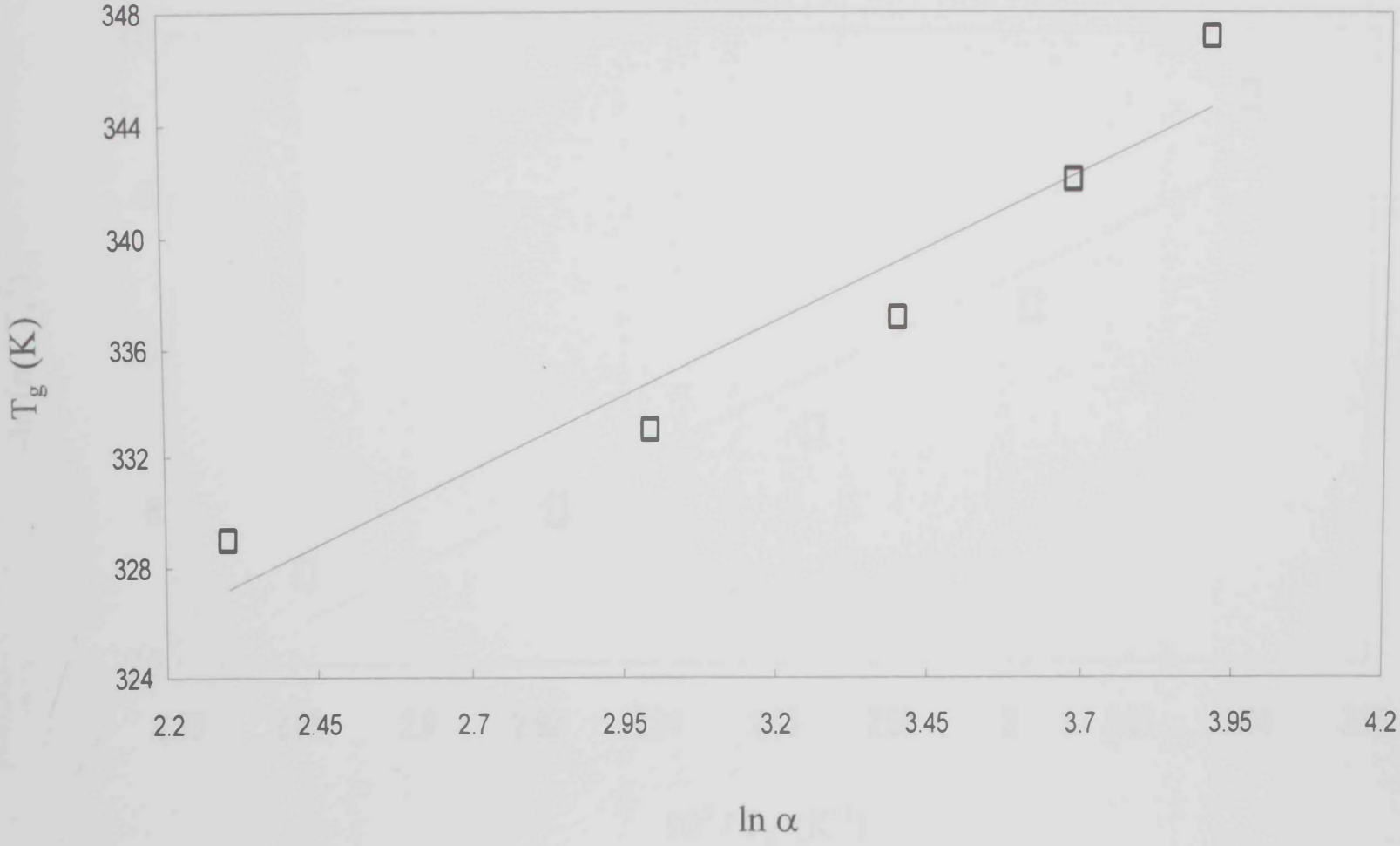

Fig. 4.49 T_g versus ln α for $Se_{80}Te_{16}Cd_4$ glassy alloy.

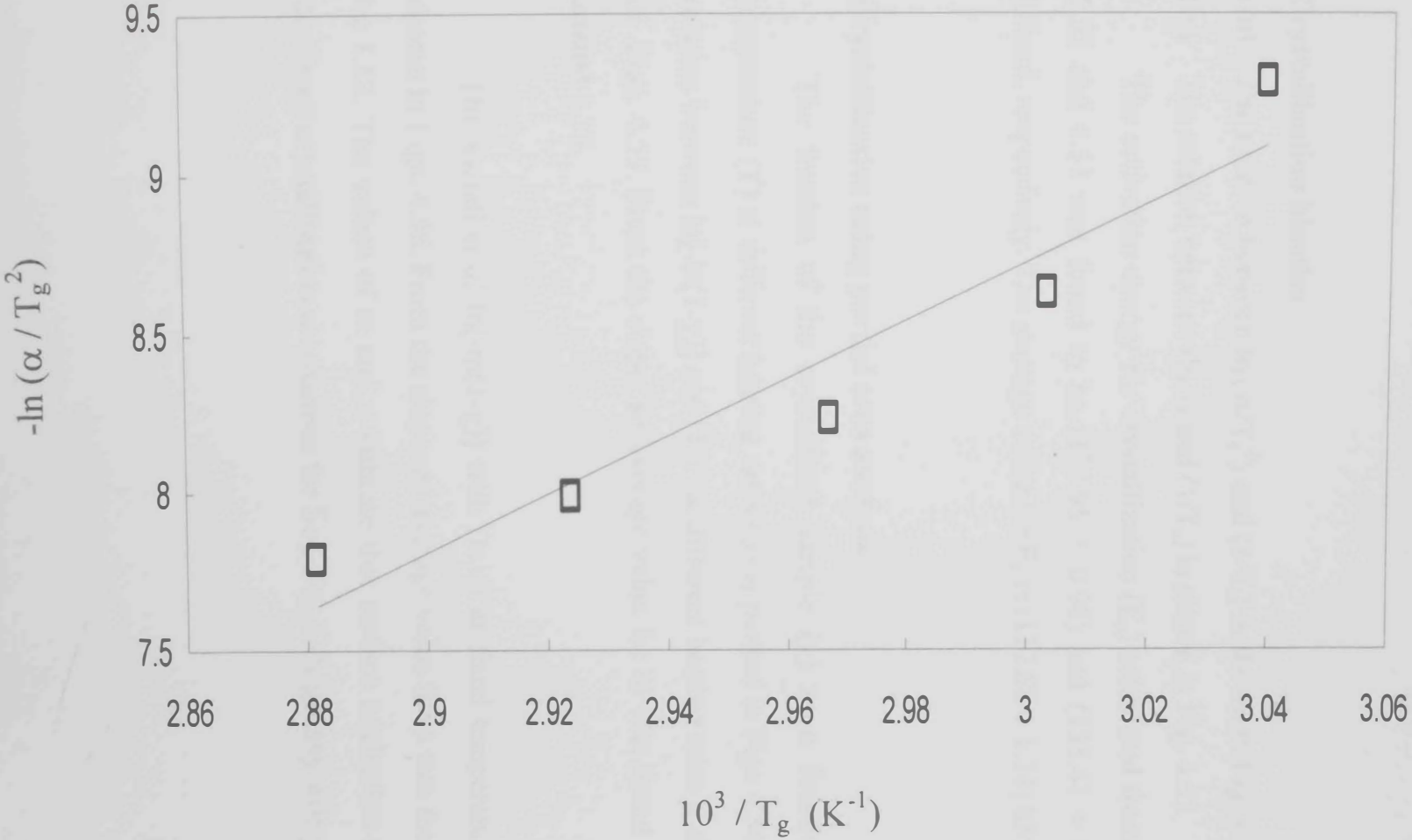

Fig 4.50 $-\ln(\alpha/T_g^2)$ versus $(10^3/T_g)$ for $Se_{80}Te_{16}Cd_4$ glassy alloy.

The activation energy for the glass transition (E_t) is calculated from Figs. 4.50 and 4.51 and was found to be (76.84 ± 0.97) and (85.66 ± 0.99) kJ/mol, respectively. The average values for E_t is (81.25 ± 1.36) kJ/mol.

Crystallization kinetics

(iii) The relation between $\ln(\alpha/T_c^2)$ and $(1/T_c)$ is shown in Fig. 4.52.

(iv) The relation between $(\ln\alpha)$ and $(1/T_c)$ is shown in Fig. 4.53

The activation energy for crystallization (E_c) calculated from Figs 5.52 and 4.53 was found to be (127.95 ± 0.98) and (135.41 ± 0.96) kJ/mol, respectively. The average value for E_c is (132.68 ± 1.34) kJ/mol.

Crystallization using partial area analysis

The fraction of the crystallized sample (χ) as a function of temperature (T) at different heating rates (α) is plotted in Figs 4.54. The relation between $\ln[-\ln(1-\chi)]$ and $(1/T)$ at different heating rates is shown in Figs. 4.55. From the slope, an average value for m was found to be around 1.13.

The variation of $\ln[-\ln(1-\chi)]$ with $(\ln\alpha)$ at fixed temperatures is shown in Figs. 4.56. From the slope, an average value for n was found to be 1.12. The values of m and n indicate that surface nucleation is the dominant crystallization mechanism for $Se_{80}Te_{16}Cd_4$ glassy alloy.

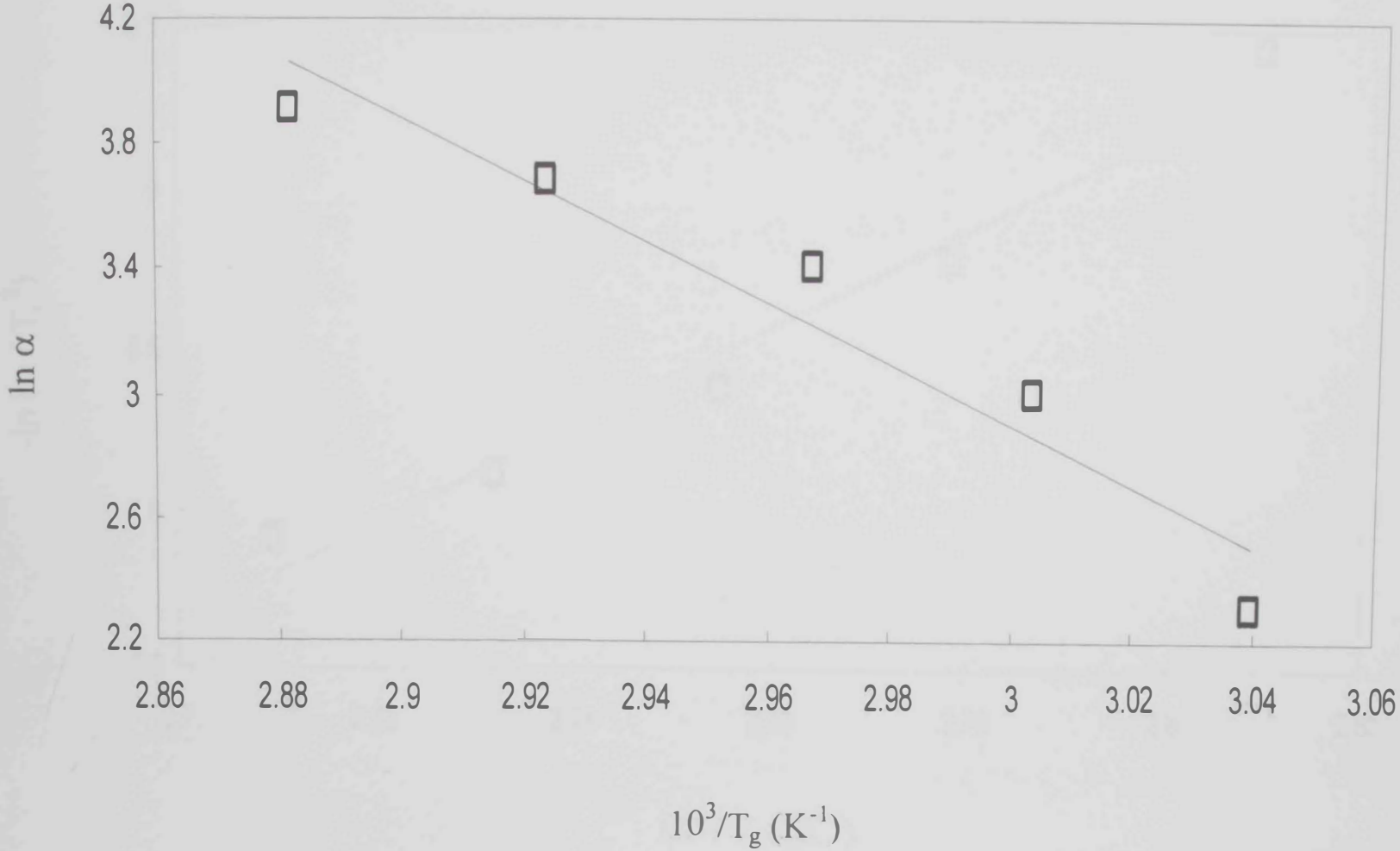

Fig 4.52 ln α versus $(10^3/T_g)$ for the $Se_{80}Te_{16}Cd_4$ glassy alloy

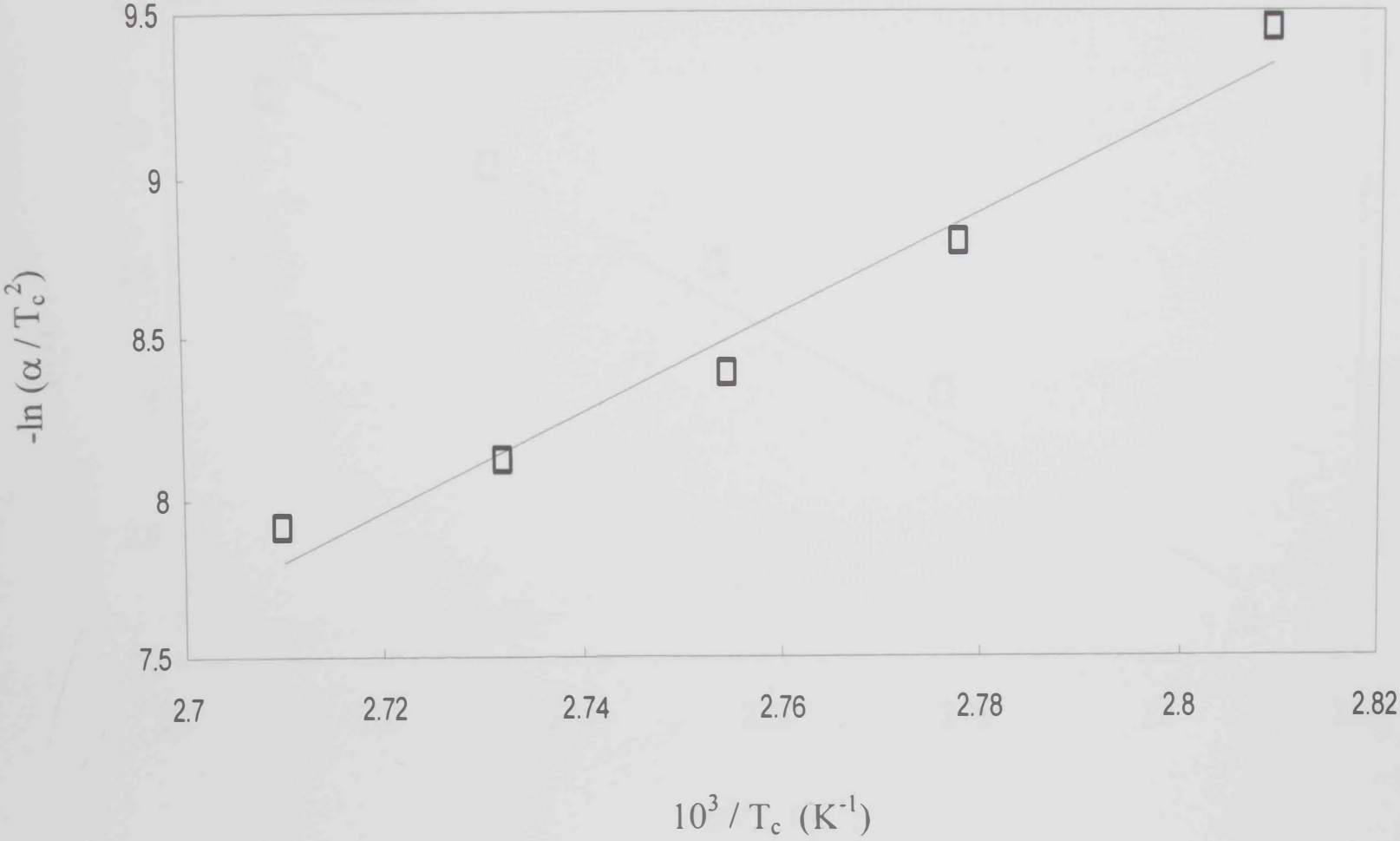

Fig 4.52 $-\ln(\alpha/T_c^2)$ versus $(10^3/T_c)$ for $Se_{80}Te_{16}Cd_4$ glassy alloy.

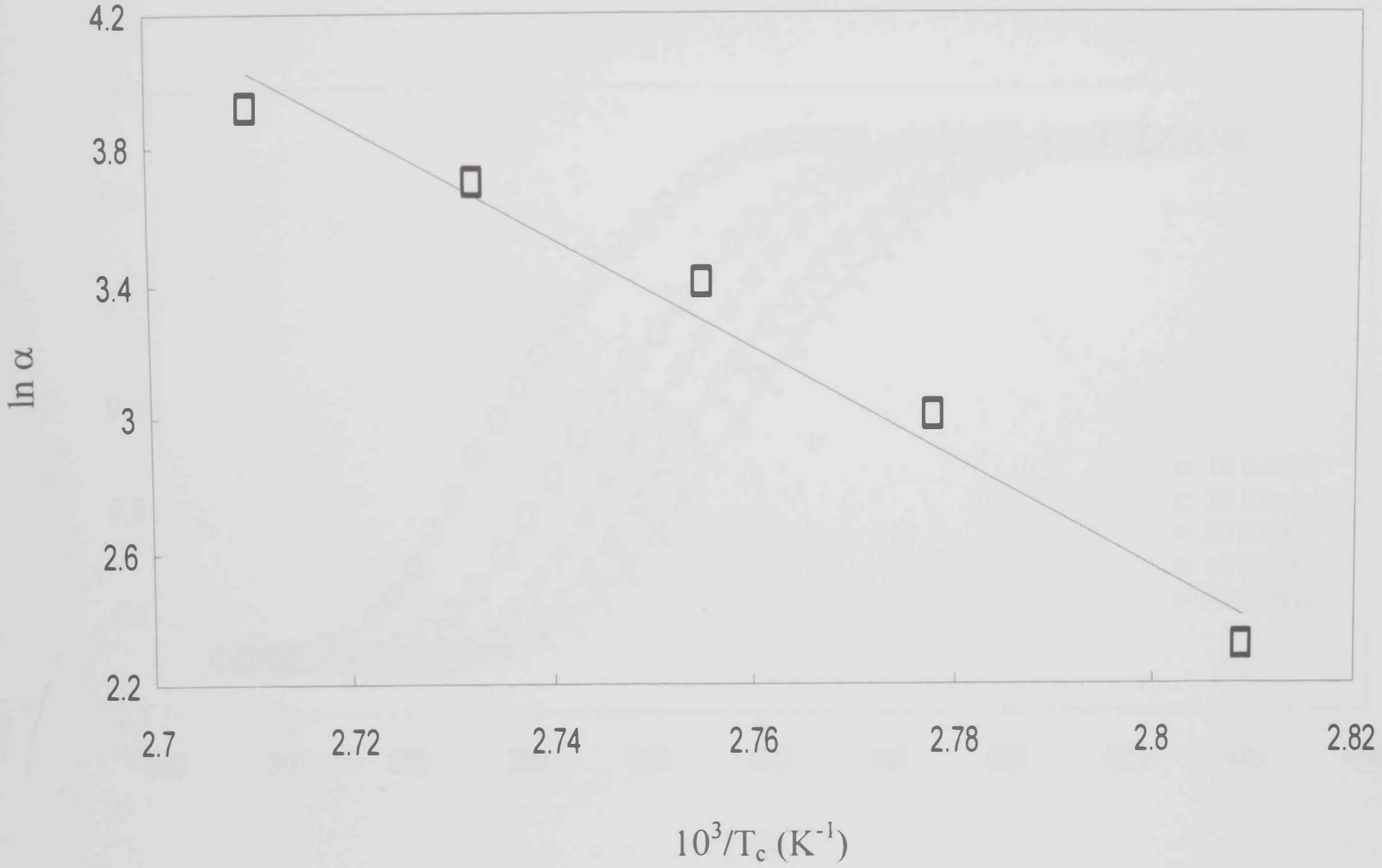

Fig 4.53 $\ln\alpha$ versus $(10^3/T_c)$ for $Se_{80}Te_{16}Cd_4$ glassy alloy

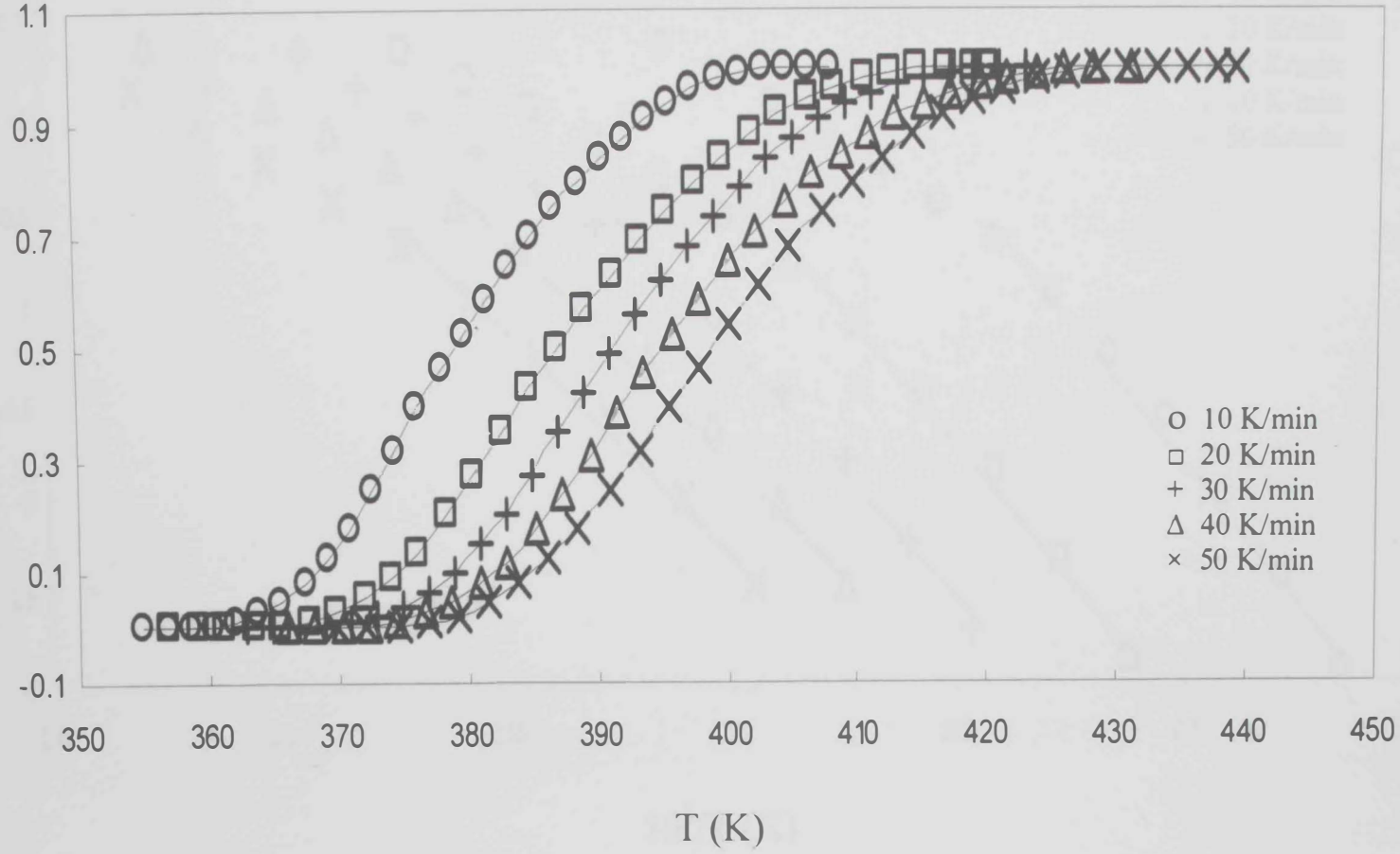

Fig. 4.54 The fraction of crystallization as a function of temperature at different heating rates for $Se_{80}Te_{16}Cd_4$ glassy alloy.

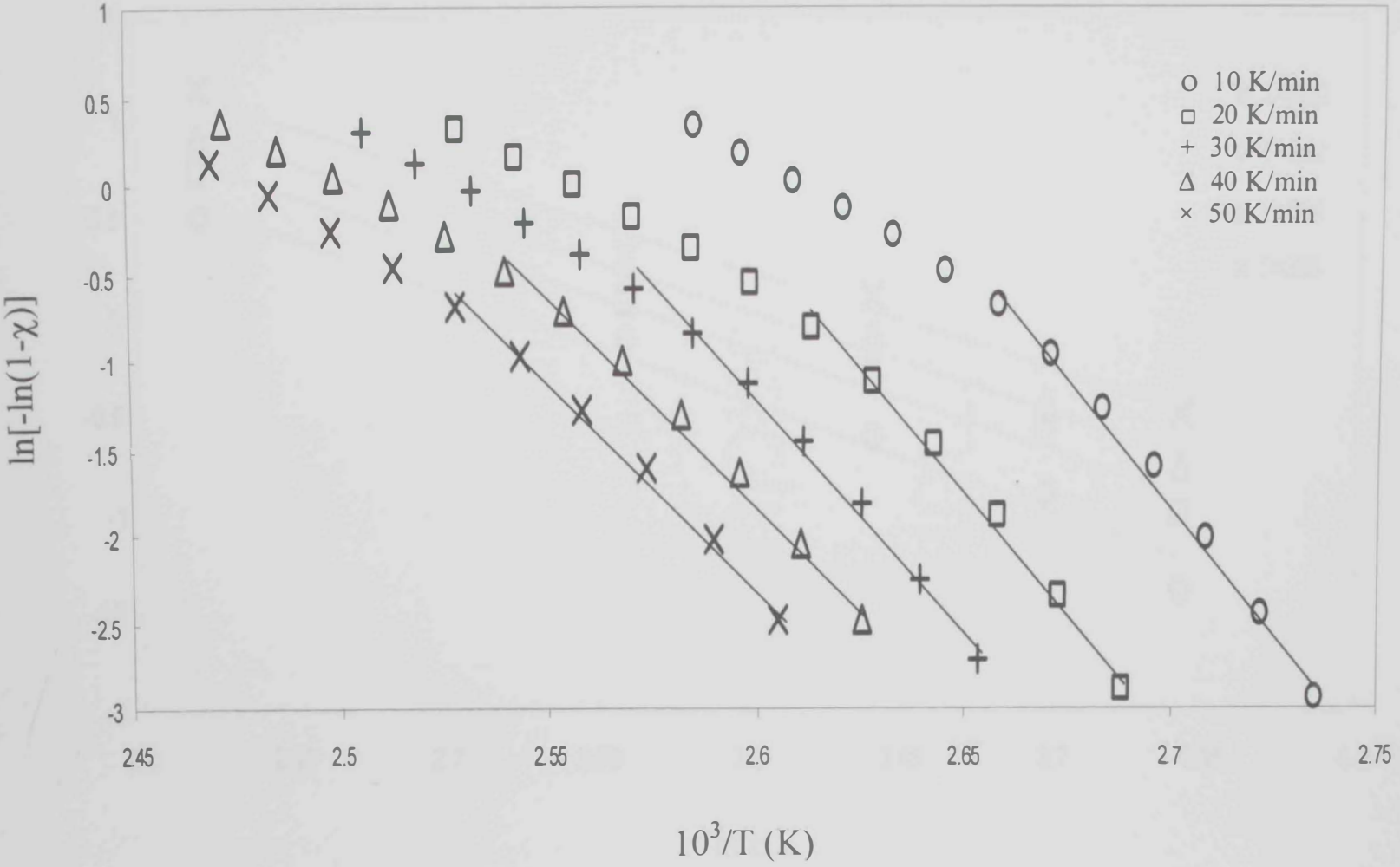

Fig. 4.55 $\ln[-\ln(1-\chi)]$ versus $(10^3/T)$ for $Se_{80}\ Te_{16}\ Cd_4$ glassy alloy.

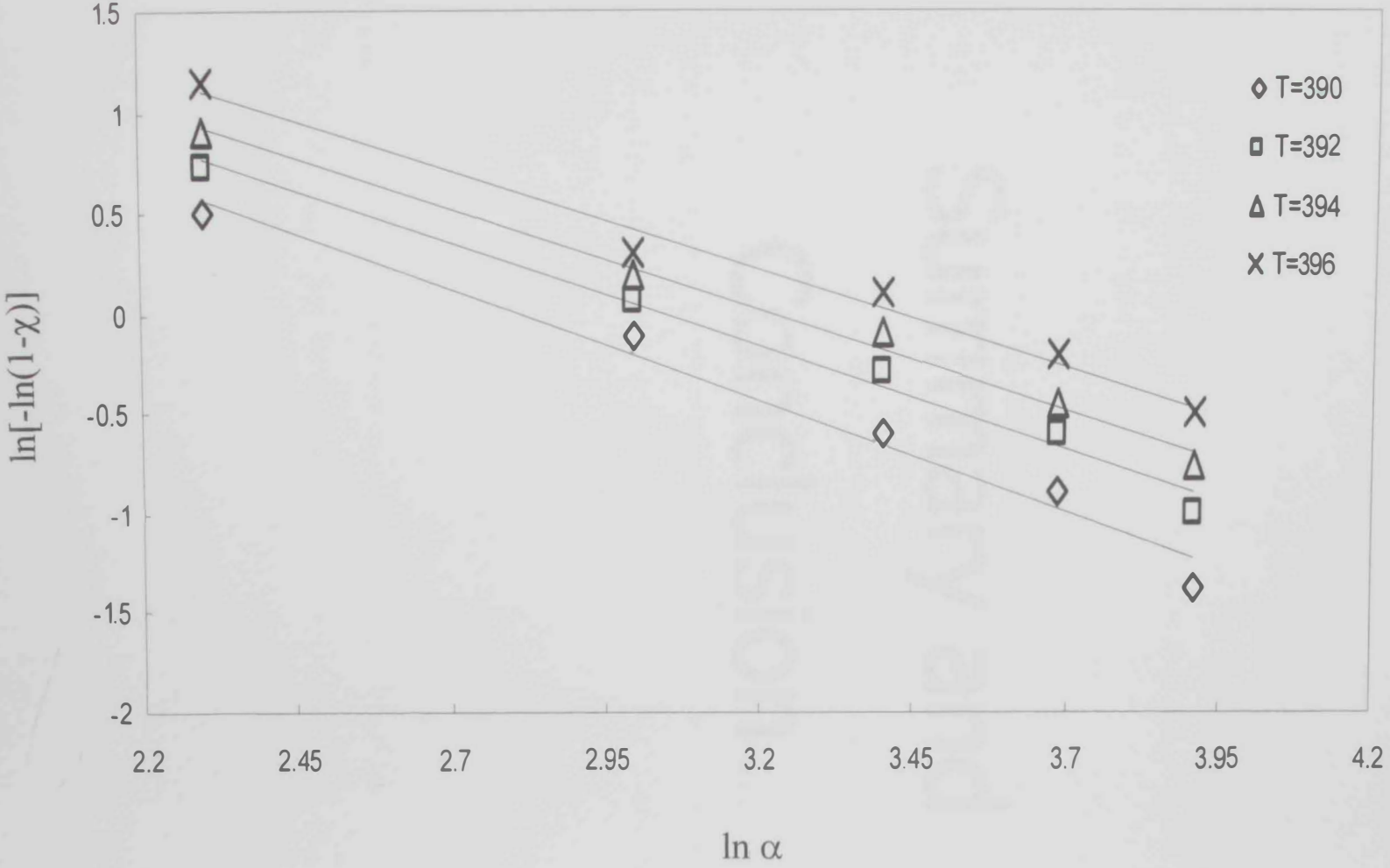

Fig. 4.56 $\ln[-\ln(1-\chi)]$ versus $\ln\alpha$ at constant temperatures for $Se_{80}\ Te_{16}\ Cd_4$ glassy alloy.

Summary and Conclusion

Summary and Conclusions

Chalcogenide glassy alloys in the system Se-Te were prepared by the melt quenching technique. Four systems were prepared. It was found that samples of $Se_{80}Te_{20-x}Sb_x$ (x = 0, 4, 6, 8, 10) and $Se_{70}Te_{30-x}Sb_x$ (x = 2, 6, 8, 10) systems were all in the glassy state. On the other hand, samples of $Se_{80}Te_{20-x}Cd_x$ (x = 2, 4, 10) and $Se_{80}Te_{20-x}Sn_x$ (x = 2, 4, 10) systems had some degree of crystallinity, except $Se_{80}Te_{16}Cd_4$ alloy which was in the glassy state.

Differential scanning calorimetry measurements were carried only on the glassy alloys. It was found that the glass transition temperature and the onset temperature of crystallization depend on the heating rate. The glass transition activation energy (E_t) was calculated by different methods and the values were in good agreement, for each glassy alloy. This indicates that any methods could be used for the calculation of E_t. The average value of E_t was found to be (from 108.12 to 127.68 kJ/mol) for $Se_{80}Te_{20-x}Sb_x$ system and (from 118.56 to 131.22 kJ/mol) for $Se_{70}Te_{30-x}Sb_x$ system.

The activation energy for crystallization (E_c) was calculated by using different equations. The values of E_c were in good agreement with each other, indicating that any equation could be applied for calculating E_c. The average value for E_c was found to be (from 122.82 to 154.65 kJ/mol) for $Se_{80}Te_{20-x}Sb_x$ system and (from 106.63 to 115.88 kJ/mol) for $Se_{70}Te_{30-x}Sb_x$ system.

Crystallization using partial area analysis were studied where the crystallization mechanism was concluded for each glassy alloy.

The difference between the crystallization temperature and glass transition temperature (T_c - T_g), which gives an indication of the thermal stability of the glasses, was calculated.

In conclusion, it was found that $Se_{80}Te_{14}Sb_6$ alloy is the most stable alloy in the $Se_{80}Te_{20-x}Sb_x$ system. All other alloys have higher tendency towards crystallization. It was also found that $Se_{70}Te_{24}Sb_6$ alloy is the most stable one in the $Se_{70}Te_{30-x}Sb_x$ system. It is interesting to note that the alloy with 6 at.% Sb is the most stable one in both systems.

Increasing Sb content for the $Se_{80}Te_{20-x}Sb_x$ system results in increasing the value of activation energy for glass transition up to 8 at.% Sb. When Sb content is increased to 10 at.%, the value of E_t decreases.

It was found that increasing Sb content for $Se_{70}Te_{30-x}Sb_x$ system results in decreasing the value of activation energy for glass transition and in increasing the value of activation energy for crystallization.

Increasing Sb content for $Se_{70}Te_{30-x}Sb_x$ system results in a linear increase in the value of T_g. While increasing Sb content causes an increase in the value of T_c up to 6 at.% Sb and then decreases slightly.

Appendices

APPENDCES

A. The program used for drawing several thermograms on the same plot:

"Using MS-Excel software"

For m ≥ 2; where m is the raw reference

i = [1, 4, 7, 10, 13]

j = [2, 5, 8, 11, 14]

o = [3, 6, 9, 12, 15]; (i, j, o) are column references

(Di) is the heating rate

Di = [10, 20, 30, 40, 50]

[R1Ci] = "The header of the Temperature Column at heating rate (Di)"

[RmCi] = [values on Temperature axis]

[R1Cj] = "The header of the Heat flow Column at heating rate (Di)"

[RmCj] = [values on Heat Flow axis]

Ts = The starting value of the measured Temperature

Hs = The starting value of the measured Heat Flow

RnCi = The last measured Temperature value, at heating rate (Di)

RnCj = The last measured Heat Flow value

(Co) is the counter for the heating rate (Di)

Co = n / (Value(RnCi – Ts))

Xi = [R1Ci → RnCi]

Yi = HLOOKUP("R1Cj ";R1C$1:R$nC$n;VALUE(RiC$o);FALSE)

Then the X-Y plot is used to present the relations at different heating rates on the same graph.

The same approach could be used for several thermograms of different samples at a fixed heating rate

B. The program for calculating the fraction (χ) crystallization functions at a particular heating rate (Di).

"Using MS-Excel software"

$m \geq 2$; where m is the raw reference

[R1C1] = "The header of the Temperature Column at heating rate (Di)"

[RmC1] = [values on Temperature axis]

[R1C2] = "The header of the Heat flow Column at heating rate (Di)"

[RmC2] = [values on Heat Flow axis]

Ts = The starting value of the measured Temperature

Hs = The starting value of the measured Heat Flow

RnCi = The last measured Temperature value, at heating rate (Di)

RnCj = The last measured Heat Flow value

Indx = [1 → n]

HMx is the maximum value of the heating rate within arrange of data

TMx is the temperature value corresponding to HMx

CMx is the cell reference corresponding to HMx

HMn is the minimum value of the heating rate within arrange of data

TMn is the temperature value corresponding to HMn

CMn is the cell reference corresponding to HMn

HMx = MAX(R2C2:RnC2)

HMn = MIN(R2C3:RnC3)

CMx = MATCH(VALUE(HMx);R2C$2:RnC$2;0)+1

CMn = MATCH(VALUE(HMn);R2C$2:RnC$2;0)+1

TMx = HLOOKUP("R1C1";R2B$2:RnC$2;CMx;FALSE)

TMn = HLOOKUP("R1C1";R2B$2:RnC$2;CMn;FALSE)

WH = 0.5*AVERAGE(VAL(R1C1):VAL([R2C1-RnC2]));

where WH is the parameter used to calculate the iteration size for crystallization Area division.

DH = ABS(L2 - (HLOOKUP("tf";B$1:C$5102;VALUE(H9)
+ A2-2;FALSE))
- (HLOOKUP("tf";B$1:C$5102;VALUE(H9)
+ A2-1;FALSE)));

where (DH) is The parameter used to calculate the baseline value.

[RmAE] = [RmDH] × [RmWH];

where (AT) is the value of the elemental areas.

AB = MATCH(TMx;R2B$2:RnB$2;0)+1

AL = MATCH(TMn;R2B$2:RnB$2;0)+1

As = INT((H10-H9)/30);

where (As) is the area calculation step parameter.

Ap = AL – AB

AT = SUM(R2AE : RpAE); where [RpAE] is the end of Area point.

[RmCTi] = RmCT{1-1}+VALUE($Ap);

where CT is the counter used for temperature positioning on x-axis.

[RmTi] = HLOOKUP("R1C1";R2B$1:RnB$n;$RmCTi;FALSE)

[RmAf] = HLOOKUP("c10";R1M$n:RnN$n;$RmCTi;FALSE)

xx =[RmAf]/ATn

X= VAL(RmTi)

Y =LN(-LN(1-xx))

Then using the X-Y plot, the fraction (χ) crystallization can be ploted.

References

References

1- W. Klement, Jr, R. H. Willnes, P. Duwez, *Nature* 187, 869 (1960).

2- K. Tanaka, Phys. Rev. B39, 1270 (1989).

3- S. R. Elliot, "*Physics of Amorphous Materials*", Longman Scientific and Technical, UK (1990)

4- N. F. Mott and E. A. Davis, "*Electronic processes in Non-crystalline Materials*" Clarendon Press, Oxford (1979).

5- William B Jensen, *J. Chem. Ed.* 9, 74 (1997)

6- Udyan Senpati, *Master Thesis*, Alfred University, NY (1994).

7- Udyan senpati, *PhD Thesis*, Alfred University, NY (1997).

8- H.R. Rawson, "*Inorganic glass forming systems*", Academic Press, New York (1967).

9- A. Pearson, "*Modern Aspects of the Vitreous State*", ed. By J. Macenzie, Butler Worths, London (1964).

10- W. H. Damhough, *Opt. Eng.* 24, 257 (1985)

11- D. Adler, "*Amorphous Semiconductors*", Butler Worths, London (1972).

12- R. Freihcs, *J. opt. Soc. Amer.* 43, 1153 (1953).

13- W. A. Fraser, *J. opt. Soc. Amer.* 43, 823 (1953).

14- F. W. Galet, D. H. Blackburn, J. S. Osmalov, D. Hubbard and M. H. Black, *J. Res. N. B. S.* 59, 83 (1957).

15- Z. U. Borisove, "*Glassy Semiconductors*" Trans. By: J. G. Adashko, Plenum Press, New York (1981).

16- R. Ruhl, R. C., *Mat. Scin.Eng.*1, 27 (1967)

17- H. Hermann, "*Treatise on Materials Science and Technology*", 20, Academic Press, New York (1981).

18- A. B. Seddon, *J. Non-cryst. Solids* 184, 111 (1995).

19- J. A. Amick, G. L. Schnable, J. L. Vossen, *J. Vac. Sc. Technol.* 14, 87 (1977).

20- W. A. Pliskin, D. R. Kerr, J. A. Perri, *Physics of Thin Films* 4, 53 (1967).

21- S. Rajagopalan, K. S. Harshavardhan, L. K. Malhotra, K. L. Chopra, *J. Non- cryst. solids* 50, 29 (1982).

22- V.Q. Nguyen, J.S. Sanghera b, J.A. Freitas, I.D. Aggarwal, I.K. Lloyd, *J. Non-Crys. Solids 3*, 248 (1999).

23- N. Afify, A Gaber, I Abdulla, H. Talaat, *Physica B.*229, 167 (1997).

24- S. R. Elliot, *Material Science and Technology* 9, 375 (1991).

25- Z. U. Borisova, "*Glassy Semiconductors Plenum*", Academic Press, New York (1981).

26- R. Kaplan, *Phys. Condens. Matters* 7, 118 (1995).

27- J. S. Sanghera, P. Hari, C. Cheney, G. Luepke, S. Singh, N. Tolk, and I. D. Aggarwal, *J. Non-Cryst. Solids* 270, 33 (200).

28- K. Hirao and K. Miura, *J. Non-Cryst. Solids* 239, 1 (1998)

29- H. Yinnon and D. R. Ullmann, *J. Non-Cryst. Solids* 54, 253 (1983)

30- S. Mahadevan, A. Giridhar and A. K. Singh, *J. Non-Cryst. Solids* 88, 11 (1986)

31- G. O. Piloyan, I. D. Rybachicov and O. S. Novikov, *Nature* 212, 1229 (1966)

32- H. J. Borcharadt, *J. Inorg. Nucl. Chem.* 12, 252 (1960).

33- A. W. Coasts and J. P. Redfren, *Nature* 201, 68 (1964).

34- M. Abramovitz and I. E. Stegun, "*Handbook of Mathematical Functions*", Dove, New York (1972).

35- I. S. Gradshteyn and I. M. Ryshik, "*Tables of Integrals Series and Products*", Academic Press, New York (1980).

36- C.D. Doyle, *Nature* 207, 290 (1965).

37- T. Ozawa, *Polymer* 12, 150 (1971).

38- H. E. Kissinger, *Anal. Chem.* 29, 1702 (1957).

39- H. E. Kissinger, *J. Res. Nat. Stand.* 57, 217 (1956)

40- M. Lasocka, *Mater. Sc. Eng.* 23, 173 (1976).

41- H. S. Chen, *J. Non-Crys. Solids*, 27, 257 (1978).

42- J. E. Shelby, *J. Non-Crys. Solids* 34, 111 (1979).

43- J. Colmenero and J. M. Barandairan, J. *Non-Cryst. Solids* 30, 363 (1978).

44- J. A. Macmillan, *J. Phys. Chem.* 42, 3497 (1965).

45- T. Hatakeyama, F. X. Quin, "*Thermal Analysis*", John Whiley & Sons, New York (1999).

46- N. Afify, J. *Non-Cryst. Solids* 126, 130 (1990).

47- M. K. Rabinal, N. R. Rao, U. S. Sangunni and E. S. R. Gopal, *Phil. Mag.* 70, 89 (1994).

48- N. Afifi, *J. Non-Cryst. Solids* 136, 67 (1991).

49- N. Afify, *J. Non-Cryst. Solids* 128, 279 (1991)

50- N. Afify, J. *Non-Cryst. Solids* 142, 247 (1992).

51- K. Matusita, T. Konatsu, and R. Yokota, *J. Mat. Sc.* 19, 291 (1984).

52- J. Calemenero and J. M. Barandiaran, *J. Non-Cryst. Solids* 30, 263 (1978).

53- R. F. Speyer and S. H. Risbud, *Phys. Chem. Glasses* 24, 26 (1983).

54- P. Dulaj, D. Barancok and A. Omderjka, *J. Non-Cryst. Solids*, 411 (1976).

ولقد تم قياس منحنيات التحليل الحراري للعينات عند معدلات تسخين مختلفة، وأوضحت هذه المنحنيات أنّ كلا من درجة التحول الزجاجي، ودرجة التحول البلوري لكل عينة تزداد قيمها بازدياد معدلات التسخين. ولقد استخدمت العلاقة بين درجة التحول الزجاجي ومعدل التسخين في حساب طاقة التنشيط الزجاجي من خلال العديد من المعادلات، ووجد أن قيمها تتفق بشكل جيد، بالنسبة لكل عينة. كذلك استخدمت العلاقة بين درجة التحول البلوري ومعدل التسخين لحساب طاقة التنشيط البلوري من خلال عدة معادلات ووجد أيضا أنها تتفق مع بعضه البعض بشكل جيد. وقد تم حساب الفرق بين درجة الحرارة للتحول الزجاجي ودرجة الحرارة للتحول البلوري، وربطه بنسب تواجد عنصر الأنتيموني في كل سبيكة ؛ وإنّ ذلك يعتبر مؤشرا على مقاومة السبيكة للتحول البلوري. وقد وجد أن العينة التي تحتوي على(٦%) من الأنتيموني، هي الأكثر ثباتا وذلك في كلا المجموعتين الأولى و الثانية السابق ذكرهما من العينات.

ملخص الرسالة

يهدف هذا البحث إلى دراسة تحول سبائك (السيلينيوم – تليريوم) من الحالة الزجاجية إلى الحالة المتبلرة، ولقد تم تحضير أربع مجموعات من هذه السبائك، وهي: (سيلينيوم[٨٠%] – تليريوم – أنتيموني)؛ (سيلينيوم[٧٠%] – تليريوم – أنتيموني)؛ (سيلينيوم[٨٠%] – تليريوم – كادميوم) و (سيلينيوم[٨٠%] – تليريوم – قصدير). ولقد تم تحضير هذه السبائك بوزن كميات عالية النقاوة (٩٩,٩٩٩%) من العناصر السابقة، ومزجها وفقا لنسبها الذرية، ووضعها في أنابيب من السيليكا تحت تفريغ (10^{-5} مم.زئبق)، وتسخين المركبات النهائية عند درجات مناسبة من الحرارة ولفترات زمنية ملائمة، ثم تم تعريض الأنابيب بمحتوياتها من السبائك لعملية التبريد الفجائي، في خليط من الماء والثلج.

ولقد أظهرت قياسات الأشعة السينية، أنّ عينات المجموعتين الأوليتين كانت كلها في الحالة الزجاجية، أما المجموعتين الأخريين من العينات فكانت في حالة شبه متبلرة نوعا ما؛ فيما عدا عينة واحدة فقط. وعلى هذا فقد تم حصر القياسات الحرارية على العينات الزجاجية فقط.

إلى والدتي الحبيبة

لكل شيء رائع

علمتني إياه

دراسة تحول سبائك من السيلينيوم- تليريوم
من الحالة اللابلورية إلى الحالة المتبلّرة

أطروحة مقدمة إلى

عمادة الدراسات العليا

جامعة الإمارات العربية المتحدة

من الطالب

فريد عبدالرحيم الغياث

إستكمالا لمتطلبات الحصول على درجة الماجستير في

علوم و هندسة المواد

بإشراف

أ. د. أسامة محمد مختار الشاذلى

قسم الفيزياء

كلية العلوم

جامعة الإمارات العربية المتحدة

أ. د. راشد عبدالرحيم السعيد

قسم الكيمياء

كلية العلوم

جامعة الإمارات العربية المتحدة

يونيو ٢٠٠٤